Università degli Studi dell'Insubria

Scuola di Dottorato dell'Università degli Studi dell'Insubria

Dottorato di Ricerca in Medicina Sperimentale e Traslazionale - XXXI CICLO

Metal nanoparticle permeation through the plasma membrane: *Xenopus laevis* oocytes as novel tools for membrane permeability evaluation and physico-chemical characterization of particle properties

Tutor: Prof.ssa **Elena Bossi**

Tesi di dottorato di:

Daniele Zanella

Matr. 711205

Anno accademico 2017-2018

Summary

Chapter 1

The biological barriers with their specific permeability limit and control the access of exogenous molecules to the interior of cells and the translocation across the adsorbing epithelia. Researchers and patients would benefit from efficient methods for intracellular delivery of a wide range of molecules (biochemically active small molecules, imaging agents, peptides, nucleic acids, proteins, drugs and micronutrients). A deep knowledge of the mechanisms underlying nanomaterial interactions with membrane and the comprehension of the effects on the cellular physiology is required, to avoid off-target adverse effects and to boost the use of these potentially revolutionary compounds in nanomedicine.

Nanotechnology and Nanomaterials

Nanoscience is the study of matter at the atomic and molecular scale, roughly in the 0.1-1000 nm range. From the visionary ideas of Richard Feynman (Nobel Prize in Physics in 1965), expressed in his speech "There's Plenty of Room at the Bottom" held at the American Physical Society in 1959[1S], the study of the smallest component of matter has gained the status of an independent, yet integrated, discipline, which is nowadays called nanotechnology, as it was baptised from Norio Taniguchi in 1974[2S]. According to the European Union's Scientific Committee on Emerging and Newly Identified Health Risks, nanotechnology is defined as "those areas of science and engineering where phenomena that take place at dimensions in the nanometre scale are utilised in the design, characterisation, production and application of materials, structures, devices and systems"[3S]. Nanomaterials (NMs) are defined as are materials that have at least one dimension in the range of 1–100 nm; it is possible to recognize materials with 1 dimension in this range (nanofilms, nanosheets), with 2

dimensions in this range (nanotubes, nanowires) and with 3 dimensions in this range (nanoparticles). One of the nanotechnology purposes is to create new products with properties and functions that differ from the corresponding bulk materials. Superior properties of NMs in terms of chemical reactivity, electrical resistance/conductivity and biological activity can be ascribed to the increased surface area to volume ratio; moreover, their dimensional range allows direct interactions with biomolecules of interest, increasing the biological relevance of NMs.

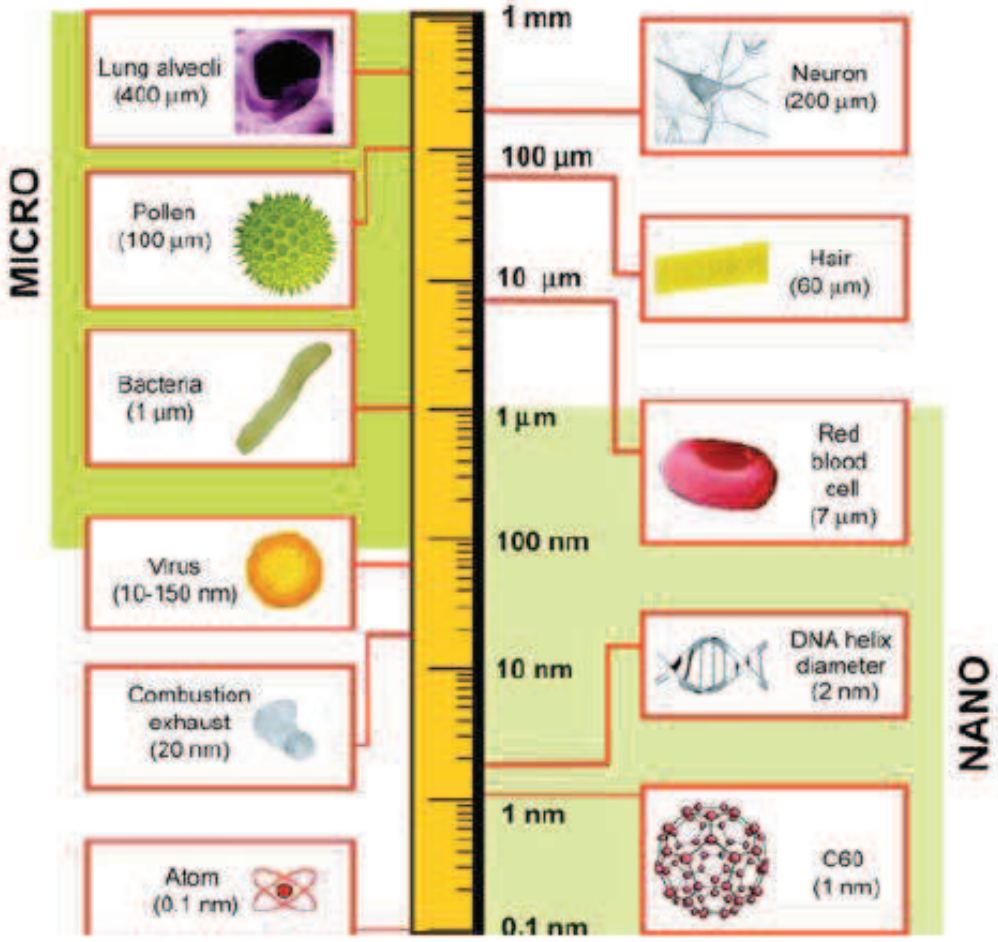

Figure 1: Logarithmical length scale showing size of nanomaterials compared to biological components and definition of "nano" and "micro" ranges[1]

NMs are now widespread in different fields[2-5], spacing from industrial application, such as catalyst[6, 7], [341], cosmetics[8-11], photovoltaic devices[342], to electronics[12], agriculture[13, 14], food safety[15-17], as well as

emerging every day more in the biomedical field as sensors[18-22], imaging tools[23-25], drug delivery agents[26-35] or as direct therapeutic agents[36, 37].

Nanoparticles

Among NMs, nanoparticles (NPs) are the ones attracting more and more interest, in areas such as biology and medicine, as well as there is concern for their possible effect on health and environment.
It is possible to classify NPs from their origin, distinguishing between natural and anthropogenic NPs (Table 1). Anthropogenic NPs can be further divided in unintentional and intentional, with the first coming from different processes as byproducts and the latter synthesized with high monodispersity and precise chemical composition[38].

Tab. 1: the main sources of nanoparticles[1, 38]

Natural	Anthropogenic	
	Unintentional	Intentional
Gas-to-particle conversions Forest fires Volcanoes (hot lava) Viruses Biogenic magnetite: magnetotactic bacteria, mollusks, arthropods, fish, birds, human brain, Ferritin (12.5 nm) Microparticles (<100 nm; activated cells)	Internal combustion engines Power plants Incinerators Jet engines Metal fumes (smelting, welding, etc.) Polymer fumes Other fumes Heated surfaces Frying, broiling, grilling Electric motors	Controlled size and shape, designed for functionality Metals, semiconductors, metal oxides, carbon, polymers Nanospheres, -wires, -needles, -tubes, -shells, -rings, -platelets Untreated, coated (nanotechnology applied to many products: cosmetics, medical, fabrics, electronics, optics, displays, etc.)

A lot of other features can be used to identify and classify NPs, such as composition, size, shape, superficial charge, and many others, that can modulate the NP interactions with the biological world[4, 26, 39-41].

Composition and structure

Four categories of NPs can be identified based on their composition[42]:

- Carbon-based: carbon is the main element constituting these NPs, being responsible for their peculiar chemical properties

and shapes (i.e hollow tubes, ellipsoids or spheres). Fullerenes, carbon nanotubes, carbon nanofibers, carbon black, graphene, and carbon onions are included under the carbon-based NMs category.

- Inorganic: these NPs include metal and metal oxide, like Au, Ag, TiO_2 and ZnO, and semiconductors such as silicon and ceramics.
- Organic-based: organic matter is the base for these NPs, from which are excluded carbon-based NPs since carbon in these NPs is just a part of a more complex and biologically inspired architecture. The utilization of noncovalent interactions for the design of molecules helps to transform the organic NMs into structures like dendrimers, micelles, liposomes and polymeric NPs.
- Composite-based: multiphase NPs with one phase on the nanoscale dimension that can either combine NPs with other NPs or NPs combined with larger or with bulk-type materials (e.g., hybrid nanofibers) or more complicated structures, such as a metalorganic framework. The composites may be any combinations of carbon-based, metal-based, or organic-based NPs with any form of metal, ceramic, or polymer bulk materials.

Size

NP size and surface area play a major role as determinants of the NP interaction with living systems[43-45]. Compared to the corresponding bulk materials, NPs are characterized by a very large specific surface area to volume ratio, which determines their high reactivity and catalytic activity. The NP sizes are suitable to interact directly with protein globules (2 to 10 nm), DNA helix (2 nm) and thickness of cell membranes (5 to 10 nm), which allows them to easily enter cells and cell organelles. The size of nanoparticles can be influenced by the tendency to form clusters in the solution[46, 47] and from the medium

characteristics[48]. In addition, the NP size largely determines how the NPs interact with the transport and defense systems of cells and the body, affecting their distribution and accumulation kinetics in the body. Larger NPs are recognized by specific defense systems of the body and absorbed by mononuclear phagocytes, which prevent them from entering other tissues, as well as it has been shown that particles 200 nm or larger tend to activate the lymphatic system and to be removed from circulation quicker[49]. Smaller particles are usually considered more effective drug carriers, potentiating the delivery across biological barriers to target tissues. NP for drug delivery may range from less than 10 nm to around 500 nm[50, 51], while for targeted drug delivery 100–200 nm NPs are preferred[52]. Size-dependent cellular uptake has been observed in different cell lines for diverse types of NP, including gold[53],[343], iron oxide[54], silica[55, 56], polystyrene NP[57, 58], QD[59], liposomes[40, 60] and polymeric NP[61, 62]. Nanoparticles can also cross the Blood Brain Barrier (BBB), providing sustained delivery of medication for diseases that were previously difficult to treat[63]. The optimum size for a nanoparticle to pass through the BBB is approximately 100 nm. At this size, immediate clearance by the lymphatic system is avoided and sufficient amount of drug can be delivered. Ultimately, NP size dictates how cell in the body ‘‘see” them and thus dictates their distribution, toxicity, and targeting ability.

PDI

With respect to particle size distribution characterization, a parameter used to define the size range of the NMs is called the “polydispersity index” (PDI). The term “polydispersity” (or “dispersity” as recommended by IUPAC) is used to describe the degree of non-uniformity of a size distribution of particles[4S, 5S]. Also known as the heterogeneity index, PDI is a number calculated from a two-parameter fit to the correlation data (the cumulants analysis). This index is

dimensionless and scaled such that values smaller than 0.05 are mainly seen with highly monodisperse standards. PDI values bigger than 0.7 indicate that the sample has a very broad particle size distribution. PDI is basically a representation of the distribution of size populations within a given sample. The numerical value of PDI ranges from 0.0 (for a perfectly uniform sample with respect to the particle size) to 1.0 (for a highly polydisperse sample with multiple particle size populations). Values of 0.2 and below are commonly deemed acceptable in practice for polymer-based nanoparticle materials.

Shape

The shape of the particles is also an important parameter that affects pathways by which particles enter the cells, lifespan and cycling time, targeting effect, ability to overcome biological barrier, because it is more likely to influence the particles in the blood transport, especially in small vessels and tumor vessels, and how cells perceive and respond[64-68]. In hydrodynamics, the shape plays an important role in the transport of particles in the fluid and is well recognized[69, 70],[344]. In particular, shape and shape correlation factors, such as aspect ratio or geometric structure, can affect the transport properties of particles and the interaction between the cells and the particles[71]. Moreover, particles shape is important for many different aspects, influencing drug delivery and tumor permeation[72], toxicity[73-78], interactions with the immune system[79-82], redox activity[83].

Surface charge and properties

The surface properties of NPs play an important role in determining the interactions of NPs with biological systems[84, 85] because are strictly involved in various biological performances of the nanoparticles[86-91] such as solubility, biodistribution, stability, cellular uptake, cytotoxicity. The experimental results of Tang and coworkers[92] showed that when the nanoparticles are dispersed in the culture medium, only positively

charged particles can be ingested by the cells. The cell membrane is negatively charged, sometimes with a small amount of positive charge of the patch; the positively charged particles are more easily adsorbed than negatively charged or neutral particles by cell membrane[93, 94].

If the particles are bound to proteins, the electrostatic difference between the positively and negatively charged particles can be eliminated.

Positively charged NPs have an enhanced capacity for opsonization, i.e., adsorption of proteins facilitating phagocytosis, including antibodies and complement components, from blood and biological fluids[95]. The adsorbed proteins, referred to as the protein corona, may affect the surface properties of NPs, aggregation characteristics and/or hydrodynamic diameter of NPs. In addition, adsorption of proteins on the NP surface leads to their conformational changes, which may decrease or completely inhibit the functional activities of the adsorbed proteins. Binding to NPs alters the protein structure, which leads to the loss of their enzymatic activity, disturbance of biological processes, and precipitation of ordered polymeric structures, e.g., amyloid fibrils[96]. This may lead to various diseases, such as amyloidosis. Thus, modification of the NP charge allows their localization and toxicity to be controlled, which could be used for developing effective systems for delivery of chemotherapeutic drugs to tumors.

Surface charge can be modified by functionalization, which can influence the interaction of cells with NPs. The surface electrostatic charges could be modified by grafting differently charged polymers. PEG (polyethylene glycol) or folic acid is often used to improve the NP intracellular uptake and ability to target specific cells[97],[98]. Other substances, such as methotrexate, polyethyleneimine, and dextran, had also been used to modify NP surfaces and their charge[345]. Xu and coworkers developed a method for changing the NP charge from negative to positive via various modifications of the surface[7].

Hydrophobicity is another crucial parameter in determining the interaction with cells. When NPs constituted of materials entirely hydrophobic or mainly composed by hydrophobic surfaces are exposed to an aqueous environment, their hydrophobic portions prefer to depart from water molecules by aggregating unsymmetrically with each other. Therefore, these hydrophobic exogenous ligands mimicking a danger signal act as an immunostimulatory alarm, being easily detected by specific surface receptors that trigger inflammation and generate an innate immune response[99]. NP surface hydrophobicity influence the uptake by APC[100] and increases opsonization by serum proteins causing higher uptake by APC and further clearance from circulation[101, 102].

Incorporation of appropriate targeting ligands, surface curvature and reactivity are among the most used modifications in nanoengineering. Coating the NP surface with polymers or surfactants like polyethylene glycol (PEG), polyethylene oxide, polyoxamer, poloxamine, and polysorbate 80 to neutralize the charge and increase the hydrophilicity of the NPs is one of the most used strategies to stabilize the particles, avoiding the recognition by the immune system[103-105],[346]. The coating of NP surface with natural cell membranes, such as red blood cells, is another approach to overcome the immune recognition and increase pharmacologically relevant characteristics of NPs without changing surface functional groups[106]. Other strategies that have also been reported are functionalization of NP surface with polysaccharides moieties, such as chitosan[107, 108] or mannose[109, 110], or addition of antibodies specific to DC receptors, such as anti-DEC205 or anti-CD40[111, 112].

Metal NPs

Metals constitute a large portion of periodic table and have a huge range of chemical activities, which controls their reactivity towards living

cells. Among inorganic NMs, metal and metal oxides NPs have thus attracted the interest of both basic and applied researches. These particles are considered promising multifunctional platforms, due to their peculiar photonic, electronic, magnetic, catalytic properties and for the resistance to corrosion and oxidation, non-reactiveness, high reduction potential, high melting point, high ionization energy and therapeutic properties, as well as for their versatile methods of synthesis and surface functionalization[347]. Due to these exceptional properties, metal NPs have been widely applied in fast moving fields like environmental remediation, water purification, antimicrobials and industries involved in manufacturing consumer goods such as cosmetic products, toothpaste, soaps, shampoos, detergents[113-115], [348]. The physico-chemical properties of metal and metal oxide NPs can be dictated by various attributes like size, shape, architecture, crystallinity and composition[116-118]. One of the characteristics that have great impact on biological applications of metal NPs is particles dissolution, which is defined as a dynamic process in which the molecules of a material moves from the surface of the NPs to the solution in which it is suspended[380]. In the case of metal and metal oxide NPs, the release of metal ions from particles is of much concern and it has been studied deeply[380-384]. Dissolution rate is dependent on various factors, from NPs physico-chemical properties (crystallinity, shape, size) to the characteristics of the dispersant medium (pH, ionic strength, presence of organic molecules[381]). The dissolution of the NPs should be assessed for each experimental condition applied, in order to determine its extent.

In the biomedical field, the most exploited metal-based NPs are silver (Ag), gold (Au) and iron (Fe) nanoparticles. Ag NPs are renowned for their biocide activity[41, 119, 120]. Au NPs, thanks to their photoactivation capability, inert character and biocompatibility, are efficiently used as therapeutic agents for cancer treatment, as medical tools for bioimaging

and biosensing[121, 122]. Iron NPs are already used successfully as imaging agents and are gaining more and more importance as drug delivery systems as therapeutic and theranostic compounds and in other medical applications[5, 36, 123-125].

In the industrial sector, Ag NPs are used in food packaging and to prolong the shelf-life of various products because of their antimicrobial properties[16, 116, 126]. Zinc oxide NPs (ZnO NPs), because of high photocatalytic efficiency, are widely employed in a variety of devices including cosmetics, toothpaste, sunscreens, fillings in medical materials, textiles, wall paints, and other building materials[349]. Titanium dioxide NPs (TiO_2 NPs), a common food additive and excipient used in nutraceuticals, pharmaceuticals and toothpaste[127-129]. However, their positive effects are constantly combined with the concern for the negative effects that these particles might have. Their interactions and effects are constantly under investigation, from controlling the environmental safety[130-135] to monitoring of the effects on human health in unintended exposure[11, 136-141].

Among metal NPs, nanostructures of iron, cobalt, and nickel are known to exhibit superparamagnetic properties and high magnetic susceptibility, as well as being relevant under the toxicological point of view. Here onward are reported some of their specific properties, applications and studies on possible toxic effects.

Iron-based NPs

Regarding elemental or zerovalent iron NPs (Fe NPs), they are widely used for the groundwater and soil remediation from pollutants[142], [350] as well as heavy metals[118, 143].

Iron oxide such as hematite (α-Fe_2O_3), maghemite (γ-Fe_2O_3) and magnetite (Fe_3O_4) are within the most studied magnetic nanoparticles. Their improved colloidal stability, biocompatibility, and magnetic properties persistence in comparison with other magnetic NMs make

them excellent candidates for biomedical applications[5, 144-146] ,[351], such as diagnostic imaging, cell labeling, site-directed drug delivery[124], anti-cancer hyperthermia therapy[125], gene delivery, tissue repair, cell separation, photothermal therapy[36] and magnetic resonance imaging[24, 25].

α-Fe_2O_3 (hematite) contains Fe^{3+} ions distributed at their octahedral sites. In the case of γ-Fe_2O_3 (maghemite), Fe^{3+} cations are distributed in octahedral and tetrahedral sites along with Fe^{2+} cation vacancies located at octahedral sites. Fe_3O_4 (magnetite) differ from other IONPs due to the presence of both Fe^{2+} and Fe^{3+} combinations, where divalent ions are organized at the octahedral sites and trivalent ions are split across the tetrahedral and octahedral sites.

Studies on their possible toxicity are systematically being conducted in many fields, from immunology to environmental sciences, to address possible problems arising from their extensive use[123, 133, 139, 147, 148].

Cobalt-based NPs

Recently, Co NPs are attractive for electromagnetic wave absorption applications such as development of wireless communications and high frequency circuit devices[352], as well as for recording media, magnetic sensors, magnetic memories, magnetic fluids, magnetic composites and catalysis[149, 150], [347], [353], [354]. Co NPs also have an intrinsic advantage in biomedical related fields, e.g., drug delivery and magnetic resonance imaging[151, 152], [355], where all these applications demand high quality and purity to avoid alteration in their magnetization or response stability. However, Co NPs aggregates are toxic on different cell lines. Toxicity is mainly due to Co ion dissolution from the Co NPs, and their effects in vivo need to be deeply investigated[153], [356].

Cobalt oxide (Co_3O_4) NPs are increasingly being used in applications like the production of pigments, sensors, in electrochemistry and in energy storage devices production[357], [358]; furthermore,

functionalization with biologically active molecules could open a path also for the exploitation of their great magnetic properties in biology[154, 155].

However, toxicity must always be considered, since cobalt is a heavy metal and can raise safety issues[25, 156, 157]. Co_3O_4 NPs can easily penetrate passing through wound, abrasions and damaged skin causing toxicity in human epidermis[359]. Under the occupational point of view, hard metal industry workers who are frequently exposed to NPs are reported to be more prone to lung cancer[158].

Nickel-based NPs

Nickel NPs (Ni NPs) find application in modern industry as catalysts, sensors and in electronics[159], [360]. Nickel oxide (NiO) NPs are utilized in various applications such as solar cells, catalysts, lithium-ion batteries, resistive RAM, light-emitting diodes, electrochemical sensors and biosensors[12, 160, 161].

However, their usage is creating concerns due to the potential risk associated to the toxicity of Ni-derived compounds that may be released from Ni NPs into the environment. The International Agency for Research on Cancer (IARC) has classified the Ni-derived compounds as "carcinogenic to humans" (Group 1) with genotoxic and mutagenic activities[162]. Ni NPs can induce lung epithelial and respiratory pathologies in human[163, 164], embryotoxicity in zebrafish and spermiotoxicity in *Ciona intestinalis*[74, 165]; NiO NPs were assessed to cause oxidative stress in different cellular models, and in vivo experiments when inhaled[166-168].

Protein Corona

To achieve a detailed understanding of NP interactions with cells, tissues, and organisms it must be taken into account that in the complex biological environment of living organisms, proteins and other

biomolecules in biological fluids (e.g., blood and lung-lining fluid) spontaneously form an adsorption layer on the NP surface, the so-called opsonization or biomolecular corona[169-174], [361] (Figure 2). The protein corona properties need to be known in detail because the adsorption layer is as much important as the NP surface in the interactions with the living organism and governs physiological responses, including cellular internalization, biodistribution, and toxicity[174-177]. Due to the high surface to volume ratios of nanomaterials, on the nanoscale the protein corona formation impact on NPs or the NP–biomolecule conjugates can heavy influence the characteristics of the nanomaterials. Many investigations have shown in detail how biomolecular adsorption can be influenced by NP properties[39, 44, 169, 172], [361].

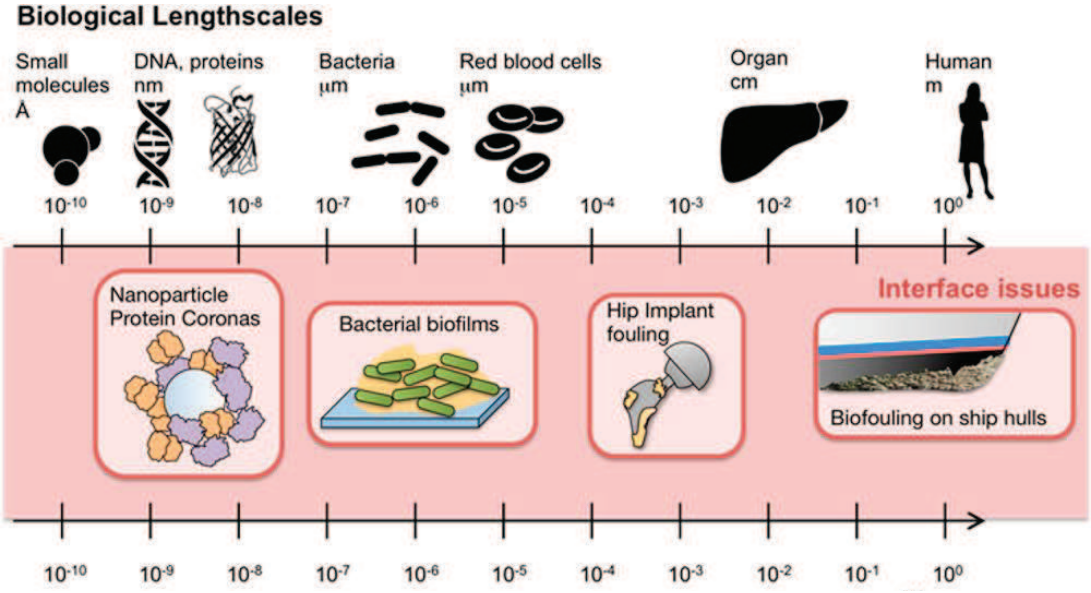

Figure 2: Biological Corona at different scales (modified from[173])

Common biological fluids are typically aqueous solutions with ions and biomolecule in high concentrations (typically hundreds of mM), which could interact with the surfaces of nanomaterials. Blood and serum are incredibly complex, with over thousands of different species of proteins at concentration greater than ~80 mg/mL, which is a completely

different environment from the organic solvents or gaseous phases in which nanomaterials are often produced.
Biofluids contain a vast number of different biomolecules, especially proteins, which may be considered as a "cloud" around the NP. Some will adsorb reversibly to the NP surface and form a monolayer. Adsorption may be accompanied by (partial) unfolding, which could expose hydrophobic moieties, that may adsorb further proteins as a second layer; polypeptide chains of globular proteins expose hydrophobic moieties and thus interact with the NP surface and other proteins in the biofluid in distinctly different ways than native proteins. NPs covered with unfolded proteins may undergo protein-mediated aggregation.

Nanotoxicology

Nanotoxicology - defined as "science of engineered nanodevices and nanostructures that deals with their effects in living organisms"[38] - is nowadays established as a key discipline in the "nano" world. Nanotoxicology research not only provides data for safety evaluation of engineered nanostructures and devices but also helps in advancing the field of nanomedicine, by providing information about their undesirable properties and means to avoid them, as well as dictating some regulatory passages in the approval of newly synthetized nanomaterials.

Toxicity

At a systemic level, many studies aim at assessing the toxicological outcomes of human exposure to NPs[1, 11, 136-141]. Many experiments are also being conducted, modelling the toxic effects of NPs on the body[178-181].

The increase in production, use, disposal of NPs and their waste treatment produces an environmental release of nanoparticulates, in

their original or modified forms[130-135]. The effect of this release needs to be considered and investigated.

However, it is the effects that NPs exert at the cellular level that mediates their toxic effects in organisms[1, 4]. A summary of the most common mechanisms of NP cytotoxicity are schematized in Figure 3:

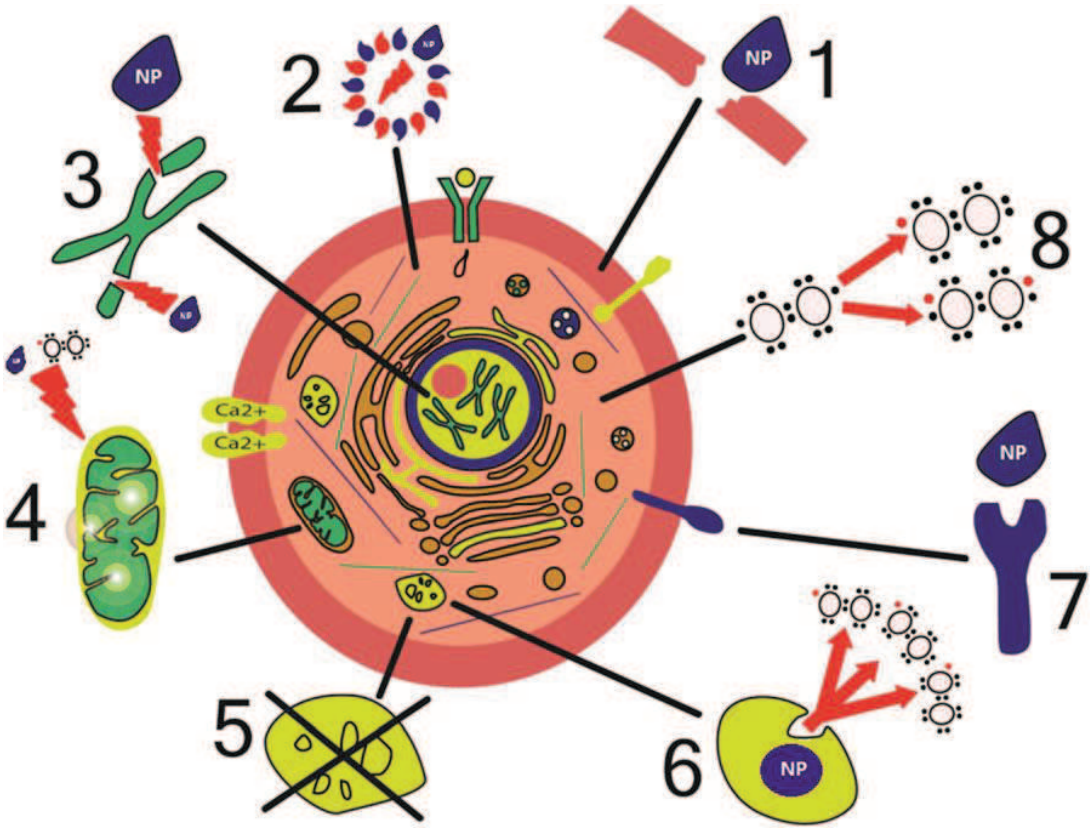

Figure 3: Main toxic effects of NPs on cells[4]

1. Cell membrane damage[182, 183], [362], [363]

2. Cytoskeleton damage[184-186]

3. Transcription disturbance and DNA damage[187-190], [364], [365]

4. Mitochondria damage and energetic metabolism imbalance[191-195]

5. Alterations of intracellular vescicles trafficking[196-198]

6. Oxidative stress induction[199-202], [364]

7. Interactions with membrane proteins, leading to membrane transport impairment or abnormal functionality[203-205]

8. Inflammatory mediators production[206-209]

Like for the NPs mechanism and activity inside the body and the interactions with cells, NP physical and chemical characteristics play a major role in causing their toxic effects[1, 3, 4, 39, 42]. According to toxicological data, the toxicity of NPs depends on various factors:

- **Dose and exposure time.** Dose is defined as the amount of a given substance that reaches the biological system; it is directly related to exposure, which is the concentration of substance in the medium (air, food or water) multiplied by the duration of contact. For NPs, rather than mass dose[38, 210, 211], toxic effects correlate better with nanoparticle surface area rather than mass dose [38, 212, 213].
- **Size, aggregation and concentration.** NPs show a size-dependent toxicity[1, 3, 4, 42]. Toxicological studies have demonstrated that small nanoparticles (<100 nm) cause adverse respiratory health effects, typically causing more inflammation than larger particles made from the same material[38, 211, 212, 214-216]. When particles smaller than 100 nm are compared, still-smaller particles are more toxic than larger ones[217, 218]. Aggregation state is strictly related to NP size, due to a more effective macrophage clearance for larger particles compared to smaller ones (that seem to easily evade this defence mechanism), leading to reduced toxicity of NP aggregates larger than 100–200 nm[38, 219]. Most aggregates are larger than 100 nm, a size that seems to be a threshold for many of the adverse health effects of small particles. A high concentration of nanoparticles would in the end can promote particle aggregation, and therefore reduce toxic effects compared to lower concentrations[214, 219, 220].

- **Surface area.** Typically, the toxicological effect of NPs increases with decreasing particle size and increasing surface area[1, 3, 42]. For the same mass of particles with the same chemical composition and crystalline structure, smaller nanoparticles have a larger specific surface area and particle number per unit mass, and thus more available surface area to interact with cellular components[221]. In some nanoparticles, toxicity was found to be a function of both size and surface area[200]. The higher surface area of nanoparticles causes a dose dependent increase in oxidation[211] and DNA damage[222] much higher than larger particles considering the same mass dose[38, 211, 216].
- **Particle shape.** NPs exhibit shape-dependent toxicity, that is, different toxicity levels at different aspect ratios (length/width)[3, 4, 39, 42, 73-78]. For example, it was found that lung cancer was associated with the presence of asbestos fibres (which are very studied for their interactions and toxicity on the biological matter) longer than 10 μm, mesothelioma with fibres longer than 5 μm, and asbestosis with fibres longer than 2 μm[223]. Long-aspect-ratio engineered nanoparticles, such as carbon nanotubes, have attracted a lot of attention due to their possible negative health effects[224-233]. Nanotubes are in general considered very toxic, inducing cell death at sufficiently high doses[233, 234], while low doses seem to be tolerated[231]. However, the multitude of morphological variants, sizes, and chemical functionalization of the surface or ends adds further complexity to the toxic effects comprehension. It is generally accepted that fibre-shaped NPs of a given material are more biologically active and toxic compared to spherical particles[235], [366].
- **Surface characteristics.** Particle surface plays a critical role in toxicity as it contacts cells and biological material and may affect the cellular uptake of particles as well as how the particles

interact with organelles and biomolecules[3, 4, 39, 236], [367]. Charged NPs tends to be more cytotoxic than their neutral forms[84], and positively charged ones act more cytotoxically than negative variants of similar sizes in nonphagocytic cells[56, 237-239], [368]. Hydrophobicity is another key-parameter and is often linked to surface charge, since NPs with hydrophobic surfaces are more cytotoxic than the respective noncoated NPs[240, 241]. Surface coatings can render noxious nontoxic NPs, while less harmful particles can be made highly toxic with the addition of active molecules on their surfaces[211, 222], [367] that leads to the creation of reactive oxygen species and the induction of inflammation.

- **Crystal structure.** Based on the crystal structure, NPs may exhibit different cellular uptake, oxidative mechanisms and subcellular localization[214, 242].

Particle Entrance Routes

The internal compartments of the body can come into contact with NPs through four main ways (Figure 4): the respiratory system[243-246], [369], the olfactory epithelium and nerves(Oberdorster 2003, messicani,), the gastrointestinal tract[247-251] and the cutaneous route[252], [370]. Nanostructures, once inhaled, ingested, or administered topically, can reach the bloodstream and be transported and accumulated at the level of various organs, exerting their effects on cells that are located there.
The interactions of NPs with biological systems, including their entrance into cells, play a key role in executing their functions and eventual toxicity. In fact, it is known that the NPs small size can easy penetrate into the cells and translocate among different cells, tissues and organs that are remote from the portal of entry to the body, ultimately representing a great risk to human health.

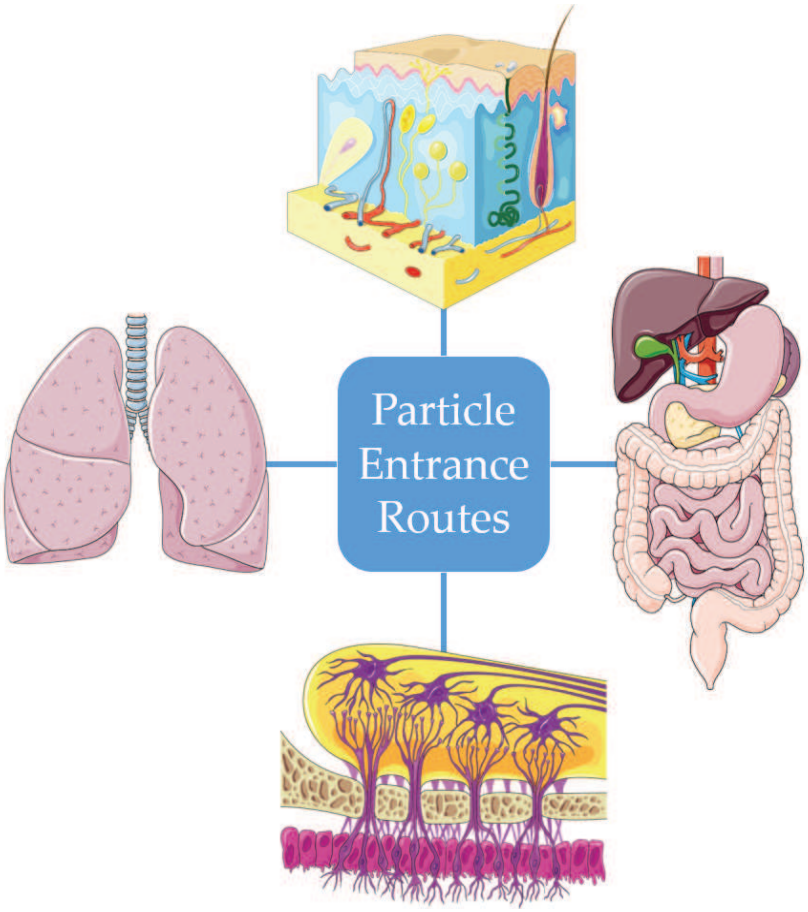

Figure 4: main NP entrance routes in the body

Systemic and tissue entrance routes

Airways are one of the main routes by which the human body comes into contact, voluntarily or accidentally, with NMs. The respiratory system consists of two parts: the upper respiratory tract, which includes the nasal cavity, the pharynx, and the larynx, and the lower respiratory tract, which includes the trachea, the bronchi and the lungs. Each bronchus is branched in small structures called bronchioles that terminate with the alveoli, where the gas exchange takes place. The particles, in general, are deposited in the whole respiratory tract, from the nasal cavity to the alveoli, through diffusional mechanisms[253].

Two possible internalization pathways, leading to different outcomes for the organism can take place in the airways: the absorption of the

particulate from the nasal mucosa that gives direct access to the brain and the deposition and accumulation in the lungs.

The nasal cavity can be divided into the respiratory region, from which the trigeminal nerve departs, and the olfactory region, from which the olfactory nerve departs[385, 386]. Along both these nerves, the movement of molecules and materials from the nasal cavity to the parenchyma of the brain occurs. The internalized materials are delivered to the origins of the nerves in the pons and cerebrum, respectively, dispersing freely throughout the brain. This process occurs via intracellular and extracellular pathways. The intracellular pathway starts with internalization of the material by an olfactory neuron, trafficking of the endocytic vesicle within the cell to the neuron's projection site, and finally release via exocytosis. The extracellular pathway begins with the material crossing the nasal epithelium to the lamina propria, before being transported externally along the length of the axon by bulk flow processes to the Central Nervous System. This internalization route has been studied extensively over the years, for its toxicological implications[137, 387-390] and recently for the possible exploitation for drug delivery bypassing the BBB[385, 386, 391, 392].

Concerning accumulation in the lungs[254, 255], the size distribution of NPs plays a major role in their ability to enter the human respiratory system. Larger particles, with a diameter between 5 and 30 μm, usually remain in the nasopharyngeal region, whereas smaller particles, with a size between 1 and 5 μm, tend to deposit in the tracheobronchial region. These inhaled materials are usually trapped in the respiratory mucus that lines the respiratory epithelium from the nose to the terminal bronchioles. NPs (0.1–1 μm) can reach the alveolar region, which is the deepest region of the respiratory system, by gravitational sedimentation and Brownian diffusion[371, 372]–**(6S)**. Overall, the size distribution of the particles markedly influences the possible target areas of the nanoparticles in the airways. Key-issues in particle deposition in the

lungs include the dynamic behaviour of particles in an aerosol, influencing the aerodynamic particle size through agglomeration or aggregation of primary particles. At the end, the particle size is crucial in determining how deep in the respiratory tract the particles can enter[255], [373]. The small NPs can thus settle and be absorbed, since the elimination mechanisms are not fast; many toxics effects can be generated because of the prolonged interaction with cells[374], as well as can be adsorbed by the pulmonary epithelium and reach the pulmonary interstitium, where they can subsequently be phagocytized by alveolar macrophages or enter the bloodstream directly or via the lymphatic pathway[136, 210, 255, 256], [373]. In conclusion, NP size is the main physicochemical property for the effects on the airways; smaller NPs are able to spread and accumulate in the deepest regions and trigger inflammations and ROS production[257-261].

Nanoparticles can also enter the human body via the gastrointestinal apparatus. It has a large surface area (200 m^2) and comprehends the mouth, the esophagus, the stomach, and the small and the large intestine and the anus, each with specific functions. This apparatus represents a mucosal barrier that selectively promotes the digestion and the absoption of nutrients. Humans can ingest directly a lot of food additives and supplements containing NPs[247, 262]. The gut route is thus potentially important for the absorption of NMs contained in consumer products[263], as well as for secondary ingestion of inhaled particles[264]. In general, the Gl tract undergoes the exposure of 'exogenous' and 'endogenous' NPs[265, 266].

Once in the gut, NPs may exert effects locally[262, 267]. For instance, the gut microbiota (the community of organisms living within the gastrointestinal tract) may have a relevant role in modulating both local and systemic biological effects of NPs[268]. NPs can also translocate into the bloodstream after crossing the GI mucosa by different routes and consequently access any organ[269].

Different chemical and physical conditions can be found along the GI, such as variations of the pH value[126] and of the pressure[270], that can influence heavily the NP characteristics and absorption.

The stomach is characterized by an acidic environment with an early-stage pH range of 1.2–2.0. When the bolus is formed, however, the pH reaches values of c.a. 5.0, followed by slow re-acidification[271]. The dissolution of NPs at a low pH promotes their further degradation in the digestive fluids.

Digestion and absorption processes are carried out by the small intestine that, at the duodenum, has a pH value between six and seven[247]. The enhancement of the absorptive surface is due to the presence of villi and enterocytes, and it is the absorption site of NPs. The major cell types in the small intestine are absorptive enterocytes, mucus secretory goblet cells and the immune sampling microfold cells (M-cells)[247, 272]. The M cells are associated with lymphocytes, immunoblasts, plasma cells and macrophages. Large NPs and microparticles can cross the intestinal epithelium through transcytosis by M-cell-uptake and persorption by M cells and the intestinal enterocytes. NPs can trigger oxidative stress, DNA damage and inflammations[273]. Moreover, NPs can cross the villi through the gaps formed in the apical zone due to a dysfunction process induced by NPs altering the morphology of the epithelium[274]. NPs paracellular uptake is a rare process but, in some disease, the tight junctions of cells can be altered, promoting the passage of NPs[247].

Another organ exposed to NPs is the skin, which is the largest organ of the body with a surface area of about 1.2–1.3 m^2 and a thickness less than 2 mm. It consists of three layers: the epidermis, dermis and hypodermis[275], [372]. The skin is a dynamic organ that has different functions, such as protection against external agents, UV protection and a selective permeable barrier. The topmost sub-layer of epidermis, *stratum corneum* poses a rate limiting barrier for diffusion[276-278]. The

dermis layer is composed of elastin and collagen fibers that provide mechanical support of skin. It is highly vascularized and permeable to solutes.

Nanomaterials contact with skin can lead to adverse consequences. Certain metals, such as nickel, are also known to cause dermatitis. Estimates of possible dermal exposure to manufactured NMs in the workplaces[158, 279], [359] have been reported. Furthermore, since 2006, NP-containing cosmetics have shown a large diffusion[280]. It has been estimated that cosmetic products contain TiO_2 NPs (70/80%), ZnO NPs (70%) and Ag NPs (20%)[375], [376]. However, the three layers of skin make it difficult for ionic molecules to penetrate through. Now, no clear evidence exists on the penetration of NM through intact or even damaged or inflamed skin into the systemic circulation[281]. It is probable that dermal exposure may lead to penetration of nanoparticles into the superficial layers of the skin, the dermis, causing there a local inflammatory reaction[158, 282], [359].

Cellular entrance routes

The design of new biological functions or the prediction of the toxicological consequences of NPs require the knowledge of their interplay, intended or incidental, with target cells. At the cellular level (Figure 5), NPs can enter into cells through endocytosis (which is the most widely described mechanism) and through direct penetration (which as enormous potential in terms of potential applications, as well as that should be monitored in terms of toxicological activity of the particles, but that has been documented for a limited number of cases). Physicochemical characteristics of NPs influence their internalization mechanism and biological barriers crossing[1, 283-285], [377]. Cell types also play a significant role, since each cell type might have different uptake mechanisms and can react differently to NPs[286, 287].

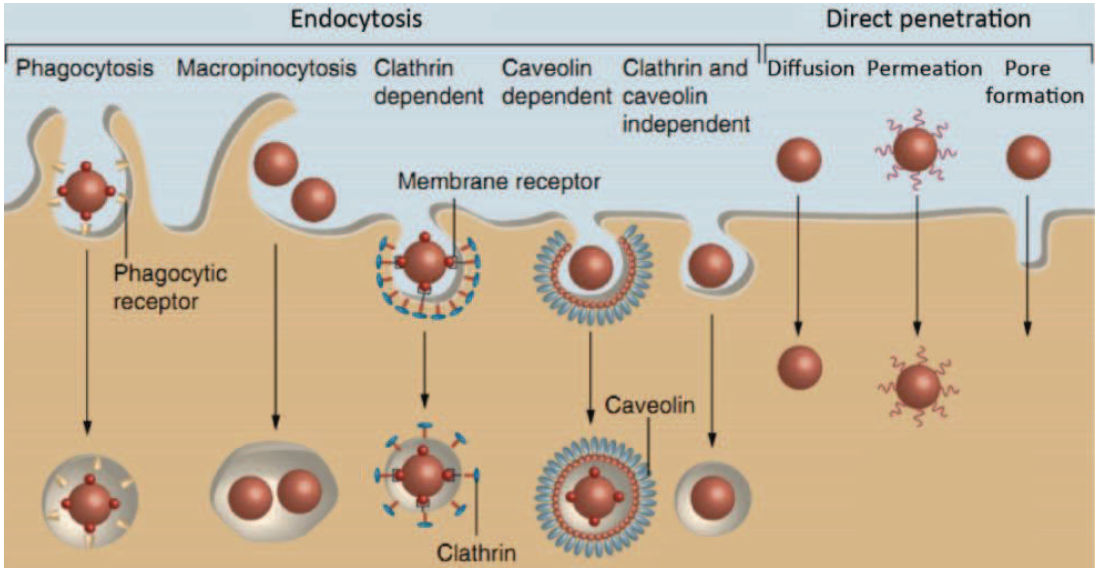

Figure 5: possible NP entrance routes in the cells[288]

Endocytosis route for NPs can be divided, according to the cellular machinery involved in the internalization processes, in phagocytosis, macropinocytosis, clathrin-mediated, caveolin-mediated, and non-clathrin and non-caveolin-mediated endocytosis[183, 288, 289]. All endocytic pathways lead to the internalization of the NPs in an intracellular vesicle. Depending on their physical properties and on the cell type, NPs can utilise all four of the endocytosis mechanisms to enter the cell. Phagocytosis is triggered in professional phagocytes (i.e., monocytes/macrophages, neutrophils, and dendritic cells) by the detection of opsonins adsorbed on the surface of the NPs, which leads to the polymerization of actin filaments at the site of ingestion and to the internalization within a vesicle, which is then transported to the lysosome for digestion, thereby forming the mature phagolysosome[210, 219, 242].

Pinocytosis (or macropinocytosis, for larger vesicle formation), is a non-specific route where the membrane invaginates (actin mediated process) and engulfs large volumes of extracellular milieu and then collapse and fuse with the plasma membrane to generate large endocytic vesicles called macropinosomes; is primarily used for the

uptake of fluids and other essential generic materials required for the cell such as salts, glucose, and amino acids[290-292].

Clathrin-mediated endocytosis is a form of receptor mediated endocytosis, which is in general very fast, occurs in all mammalian cells and carries out the continuous uptake of essential nutrients. The peptide clathrin, binds to the protein known as adaptor protein 2 which is bound to the receptor protein embedded in the inner membrane of the cell. The membrane bound clathrin molecules link with each other, forming a spherical cage and leading to the formation of a vesicle, which is subsequently released with the aid of dynamin (a GTPase that wraps itself around the vesicle neck and constricts, collapsing the neck and freeing the vesicle from the membrane) following the ligand binding[290, 293-299].

In caveolin dependent endocytosis, the protein caveolin integrates itself within the cholesterol rafts present in the membrane. This leads to the formation of caveolae, which are static, flask-shaped invaginations of the plasma membrane, whose release is dynamin-mediated. It is usually involved in the transport of serum proteins and its uptake rate is relatively slow[300-303].

However, increasing evidences are nowadays present, sustaining the hypothesis that NPs do not necessarily undertake the endocytosis process to enter a cell; this mechanism shall be treated in deeper details in the following subsection.

Direct Membrane Penetration

Understanding in more details the interactions occurring between NPs and the cellular membrane that lead to membrane direct crossing would be of extreme importance in establishing a new path to get access to the cell cytoplasm, opening new possibilities in the nanomedicine world. The endocytosed nanoparticles are confined in the endosome, and their "escape" is very complicated even with strategies developed ad hoc and

with low success rate; their overall functionality is thus limited to the endosome, with very low therapeutic efficacy. By directly penetrating the membrane, there will be no lipids coated on their surfaces and NPs will be free to exert their effect where they will be designed to. However, there is very limited information available on direct membrane crossing and on which NP characteristics dictate this mechanism, as well as on which characteristic of the cell or of the cell microenvironment could play a role in this. Studies reported that the intracellular localization of some nanomaterials may be related to alternative pathways for particles to enter cells[304-307].

First, it must be considered that the plasma membrane is a highly complex system, acting as a cellular barrier with selective permeability to maintain a homeostatic environment within the cell. The cell membrane consists of a self-assembled bilayer of a mixture of different lipids and proteins, it is responsive to external stimuli such as chemical and mechanical forces, electrical and thermal stresses, and it is responsible for communicating with other cell membranes and transducing signals inside. The proteins embedded in the membrane have different roles, these proteins included channels, receptors, transporters, and cellular adhesion molecules. To add further complexity, approaching the cell membrane the NPs will encounter a layer of negatively charged oligosaccharides (glycolipids and glycoproteins), which has several functions and also acts as receptor for macromolecule internalisation[308] or as a macromolecular repellent, further complicating the internalisation behaviour of NPs[309]. Cell membrane integral proteoglycans have been demonstrated to have a key role in binding of nanoparticle-sized lipoproteins[310], as well as lipopolysaccharide membrane components dramatically affect binding of amphiphilic macromolecules[311, 312], [378]. Charge inhomogeneity on the cell membrane surface adds even further complexity, with positively

charged NPs are believed to be attached to negatively charged areas[217, 313].

It is clear that NPs interact with a biological barrier of great complexity; hence, different mechanisms have been proposed to explain this phenomenon according to the difference that can be found in the membrane characteristics. The mechanisms described or hypothesized range from passive diffusion through membrane pores or specialized membrane transport protein channels[308, 314], to the occurring of van der Waals forces, electrostatic charges, steric interactions, physical interactions or interfacial tension effects leading to passive permeation[141, 304, 305], [379], to direct permeation through the cell membrane inserting into the hydrophobic membrane interiors and then leaving from the membrane[310, 311] and to the creation of nanometer-size pores on the membrane to translocate[312, 315], [378]. Different experimental approaches have been performed, to discriminate and identify among the particles properties some "guidelines", some indications of which are the most influent characteristics that dictate the membrane direct permeation.

Molecular dynamics computer simulation studies have been used to recreate through computational models the bio-nano interface and mimicking the hypothesized interactions[288]. This approach is very powerful and led to the identification of some conditions in which effective membrane penetration could be potentially achieved. These can be due to NPs charge[316-319], NPs surface properties[320]. Molecular dynamics study suggests different experimental conditions to monitor the NPs possible effects[316, 321-323]. Simulations are thus very useful, but their results need to be verified through practical experiments.

The use of artificial membranes and liposomes could address some of the issues related to membrane complexity. These tools may provide a membrane platform of controlled composition and with tuneable

properties, resulting suitable to focus mainly on the NPs-related characteristics.

Interesting results have been achieved using liposomes, supported lipid membranes or bilayer models and experimental techniques involving fluorescent probes, microscopy. Electrophysiology and the determination of physical characteristics of the membrane has been also applied.

Passive permeation was observed and related to particle charge, surface characteristics and chemical composition[324-328][379][329], or to particle size[305, 330], or to the combined effects of these parameters[315, 331, 332]. These studies are considered valuable to optimize engineered particles composition and surface characteristics but remain a simplification of a more complex situation (for example, considering protein role in the interactions in these models is impossible). The use of cells remains thus inevitable, to verify the simulations and in the vitro data and to test the real interactions occurring among membrane and NPs.

A wide range of approaches has been applied to determine the effects of membrane direct crossing in physiological conditions in cells. The experimental studies conducted focused on different aspects of cell-NP interactions, from the role of physicochemical parameters alone or in combination, such as charge, size and aggregation state[182, 305, 328, 333-336], and studying other possible mechanisms or issues[304, 337, 338]. Through fluorescent probes, the physiological parameters of the cells were monitored, to assess changes in cellular potential and membrane integrity, and by microscopy was verified the intracellular presence of the particles[334, 335] [304, 336]. A study from Chen and coworkers reported the direct effects of NP interactions on cell membranes by electrophysiology[333], highlighting that the access to the cytoplasm is paralleled by the formation of nanoscale defect, which could account for a pore.

However, it is not fully understood which chemical and physical properties of the cellular membrane and particles (or what combination of these properties) are responsible for the translocation of nanomaterials into the cells, the nucleus and organelles, either in vitro or in vivo, and the comprehension of this entrance route is far from being achieved. The complexity of the processes involved in nanomaterial uptake by cells and the complexity of the cell membranes make these interactions more difficult to study and to understand in real time.

In this scenario, we focused on a special kind of cell: the *Xenopus laevis* oocytes, to develop a platform for the screening of the effect of NPs on the membranes. These cells are suitable for study passive permeation mechanism for their resting state, where the endocytotic mechanism are extremely reduced in standard condition. Moreover, these cells are easy to maintain in saline solution giving, the possibility to test NPs in the absence of protein in the experimental medium (avoiding protein corona).

These cells could provide a useful tool, which can be used to work with fluorescent probes to monitor intracellular environment for the presence of a specific ions or for a change in cytoplasm condition such as pH or voltage. Electrophysiological techniques, and in particular two electrodes voltage clamp, in *Xenopus* oocytes allow to follow quite easily membrane modification such as endocytosis phenomena or the opening of specific and unspecific conductances. Furthermore, the use of these cells as heterologous expression system allows to study selected active transport phenomena by overexpressing the target membrane proteins, it is possible to achieve high signals from these cells and to easily detect the protein response to the various stimuli applied.

The passive diffusion mechanism, although occurring rarely, is by far the most interesting of the described mechanisms and increasing the knowledge about the particles properties and the cellular environment

implicated in this phenomenon would be of extreme importance for newly designed particles and therapies.

Outline of the project

This Ph.D. thesis is in the form of collection of papers. Each paper constitutes a single chapter, from 2 to 4. Chapter 5 is a complete set of experiments just concluded. This is the scientific production of the research work conducted during my three years as a Ph.D. student in the Laboratory of Cellular and Molecular Physiology (LFCM) at the Department of Biotechnology and Life Sciences of the University of Insubria, under the supervision of my tutor Prof. Elena Bossi. The research was conducted in collaboration with the Laboratory of Cellular Biology of Prof. Giovanni Bernardini and Prof. Rosalba Gornati.

Prof. Elena Bossi is an electrophysiologist with experience in the use of the *Xenopus laevis* oocytes as heterologous expression system. During the last 5 years the membrane transporters form *Dictyostelium discoideum*, NRAMP1 and 2, and the rat transporter (rDMT1) have been studied in the LFCM since they are involved in the iron transport and have become the starting point of my thesis. In the beginning of my work I have investigated the permeation of iron ions with the use of *Xenopus laevis* oocytes heterologously expressing rDMT1 and injected with calcein. Calcein is a fluorescent probe whose fluorescent signal is quenched by divalent metal ions.

After establishing the efficacy of the method for the detection of free intracellular divalent metal ions, I have tested calcein-injected oocytes in the presence of metal NPs provided from Prof. Bernardini research group. This was made to understand the metal NP related toxicity, which is usually associated with the presence of the realized ions inside the cytosol[154, 339]. The oocytes were not injected with any metal transporters and were exposed to NPs to verify the effect in the absence of permeation pathways for metal ions.

Testing oocytes with cobalt-based NPs (Co and Co_3O_4 NPs) showed a significant difference in the intracellular calcein fluorescence after exposure, since it was quenched by Co_3O_4 NPs but not by Co NPs. The

quenching was significantly different from that registered in control oocytes and was abolished when Co_3O_4 NPs were coated with BSA, pointing out a role of the NPs surface characteristics in causing the internalization. Endocytosis inhibitors did not alter the effect of the NPs exposure, suggesting that the entrance of metal and the consequent quenching could be due to a passive permeation mechanism followed by small intracellular dissolution of the NPs.

The aims of my work were to investigate and understand the mechanism of the metals entrance in the cell and to verify the passive permeation hypothesis.

These first findings were originally published in 2016 in the journal Scientific Reports as:

Cobalt oxide nanoparticles can enter inside the cells by crossing plasma membranes

Elena Bossi, Daniele Zanella, Rosalba Gornati and Giovanni Bernardini

Scientific Reports | 6:22254 | DOI: 10.1038/srep22254

The article is quoted in full in Chapter 2 of this thesis.

After this, I started to test different NPs with the fluorescence probe, to identify NPs behaving similarly or differently from Co or Co_3O_4 NPs and to link the effects with their physico-chemical properties.

I investigated if the NP passage through the membrane could be associated with modifications of membrane biophysical parameters; this method was suggested by a paper of Dr. Annalisa Bernareggi and Prof. Zabucchi from the University of Trieste, whose experimental activities on Asbestos fibers gave us some precious tips[340].

We began with iron-based NPs, namely Fe_3O_4 and Fe NPs, that are already used in medical and industrial applications. The fluorescence probe method allowed to verify that Fe_3O_4 NPs induced intracellular calcein quenching as a consequence of iron increase in the cytoplasm, while Fe NPs and Fe_3O_4@BSA NPs did not. Applying specifically

designed two electrode voltage clamp protocols, it was determined that the quenching is associated with modification of biophysical parameters like resistance, resting potential transmembrane current. Neither Fe NPs nor Fe_3O_4@BSA NPs altered these parameters.
Furthermore, these modifications occurred only in oocytes tested within 5 min from the addition of NPs and disappeared after 20 min. The characterization of the NPs properties and behaviour in experimental medium was conducted in collaboration with the Biomineral Research group of Prof. Jonathan J. Powell of the University of Cambridge. Particles were determined to be neutral, but a difference in sizes emerged, with a submicron population of Fe_3O_4 NPs delineating precisely and stable for 5 min, underlining that these smaller Fe_3O_4 particles could be responsible for the effect described.
Moreover, experiment conducted with aggregated particles (30 min standing time before application) demonstrated that when all Fe_3O_4 NPs were aggregated there were no modification in membrane permeability and in calcein intracellular fluorescence. BSA role in the modification NPs properties was also confirmed.
The combination of fluorescence approach, electrophysiology and physico-chemical characterizations gave a more precise picture, leading to the publication of one work in 2017 on the journal Scientific Reports as:

Iron oxide nanoparticles can cross plasma membranes
Daniele Zanella, Elena Bossi, Rosalba Gornati, Carlos Bastos, Nuno Faria and Giovanni Bernardini
Scientific Reports | 7: 11413 | DOI:10.1038/s41598-017-11535-z

The paper is quoted in Chapter 3 in full.
To check if what we have reported for Fe_3O_4 was true also for Co_3O_4 and to complete the panel of transition metal-based NPs, the two electrode voltage clap techniques was applied to nickel and cobalt-based NPs.

Co_3O_4 NPs resulted able to modify cell membrane biophysical parameters similarly to Fe_3O_4 NPs, while Co were not and the coating of BSA stabilized the particles against each other as well as towards the membrane, thereby preventing the membrane modifications.
Ni-based NPs on the other hand resulted ineffective both in fluorescence approach and in electrophysiology. However, in the case of NiO particles, a submicron population was present for the whole experiment length; this presence allowed us to narrow the size range we hypothesized to be implied in the membrane modifications, since from the comparison between Co_3O_4 (effective) and NiO (ineffective) we were able to notice that Co_3O_4 possess an unstable submicron population below 200 nm, while NiO never go below this threshold. Aggregation experiments again confirmed the importance of the population <200 nm Co_3O_4 in causing the described modifications in membrane biophysical parameters and calcein intracellular fluorescence.
These data have been collected in a new manuscript and submitted to the journal Nanotoxicology.

<u>The direct permeation of nanoparticles through the plasma membrane transiently modifies its properties</u>
Daniele Zanella, Elena Bossi, Rosalba Gornati, Nuno Faria, Jonathan J. Powell and Giovanni Bernardini

The article submitted form is quoted in Chapter 4
Chapter 5 is the synthesis of the work conducted on Fe_2O_3 NPs and on their surface coated form, modified covalently with the binding of APTES, an organosilane that could give to the particles a net positive charge. These particles are interesting for their magnetic properties, and understanding if they could undergo passive permeation entrance into cells would be of great interest.
Particles were synthesized by Dr. Ilaria Armenia of Prof. Bernardini group.

The data collected show that neither Fe_2O_3 NPs nor Fe_2O_3-APTES NPs were able to modify membrane and reduce intracellular calcein fluorescence. Their physico-chemical characterization demonstrated that Fe_2O_3 NPs were neutral and aggregated promptly after the addition in the experimental medium. Fe_2O_3-APTES NPs on the other hand had free amino groups on their surface, hence a positive charge was expected, but they resulted neutral; the coating operated a partial stabilization, with the presence of a population around 100 nm that however did not interact with cell membranes.

Chapter 6 provides a more integrated framework of the work conducted, highlighting for each particle type the finding related to membrane effect and the link to the physico-chemical properties, and some concluding remarks dealing with the passive permeation mechanism we have proposed.

Bibliography

1. Buzea, C., Pacheco, II, and K. Robbie, Nanomaterials and nanoparticles: sources and toxicity. Biointerphases, 2007. 2(4): p. MR17-71.
2. Pandey, R.K. and V.K. Prajapati, Molecular and immunological toxic effects of nanoparticles. Int J Biol Macromol, 2018. 107(Pt A): p. 1278-1293.
3. Huang, Y.W., M. Cambre, and H.J. Lee, The Toxicity of Nanoparticles Depends on Multiple Molecular and Physicochemical Mechanisms. Int J Mol Sci, 2017. 18(12).
4. Sukhanova, A., et al., Dependence of Nanoparticle Toxicity on Their Physical and Chemical Properties. Nanoscale Res Lett, 2018. 13(1): p. 44.
5. Vallabani, N.V.S. and S. Singh, Recent advances and future prospects of iron oxide nanoparticles in biomedicine and diagnostics. 3 Biotech, 2018. 8(6): p. 279.
6. Nasrollahzadeh, M., M. Bagherzadeh, and H. Karimi, Preparation, characterization and catalytic activity of CoFe2O4 nanoparticles as a magnetically recoverable catalyst for selective oxidation of benzyl alcohol to benzaldehyde and reduction of organic dyes. J Colloid Interface Sci, 2016. 465: p. 271-8.
7. Xu, P., et al., Targeted charge-reversal nanoparticles for nuclear drug delivery. Angew Chem Int Ed Engl, 2007. 46(26): p. 4999-5002.
8. Lohani, A., et al., Nanotechnology-based cosmeceuticals. ISRN Dermatol, 2014. 2014: p. 843687.
9. Tichota, D.M., et al., Design, characterization, and clinical evaluation of argan oil nanostructured lipid carriers to improve skin hydration. Int J Nanomedicine, 2014. 9: p. 3855-64.
10. Alarifi, S., D. Ali, and S. Alkahtani, Nanoalumina induces apoptosis by impairing antioxidant enzyme systems in human hepatocarcinoma cells. Int J Nanomedicine, 2015. 10: p. 3751-60.
11. Runa, S., M. Hussey, and C.K. Payne, Nanoparticle-Cell Interactions: Relevance for Public Health. J Phys Chem B, 2018. 122(3): p. 1009-1016.
12. Zhu, F.Q., et al., Magnetic bistability and controllable reversal of asymmetric ferromagnetic nanorings. Phys Rev Lett, 2006. 96(2): p. 027205.
13. Zhang, X., et al., A Magnetic Nanoparticle Based Enzyme-Linked Immunosorbent Assay for Sensitive Quantification of Zearalenone in Cereal and Feed Samples. Toxins (Basel), 2015. 7(10): p. 4216-31.
14. Burke, D.J., et al., Iron Oxide and Titanium Dioxide Nanoparticle Effects on Plant Performance and Root Associated Microbes. Int J Mol Sci, 2015. 16(10): p. 23630-50.
15. Pyrgiotakis, G., et al., Optimization of a nanotechnology based antimicrobial platform for food safety applications using Engineered Water Nanostructures (EWNS). Sci Rep, 2016. 6: p. 21073.
16. Sharma, C., et al., Nanotechnology: An Untapped Resource for Food Packaging. Front Microbiol, 2017. 8: p. 1735.
17. Bulbul, G., A. Hayat, and S. Andreescu, Portable Nanoparticle-Based Sensors for Food Safety Assessment. Sensors (Basel), 2015. 15(12): p. 30736-58.
18. Ju, Y., et al., Monodisperse Au-Fe2C Janus Nanoparticles: An Attractive Multifunctional Material for Triple-Modal Imaging-Guided Tumor Photothermal Therapy. ACS Nano, 2017. 11(9): p. 9239-9248.
19. Xie, J., et al., PET/NIRF/MRI triple functional iron oxide nanoparticles. Biomaterials, 2010. 31(11): p. 3016-22.
20. Chen, Z., et al., Dual enzyme-like activities of iron oxide nanoparticles and their implication for diminishing cytotoxicity. ACS Nano, 2012. 6(5): p. 4001-12.

21. Wu, Q., et al., Microgel coating of magnetic nanoparticles via bienzyme-mediated free-radical polymerization for colorimetric detection of glucose. Nanoscale, 2015. 7(40): p. 16578-82.
22. Yu, F., et al., The artificial peroxidase activity of magnetic iron oxide nanoparticles and its application to glucose detection. Biomaterials, 2009. 30(27): p. 4716-22.
23. Aye, M., et al., Genotoxic and mutagenic effects of lipid-coated CdSe/ZnS quantum dots. Mutat Res, 2013. 750(1-2): p. 129-38.
24. Mahmoudi, M., et al., A new approach for the in vitro identification of the cytotoxicity of superparamagnetic iron oxide nanoparticles. Colloids Surf B Biointerfaces, 2010. 75(1): p. 300-9.
25. Rajiv, S., et al., Comparative cytotoxicity and genotoxicity of cobalt (II, III) oxide, iron (III) oxide, silicon dioxide, and aluminum oxide nanoparticles on human lymphocytes in vitro. Hum Exp Toxicol, 2016. 35(2): p. 170-83.
26. Zhang, J., et al., Effects of major parameters of nanoparticles on their physical and chemical properties and recent application of nanodrug delivery system in targeted chemotherapy. Int J Nanomedicine, 2017. 12: p. 8483-8493.
27. Gao, J., et al., Liposome encapsulated of temozolomide for the treatment of glioma tumor: preparation, characterization and evaluation. Drug Discov Ther, 2015. 9(3): p. 205-12.
28. Liu, P., et al., Tf-PEG-PLL-PLGA nanoparticles enhanced chemosensitivity for hypoxia-responsive tumor cells. Onco Targets Ther, 2016. 9: p. 5049-59.
29. Li, Y.M., et al., Mercaptan acids modified amphiphilic copolymers for efficient loading and release of doxorubicin. Colloids Surf B Biointerfaces, 2017. 153: p. 220-228.
30. Shaarani, S., S.S. Hamid, and N.H. Mohd Kaus, The Influence of Pluronic F68 and F127 Nanocarrier on Physicochemical Properties, In vitro Release, and Antiproliferative Activity of Thymoquinone Drug. Pharmacognosy Res, 2017. 9(1): p. 12-20.
31. Mishra, B., B.B. Patel, and S. Tiwari, Colloidal nanocarriers: a review on formulation technology, types and applications toward targeted drug delivery. Nanomedicine, 2010. 6(1): p. 9-24.
32. Dong, X., et al., Simultaneous monitoring of the drug release and antitumor effect of a novel drug delivery system-MWCNTs/DOX/TC. Drug Deliv, 2017. 24(1): p. 143-151.
33. Biswas, N., Modified mesoporous silica nanoparticles for enhancing oral bioavailability and antihypertensive activity of poorly water soluble valsartan. Eur J Pharm Sci, 2017. 99: p. 152-160.
34. Hamzawy, M.A., et al., Antitumor activity of intratracheal inhalation of temozolomide (TMZ) loaded into gold nanoparticles and/or liposomes against urethane-induced lung cancer in BALB/c mice. Drug Deliv, 2017. 24(1): p. 599-607.
35. Yang, W., et al., Targeting cancer cells with biotin-dendrimer conjugates. Eur J Med Chem, 2009. 44(2): p. 862-8.
36. Estelrich, J. and M.A. Busquets, Iron Oxide Nanoparticles in Photothermal Therapy. Molecules, 2018. 23(7).
37. Ren, Y., et al., Multifunctional magnetic Fe3O4 nanoparticles combined with chemotherapy and hyperthermia to overcome multidrug resistance. Int J Nanomedicine, 2012. 7: p. 2261-9.
38. Oberdorster, G., E. Oberdorster, and J. Oberdorster, Nanotoxicology: an emerging discipline evolving from studies of ultrafine particles. Environ Health Perspect, 2005. 113(7): p. 823-39.
39. Albanese, A., P.S. Tang, and W.C. Chan, The effect of nanoparticle size, shape, and surface chemistry on biological systems. Annu Rev Biomed Eng, 2012. 14: p. 1-16.
40. Danaei, M., et al., Impact of Particle Size and Polydispersity Index on the Clinical Applications of Lipidic Nanocarrier Systems. Pharmaceutics, 2018. 10(2).

41. Pareek, V., R. Gupta, and J. Panwar, Do physico-chemical properties of silver nanoparticles decide their interaction with biological media and bactericidal action? A review. Mater Sci Eng C Mater Biol Appl, 2018. 90: p. 739-749.
42. Jeevanandam, J., et al., Review on nanoparticles and nanostructured materials: history, sources, toxicity and regulations. Beilstein J Nanotechnol, 2018. 9: p. 1050-1074.
43. Hoshyar, N., et al., The effect of nanoparticle size on in vivo pharmacokinetics and cellular interaction. Nanomedicine (Lond), 2016. 11(6): p. 673-92.
44. Shang, L., K. Nienhaus, and G.U. Nienhaus, Engineered nanoparticles interacting with cells: size matters. J Nanobiotechnology, 2014. 12: p. 5.
45. Gratton, S.E., et al., The effect of particle design on cellular internalization pathways. Proc Natl Acad Sci U S A, 2008. 105(33): p. 11613-8.
46. Benne, N., et al., Orchestrating immune responses: How size, shape and rigidity affect the immunogenicity of particulate vaccines. J Control Release, 2016. 234: p. 124-34.
47. Silva, A.L., et al., PLGA particulate delivery systems for subunit vaccines: Linking particle properties to immunogenicity. Hum Vaccin Immunother, 2016. 12(4): p. 1056-69.
48. Pfeiffer, C., et al., Interaction of colloidal nanoparticles with their local environment: the (ionic) nanoenvironment around nanoparticles is different from bulk and determines the physico-chemical properties of the nanoparticles. J R Soc Interface, 2014. 11(96): p. 20130931.
49. Prokop, A. and J.M. Davidson, Nanovehicular intracellular delivery systems. J Pharm Sci, 2008. 97(9): p. 3518-90.
50. Link, A., et al., Innate immunity mediates follicular transport of particulate but not soluble protein antigen. J Immunol, 2012. 188(8): p. 3724-33.
51. Manolova, V., et al., Nanoparticles target distinct dendritic cell populations according to their size. Eur J Immunol, 2008. 38(5): p. 1404-13.
52. Oyewumi, M.O., A. Kumar, and Z. Cui, Nano-microparticles as immune adjuvants: correlating particle sizes and the resultant immune responses. Expert Rev Vaccines, 2010. 9(9): p. 1095-107.
53. Wang, S.H., et al., Size-dependent endocytosis of gold nanoparticles studied by three-dimensional mapping of plasmonic scattering images. J Nanobiotechnology, 2010. 8: p. 33.
54. Huang, J., et al., Effects of nanoparticle size on cellular uptake and liver MRI with polyvinylpyrrolidone-coated iron oxide nanoparticles. ACS Nano, 2010. 4(12): p. 7151-60.
55. Lu, F., et al., Size effect on cell uptake in well-suspended, uniform mesoporous silica nanoparticles. Small, 2009. 5(12): p. 1408-13.
56. Oh, W.K., et al., Cellular uptake, cytotoxicity, and innate immune response of silica-titania hollow nanoparticles based on size and surface functionality. ACS Nano, 2010. 4(9): p. 5301-13.
57. Zauner, W., N.A. Farrow, and A.M. Haines, In vitro uptake of polystyrene microspheres: effect of particle size, cell line and cell density. J Control Release, 2001. 71(1): p. 39-51.
58. Varela, J.A., et al., Quantifying size-dependent interactions between fluorescently labeled polystyrene nanoparticles and mammalian cells. J Nanobiotechnology, 2012. 10: p. 39.
59. Osaki, F., et al., A quantum dot conjugated sugar ball and its cellular uptake. On the size effects of endocytosis in the subviral region. J Am Chem Soc, 2004. 126(21): p. 6520-1.
60. Chono, S., et al., Uptake characteristics of liposomes by rat alveolar macrophages: influence of particle size and surface mannose modification. J Pharm Pharmacol, 2007. 59(1): p. 75-80.
61. Foged, C., et al., Particle size and surface charge affect particle uptake by human dendritic cells in an in vitro model. Int J Pharm, 2005. 298(2): p. 315-22.

62. Cortez, C., et al., Influence of size, surface, cell line, and kinetic properties on the specific binding of A33 antigen-targeted multilayered particles and capsules to colorectal cancer cells. ACS Nano, 2007. 1(2): p. 93-102.
63. McMillan, J., E. Batrakova, and H.E. Gendelman, Cell delivery of therapeutic nanoparticles. Prog Mol Biol Transl Sci, 2011. 104: p. 563-601.
64. Bartczak, D., et al., Interactions of human endothelial cells with gold nanoparticles of different morphologies. Small, 2012. 8(1): p. 122-30.
65. Culver, K.S., et al., Shape-Dependent Relaxivity of Nanoparticle-Based T1 Magnetic Resonance Imaging Contrast Agents. J Phys Chem C Nanomater Interfaces, 2016. 120(38): p. 22103-22109.
66. Rampersaud, S., et al., The Effect of Cage Shape on Nanoparticle-Based Drug Carriers: Anticancer Drug Release and Efficacy via Receptor Blockade Using Dextran-Coated Iron Oxide Nanocages. Nano Lett, 2016. 16(12): p. 7357-7363.
67. Moghimi, S.M., A.C. Hunter, and J.C. Murray, Long-circulating and target-specific nanoparticles: theory to practice. Pharmacol Rev, 2001. 53(2): p. 283-318.
68. Chithrani, B.D. and W.C. Chan, Elucidating the mechanism of cellular uptake and removal of protein-coated gold nanoparticles of different sizes and shapes. Nano Lett, 2007. 7(6): p. 1542-50.
69. Lamprecht, A., U. Schafer, and C.M. Lehr, Size-dependent bioadhesion of micro- and nanoparticulate carriers to the inflamed colonic mucosa. Pharm Res, 2001. 18(6): p. 788-93.
70. Chatterjee, T., et al., Structure and function of Vibrio cholerae accessory cholera enterotoxin in presence of gold nanoparticles: Dependence on morphology. Biochim Biophys Acta Gen Subj, 2017. 1861(5 Pt A): p. 977-986.
71. Nishiyama, N., Nanomedicine: nanocarriers shape up for long life. Nat Nanotechnol, 2007. 2(4): p. 203-4.
72. Black, K.C., et al., Radioactive 198Au-doped nanostructures with different shapes for in vivo analyses of their biodistribution, tumor uptake, and intratumoral distribution. ACS Nano, 2014. 8(5): p. 4385-94.
73. Kong, B., et al., Experimental considerations on the cytotoxicity of nanoparticles. Nanomedicine (Lond), 2011. 6(5): p. 929-41.
74. Ispas, C., et al., Toxicity and developmental defects of different sizes and shape nickel nanoparticles in zebrafish. Environ Sci Technol, 2009. 43(16): p. 6349-56.
75. Favi, P.M., et al., Shape and surface effects on the cytotoxicity of nanoparticles: Gold nanospheres versus gold nanostars. J Biomed Mater Res A, 2015. 103(11): p. 3449-62.
76. Hamilton, R.F., et al., Particle length-dependent titanium dioxide nanomaterials toxicity and bioactivity. Part Fibre Toxicol, 2009. 6: p. 35.
77. Park, K.H., et al., Single-walled carbon nanotubes are a new class of ion channel blockers. J Biol Chem, 2003. 278(50): p. 50212-6.
78. Zhao, X., et al., Cytotoxicity of hydroxyapatite nanoparticles is shape and cell dependent. Arch Toxicol, 2013. 87(6): p. 1037-52.
79. Najafi-Hajivar, S., et al., Overview on experimental models of interactions between nanoparticles and the immune system. Biomed Pharmacother, 2016. 83: p. 1365-1378.
80. Getts, D.R., et al., Harnessing nanoparticles for immune modulation. Trends Immunol, 2015. 36(7): p. 419-27.
81. Mostaghaci, B., et al., Transfection system of amino-functionalized calcium phosphate nanoparticles: in vitro efficacy, biodegradability, and immunogenicity study. ACS Appl Mater Interfaces, 2015. 7(9): p. 5124-33.
82. Wibroe, P.P., et al., Bypassing adverse injection reactions to nanoparticles through shape modification and attachment to erythrocytes. Nat Nanotechnol, 2017. 12(6): p. 589-594.

83. Sun, B., et al., Engineering an effective immune adjuvant by designed control of shape and crystallinity of aluminum oxyhydroxide nanoparticles. ACS Nano, 2013. 7(12): p. 10834-49.
84. Schaeublin, N.M., et al., Surface charge of gold nanoparticles mediates mechanism of toxicity. Nanoscale, 2011. 3(2): p. 410-20.
85. El Badawy, A.M., et al., Surface charge-dependent toxicity of silver nanoparticles. Environ Sci Technol, 2011. 45(1): p. 283-7.
86. Peng, Y., et al., Impacts of interfacial charge transfer on nanoparticle electrocatalytic activity towards oxygen reduction. Phys Chem Chem Phys, 2017. 19(14): p. 9336-9348.
87. Mou, Y., et al., The Effect of Superparamagnetic Iron Oxide Nanoparticle Surface Charge on Antigen Cross-Presentation. Nanoscale Res Lett, 2017. 12(1): p. 52.
88. Bantz, C., et al., The surface properties of nanoparticles determine the agglomeration state and the size of the particles under physiological conditions. Beilstein J Nanotechnol, 2014. 5: p. 1774-1786.
89. Arvizo, R.R., et al., Effect of nanoparticle surface charge at the plasma membrane and beyond. Nano Lett, 2010. 10(7): p. 2543-8.
90. Liu, Y., et al., Intracellular dynamics of cationic and anionic polystyrene nanoparticles without direct interaction with mitotic spindle and chromosomes. Biomaterials, 2011. 32(32): p. 8291-303.
91. Frohlich, E., The role of surface charge in cellular uptake and cytotoxicity of medical nanoparticles. Int J Nanomedicine, 2012. 7: p. 5577-91.
92. Tang, J., et al., Preparation of optimized lipid-coated calcium phosphate nanoparticles for enhanced in vitro gene delivery to breast cancer cells. J Mater Chem B, 2015. 3(33): p. 6805-6812.
93. Holgate, S.T., Exposure, uptake, distribution and toxicity of nanomaterials in humans. J Biomed Nanotechnol, 2010. 6(1): p. 1-19.
94. Leonenko, Z., E. Finot, and M. Amrein, Adhesive interaction measured between AFM probe and lung epithelial type II cells. Ultramicroscopy, 2007. 107(10-11): p. 948-53.
95. Alexis, F., et al., Factors affecting the clearance and biodistribution of polymeric nanoparticles. Mol Pharm, 2008. 5(4): p. 505-15.
96. Sukhanova, A., et al., Implications of protein structure instability: from physiological to pathological secondary structure. Biopolymers, 2012. 97(8): p. 577-88.
97. Zhang, Y., N. Kohler, and M. Zhang, Surface modification of superparamagnetic magnetite nanoparticles and their intracellular uptake. Biomaterials, 2002. 23(7): p. 1553-61.
98. Cheyne, R.W., et al., Synthesis and characterisation of biologically compatible TiO2 nanoparticles. Nanoscale Res Lett, 2011. 6(1): p. 423.
99. Seong, S.Y. and P. Matzinger, Hydrophobicity: an ancient damage-associated molecular pattern that initiates innate immune responses. Nat Rev Immunol, 2004. 4(6): p. 469-78.
100. Verma, A. and F. Stellacci, Effect of surface properties on nanoparticle-cell interactions. Small, 2010. 6(1): p. 12-21.
101. Badiee, A., et al., Micro/nanoparticle adjuvants for antileishmanial vaccines: present and future trends. Vaccine, 2013. 31(5): p. 735-49.
102. Xu, J., et al., Functional characterization of bitter-taste receptors expressed in mammalian testis. Mol Hum Reprod, 2013. 19(1): p. 17-28.
103. Uner, M. and G. Yener, Importance of solid lipid nanoparticles (SLN) in various administration routes and future perspectives. Int J Nanomedicine, 2007. 2(3): p. 289-300.
104. Araujo, L., R. Lobenberg, and J. Kreuter, Influence of the surfactant concentration on the body distribution of nanoparticles. J Drug Target, 1999. 6(5): p. 373-85.
105. Labhasetwar, V., et al., Arterial uptake of biodegradable nanoparticles: effect of surface modifications. J Pharm Sci, 1998. 87(10): p. 1229-34.

106. Chambers, E. and S. Mitragotri, Long circulating nanoparticles via adhesion on red blood cells: mechanism and extended circulation. Exp Biol Med (Maywood), 2007. 232(7): p. 958-66.
107. Chellat, F., et al., Metalloproteinase and cytokine production by THP-1 macrophages following exposure to chitosan-DNA nanoparticles. Biomaterials, 2005. 26(9): p. 961-70.
108. Shi, S.F., et al., Biocompatibility of chitosan-coated iron oxide nanoparticles with osteoblast cells. Int J Nanomedicine, 2012. 7: p. 5593-602.
109. Silva, J.M., et al., Development of functionalized nanoparticles for vaccine delivery to dendritic cells: a mechanistic approach. Nanomedicine (Lond), 2014. 9(17): p. 2639-56.
110. Carrillo-Conde, B., et al., Mannose-functionalized "pathogen-like" polyanhydride nanoparticles target C-type lectin receptors on dendritic cells. Mol Pharm, 2011. 8(5): p. 1877-86.
111. Macho-Fernandez, E., et al., Targeted delivery of alpha-galactosylceramide to CD8alpha+ dendritic cells optimizes type I NKT cell-based antitumor responses. J Immunol, 2014. 193(2): p. 961-9.
112. Cruz, L.J., et al., Targeting nanoparticles to CD40, DEC-205 or CD11c molecules on dendritic cells for efficient CD8(+) T cell response: a comparative study. J Control Release, 2014. 192: p. 209-18.
113. Hajipour, M.J., et al., Antibacterial properties of nanoparticles. Trends Biotechnol, 2012. 30(10): p. 499-511.
114. Lemire, J.A., J.J. Harrison, and R.J. Turner, Antimicrobial activity of metals: mechanisms, molecular targets and applications. Nat Rev Microbiol, 2013. 11(6): p. 371-84.
115. Wu, M.C., et al., Nitrogen-doped anatase nanofibers decorated with noble metal nanoparticles for photocatalytic production of hydrogen. ACS Nano, 2011. 5(6): p. 5025-30.
116. Li, J., et al., Engineering noble metal nanomaterials for environmental applications. Nanoscale, 2015. 7(17): p. 7502-19.
117. Teske, S.S. and C.S. Detweiler, The biomechanisms of metal and metal-oxide nanoparticles' interactions with cells. Int J Environ Res Public Health, 2015. 12(2): p. 1112-34.
118. Wang, P., et al., Nanotechnology: A New Opportunity in Plant Sciences. Trends Plant Sci, 2016. 21(8): p. 699-712.
119. Slavin, Y.N., et al., Metal nanoparticles: understanding the mechanisms behind antibacterial activity. J Nanobiotechnology, 2017. 15(1): p. 65.
120. Malekkhaiat Haffner, S. and M. Malmsten, Membrane interactions and antimicrobial effects of inorganic nanoparticles. Adv Colloid Interface Sci, 2017. 248: p. 105-128.
121. Popescu, R.C. and A.M. Grumezescu, Metal based frameworks for drug delivery systems. Curr Top Med Chem, 2015. 15(15): p. 1532-42.
122. McQuaid, H.N., et al., Imaging and radiation effects of gold nanoparticles in tumour cells. Sci Rep, 2016. 6: p. 19442.
123. Arias, L.S., et al., Iron Oxide Nanoparticles for Biomedical Applications: A Perspective on Synthesis, Drugs, Antimicrobial Activity, and Toxicity. Antibiotics (Basel), 2018. 7(2).
124. Shen, L., B. Li, and Y. Qiao, Fe(3)O(4) Nanoparticles in Targeted Drug/Gene Delivery Systems. Materials (Basel), 2018. 11(2).
125. Saeed, M., W. Ren, and A. Wu, Therapeutic applications of iron oxide based nanoparticles in cancer: basic concepts and recent advances. Biomater Sci, 2018. 6(4): p. 708-725.
126. Frohlich, E.E. and E. Frohlich, Cytotoxicity of Nanoparticles Contained in Food on Intestinal Cells and the Gut Microbiota. Int J Mol Sci, 2016. 17(4): p. 509.
127. Schulte, P.A., et al., Assessing the protection of the nanomaterial workforce. Nanotoxicology, 2016. 10(7): p. 1013-9.

128. Pele, L.C., et al., Pharmaceutical/food grade titanium dioxide particles are absorbed into the bloodstream of human volunteers. Part Fibre Toxicol, 2015. 12: p. 26.
129. Tomankova, K., et al., Reprint of: Cytotoxicity, cell uptake and microscopic analysis of titanium dioxide and silver nanoparticles in vitro. Food Chem Toxicol, 2015. 85: p. 20-30.
130. Amde, M., et al., Transformation and bioavailability of metal oxide nanoparticles in aquatic and terrestrial environments. A review. Environ Pollut, 2017. 230: p. 250-267.
131. Bundschuh, M., et al., Nanoparticles in the environment: where do we come from, where do we go to? Environ Sci Eur, 2018. 30(1): p. 6.
132. Hou, J., et al., Toxic effects of different types of zinc oxide nanoparticles on algae, plants, invertebrates, vertebrates and microorganisms. Chemosphere, 2018. 193: p. 852-860.
133. Lei, C., et al., Environmental transformations and ecological effects of iron-based nanoparticles. Environ Pollut, 2018. 232: p. 10-30.
134. Bhuvaneshwari, M., et al., Toxicity, accumulation, and trophic transfer of chemically and biologically synthesized nano zero valent iron in a two species freshwater food chain. Aquat Toxicol, 2017. 183: p. 63-75.
135. Rastogi, A., et al., Impact of Metal and Metal Oxide Nanoparticles on Plant: A Critical Review. Front Chem, 2017. 5: p. 78.
136. Pietroiusti, A., et al., Nanomaterial exposure, toxicity, and impact on human health. Wiley Interdiscip Rev Nanomed Nanobiotechnol, 2018.
137. Maher, B.A., et al., Magnetite pollution nanoparticles in the human brain. Proc Natl Acad Sci U S A, 2016. 113(39): p. 10797-801.
138. De Matteis, V., Exposure to Inorganic Nanoparticles: Routes of Entry, Immune Response, Biodistribution and In Vitro/In Vivo Toxicity Evaluation. Toxics, 2017. 5(4).
139. Kornberg, T.G., et al., Potential Toxicity and Underlying Mechanisms Associated with Pulmonary Exposure to Iron Oxide Nanoparticles: Conflicting Literature and Unclear Risk. Nanomaterials (Basel), 2017. 7(10).
140. Frohlich, E. and E. Roblegg, Oral uptake of nanoparticles: human relevance and the role of in vitro systems. Arch Toxicol, 2016. 90(10): p. 2297-314.
141. Peters, A., et al., Translocation and potential neurological effects of fine and ultrafine particles a critical update. Part Fibre Toxicol, 2006. 3: p. 13.
142. Cundy, A.B., L. Hopkinson, and R.L. Whitby, Use of iron-based technologies in contaminated land and groundwater remediation: a review. Sci Total Environ, 2008. 400(1-3): p. 42-51.
143. Liu, T.Y., et al., Effects of physicochemical factors on Cr(VI) removal from leachate by zero-valent iron and alpha-Fe(2)O(3) nanoparticles. Water Sci Technol, 2010. 61(11): p. 2759-67.
144. Huang, D.M., et al., The promotion of human mesenchymal stem cell proliferation by superparamagnetic iron oxide nanoparticles. Biomaterials, 2009. 30(22): p. 3645-51.
145. Martinkova, P., et al., Iron Oxide Nanoparticles: Innovative Tool in Cancer Diagnosis and Therapy. Adv Healthc Mater, 2018. 7(5).
146. Wu, W., et al., Recent progress on magnetic iron oxide nanoparticles: synthesis, surface functional strategies and biomedical applications. Sci Technol Adv Mater, 2015. 16(2): p. 023501.
147. Patil, R.M., et al., Comprehensive cytotoxicity studies of superparamagnetic iron oxide nanoparticles. Biochem Biophys Rep, 2018. 13: p. 63-72.
148. Shah, A. and M.A. Dobrovolskaia, Immunological effects of iron oxide nanoparticles and iron-based complex drug formulations: Therapeutic benefits, toxicity, mechanistic insights, and translational considerations. Nanomedicine, 2018. 14(3): p. 977-990.
149. Puntes, V.F., K.M. Krishnan, and A.P. Alivisatos, Colloidal nanocrystal shape and size control: the case of cobalt. Science, 2001. 291(5511): p. 2115-7.

150. Dumestre, F., et al., Shape control of thermodynamically stable cobalt nanorods through organometallic chemistry. Angew Chem Int Ed Engl, 2002. 41(22): p. 4286-9.
151. Bouchard, L.S., et al., Picomolar sensitivity MRI and photoacoustic imaging of cobalt nanoparticles. Proc Natl Acad Sci U S A, 2009. 106(11): p. 4085-9.
152. Lacroix, L.M., et al., New generation of magnetic and luminescent nanoparticles for in vivo real-time imaging. Interface Focus, 2013. 3(3): p. 20120103.
153. Horev-Azaria, L., et al., Predictive toxicology of cobalt nanoparticles and ions: comparative in vitro study of different cellular models using methods of knowledge discovery from data. Toxicol Sci, 2011. 122(2): p. 489-501.
154. Papis, E., et al., Engineered cobalt oxide nanoparticles readily enter cells. Toxicol Lett, 2009. 189(3): p. 253-9.
155. Vismara, E., et al., Non-covalent synthesis of metal oxide nanoparticle-heparin hybrid systems: a new approach to bioactive nanoparticles. Int J Mol Sci, 2013. 14(7): p. 13463-81.
156. Bava, A., et al., Heparin and carboxymethylchitosan metal nanoparticles: an evaluation of their cytotoxicity. Biomed Res Int, 2013. 2013: p. 314091.
157. Ortega, R., et al., Low-solubility particles and a Trojan-horse type mechanism of toxicity: the case of cobalt oxide on human lung cells. Part Fibre Toxicol, 2014. 11: p. 14.
158. Murray, A.R., et al., Oxidative stress and dermal toxicity of iron oxide nanoparticles in vitro. Cell Biochem Biophys, 2013. 67(2): p. 461-76.
159. Wessells, C.D., et al., Nickel hexacyanoferrate nanoparticle electrodes for aqueous sodium and potassium ion batteries. Nano Lett, 2011. 11(12): p. 5421-5.
160. Salimi, A., et al., Direct electrochemistry and electrocatalytic activity of catalase immobilized onto electrodeposited nano-scale islands of nickel oxide. Biophys Chem, 2007. 125(2-3): p. 540-8.
161. Rao, K.V. and C.S. Sunandana, Effect of fuel to oxidizer ratio on the structure, micro structure and EPR of combustion synthesized NiO nanoparticles. J Nanosci Nanotechnol, 2008. 8(8): p. 4247-53.
162. Kasprzak, K.S., F.W. Sunderman, Jr., and K. Salnikow, Nickel carcinogenesis. Mutat Res, 2003. 533(1-2): p. 67-97.
163. Ahamed, M., Toxic response of nickel nanoparticles in human lung epithelial A549 cells. Toxicol In Vitro, 2011. 25(4): p. 930-6.
164. Phillips, J.I., et al., Pulmonary and systemic toxicity following exposure to nickel nanoparticles. Am J Ind Med, 2010. 53(8): p. 763-7.
165. Gallo, A., et al., Spermiotoxicity of nickel nanoparticles in the marine invertebrate Ciona intestinalis (ascidians). Nanotoxicology, 2016. 10(8): p. 1096-104.
166. Ahamed, M., et al., Nickel oxide nanoparticles exert cytotoxicity via oxidative stress and induce apoptotic response in human liver cells (HepG2). Chemosphere, 2013. 93(10): p. 2514-22.
167. Horie, M., et al., Evaluation of acute oxidative stress induced by NiO nanoparticles in vivo and in vitro. J Occup Health, 2011. 53(2): p. 64-74.
168. Horie, M., et al., Comparison of the Pulmonary Oxidative Stress Caused by Intratracheal Instillation and Inhalation of NiO Nanoparticles when Equivalent Amounts of NiO Are Retained in the Lung. Antioxidants (Basel), 2016. 5(1).
169. Docter, D., et al., The nanoparticle biomolecule corona: lessons learned - challenge accepted? Chem Soc Rev, 2015. 44(17): p. 6094-121.
170. Cedervall, T., et al., Understanding the nanoparticle-protein corona using methods to quantify exchange rates and affinities of proteins for nanoparticles. Proc Natl Acad Sci U S A, 2007. 104(7): p. 2050-5.
171. Treuel, L., X. Jiang, and G.U. Nienhaus, New views on cellular uptake and trafficking of manufactured nanoparticles. J R Soc Interface, 2013. 10(82): p. 20120939.

172. Lane, L.A., et al., Physical chemistry of nanomedicine: understanding the complex behaviors of nanoparticles in vivo. Annu Rev Phys Chem, 2015. 66: p. 521-47.
173. Rodriguez-Quijada, C., et al., Physical Properties of Biomolecules at the Nanomaterial Interface. J Phys Chem B, 2018. 122(11): p. 2827-2840.
174. Barbero, F., et al., Formation of the Protein Corona: The Interface between Nanoparticles and the Immune System. Semin Immunol, 2017. 34: p. 52-60.
175. Lesniak, A., et al., Effects of the presence or absence of a protein corona on silica nanoparticle uptake and impact on cells. ACS Nano, 2012. 6(7): p. 5845-57.
176. Duran, N., et al., Silver nanoparticle protein corona and toxicity: a mini-review. J Nanobiotechnology, 2015. 13: p. 55.
177. Walczyk, D., et al., What the cell "sees" in bionanoscience. J Am Chem Soc, 2010. 132(16): p. 5761-8.
178. Radomski, A., et al., Nanoparticle-induced platelet aggregation and vascular thrombosis. Br J Pharmacol, 2005. 146(6): p. 882-93.
179. Madl, A.K., et al., Nanoparticles, lung injury, and the role of oxidant stress. Annu Rev Physiol, 2014. 76: p. 447-65.
180. Lucchini, R.G., et al., Neurological impacts from inhalation of pollutants and the nose-brain connection. Neurotoxicology, 2012. 33(4): p. 838-41.
181. Zhu, M.T., et al., Particokinetics and extrapulmonary translocation of intratracheally instilled ferric oxide nanoparticles in rats and the potential health risk assessment. Toxicol Sci, 2009. 107(2): p. 342-51.
182. Ruenraroengsak, P., et al., Respiratory epithelial cytotoxicity and membrane damage (holes) caused by amine-modified nanoparticles. Nanotoxicology, 2012. 6(1): p. 94-108.
183. Zhao, F., et al., Cellular uptake, intracellular trafficking, and cytotoxicity of nanomaterials. Small, 2011. 7(10): p. 1322-37.
184. Mao, Z., et al., Titanium dioxide nanoparticles alter cellular morphology via disturbing the microtubule dynamics. Nanoscale, 2015. 7(18): p. 8466-75.
185. Wu, X., et al., Toxic effects of iron oxide nanoparticles on human umbilical vein endothelial cells. Int J Nanomedicine, 2010. 5: p. 385-99.
186. Gheshlaghi, Z.N., et al., Toxicity and interaction of titanium dioxide nanoparticles with microtubule protein. Acta Biochim Biophys Sin (Shanghai), 2008. 40(9): p. 777-82.
187. Schmid, G., The relevance of shape and size of Au55 clusters. Chem Soc Rev, 2008. 37(9): p. 1909-30.
188. Zinchenko, A.A., F. Luckel, and K. Yoshikawa, Transcription of giant DNA complexed with cationic nanoparticles as a simple model of chromatin. Biophys J, 2007. 92(4): p. 1318-25.
189. Chen, M. and A. von Mikecz, Formation of nucleoplasmic protein aggregates impairs nuclear function in response to SiO2 nanoparticles. Exp Cell Res, 2005. 305(1): p. 51-62.
190. Li, N., et al., Interaction Between Nano-Anatase TiO(2) and Liver DNA from Mice In Vivo. Nanoscale Res Lett, 2009. 5(1): p. 108-115.
191. Nguyen, K.C., et al., Mitochondrial Toxicity of Cadmium Telluride Quantum Dot Nanoparticles in Mammalian Hepatocytes. Toxicol Sci, 2015. 146(1): p. 31-42.
192. Freyre-Fonseca, V., et al., Titanium dioxide nanoparticles impair lung mitochondrial function. Toxicol Lett, 2011. 202(2): p. 111-9.
193. Teodoro, J.S., et al., Assessment of the toxicity of silver nanoparticles in vitro: a mitochondrial perspective. Toxicol In Vitro, 2011. 25(3): p. 664-70.
194. AshaRani, P.V., et al., Cytotoxicity and genotoxicity of silver nanoparticles in human cells. ACS Nano, 2009. 3(2): p. 279-90.
195. Piao, M.J., et al., Silver nanoparticles induce oxidative cell damage in human liver cells through inhibition of reduced glutathione and induction of mitochondria-involved apoptosis. Toxicol Lett, 2011. 201(1): p. 92-100.

196. Puppi, J., et al., Use of a clinically approved iron oxide MRI contrast agent to label human hepatocytes. Cell Transplant, 2011. 20(6): p. 963-75.
197. Vercauteren, D., et al., Dynamic colocalization microscopy to characterize intracellular trafficking of nanomedicines. ACS Nano, 2011. 5(10): p. 7874-84.
198. Asati, A., et al., Surface-charge-dependent cell localization and cytotoxicity of cerium oxide nanoparticles. ACS Nano, 2010. 4(9): p. 5321-31.
199. Sabella, S., et al., A general mechanism for intracellular toxicity of metal-containing nanoparticles. Nanoscale, 2014. 6(12): p. 7052-61.
200. Jiang, W., et al., Nanoparticle-mediated cellular response is size-dependent. Nat Nanotechnol, 2008. 3(3): p. 145-50.
201. Singh, B.R., et al., ROS-mediated apoptotic cell death in prostate cancer LNCaP cells induced by biosurfactant stabilized CdS quantum dots. Biomaterials, 2012. 33(23): p. 5753-67.
202. Ambrosone, A., et al., Mechanisms underlying toxicity induced by CdTe quantum dots determined in an invertebrate model organism. Biomaterials, 2012. 33(7): p. 1991-2000.
203. Peuschel, H., et al., c-Src-mediated activation of Erk1/2 is a reaction of epithelial cells to carbon nanoparticle treatment and may be a target for a molecular preventive strategy. Biol Chem, 2010. 391(11): p. 1327-32.
204. Brown, D.M., et al., The effects of PM10 particles and oxidative stress on macrophages and lung epithelial cells: modulating effects of calcium-signaling antagonists. Am J Physiol Lung Cell Mol Physiol, 2007. 292(6): p. L1444-51.
205. Sydlik, U., et al., Ultrafine carbon particles induce apoptosis and proliferation in rat lung epithelial cells via specific signaling pathways both using EGF-R. Am J Physiol Lung Cell Mol Physiol, 2006. 291(4): p. L725-33.
206. Kostura, L., et al., Feridex labeling of mesenchymal stem cells inhibits chondrogenesis but not adipogenesis or osteogenesis. NMR Biomed, 2004. 17(7): p. 513-7.
207. Chen, Y.C., et al., The inhibitory effect of superparamagnetic iron oxide nanoparticle (Ferucarbotran) on osteogenic differentiation and its signaling mechanism in human mesenchymal stem cells. Toxicol Appl Pharmacol, 2010. 245(2): p. 272-9.
208. Choi, S.J., J.M. Oh, and J.H. Choy, Toxicological effects of inorganic nanoparticles on human lung cancer A549 cells. J Inorg Biochem, 2009. 103(3): p. 463-71.
209. Park, E.J. and K. Park, Oxidative stress and pro-inflammatory responses induced by silica nanoparticles in vivo and in vitro. Toxicol Lett, 2009. 184(1): p. 18-25.
210. Hoet, P.H., I. Bruske-Hohlfeld, and O.V. Salata, Nanoparticles - known and unknown health risks. J Nanobiotechnology, 2004. 2(1): p. 12.
211. Donaldson, K. and V. Stone, Current hypotheses on the mechanisms of toxicity of ultrafine particles. Ann Ist Super Sanita, 2003. 39(3): p. 405-10.
212. Oberdorster, G., J. Ferin, and B.E. Lehnert, Correlation between particle size, in vivo particle persistence, and lung injury. Environ Health Perspect, 1994. 102 Suppl 5: p. 173-9.
213. Stoeger, T., et al., Instillation of six different ultrafine carbon particles indicates a surface area threshold dose for acute lung inflammation in mice. Environ Health Perspect, 2006. 114(3): p. 328-33.
214. Gurr, J.R., et al., Ultrafine titanium dioxide particles in the absence of photoactivation can induce oxidative damage to human bronchial epithelial cells. Toxicology, 2005. 213(1-2): p. 66-73.
215. Wilson, M.R., et al., Interactions between ultrafine particles and transition metals in vivo and in vitro. Toxicol Appl Pharmacol, 2002. 184(3): p. 172-9.
216. Ferin, J., G. Oberdorster, and D.P. Penney, Pulmonary retention of ultrafine and fine particles in rats. Am J Respir Cell Mol Biol, 1992. 6(5): p. 535-42.

217. Zhang, Y., et al., Analysis of the cytotoxicity of differentially sized titanium dioxide nanoparticles in murine MC3T3-E1 preosteoblasts. J Mater Sci Mater Med, 2011. 22(8): p. 1933-45.
218. Ivask, A., et al., Size-dependent toxicity of silver nanoparticles to bacteria, yeast, algae, crustaceans and mammalian cells in vitro. PLoS One, 2014. 9(7): p. e102108.
219. Takenaka, S., et al., Pulmonary and systemic distribution of inhaled ultrafine silver particles in rats. Environ Health Perspect, 2001. 109 Suppl 4: p. 547-51.
220. Churg, A., B. Stevens, and J.L. Wright, Comparison of the uptake of fine and ultrafine TiO2 in a tracheal explant system. Am J Physiol, 1998. 274(1 Pt 1): p. L81-6.
221. Roduner, E., Size matters: why nanomaterials are different. Chem Soc Rev, 2006. 35(7): p. 583-92.
222. Risom, L., P. Moller, and S. Loft, Oxidative stress-induced DNA damage by particulate air pollution. Mutat Res, 2005. 592(1-2): p. 119-37.
223. Lippmann, M., Effects of fiber characteristics on lung deposition, retention, and disease. Environ Health Perspect, 1990. 88: p. 311-7.
224. Muller, J., et al., Respiratory toxicity of multi-wall carbon nanotubes. Toxicol Appl Pharmacol, 2005. 207(3): p. 221-31.
225. Monteiro-Riviere, N.A., et al., Multi-walled carbon nanotube interactions with human epidermal keratinocytes. Toxicol Lett, 2005. 155(3): p. 377-84.
226. Shvedova, A.A., et al., Unusual inflammatory and fibrogenic pulmonary responses to single-walled carbon nanotubes in mice. Am J Physiol Lung Cell Mol Physiol, 2005. 289(5): p. L698-708.
227. Warheit, D.B., et al., Comparative pulmonary toxicity assessment of single-wall carbon nanotubes in rats. Toxicol Sci, 2004. 77(1): p. 117-25.
228. Lam, C.W., et al., Pulmonary toxicity of single-wall carbon nanotubes in mice 7 and 90 days after intratracheal instillation. Toxicol Sci, 2004. 77(1): p. 126-34.
229. Maynard, A.D., et al., Exposure to carbon nanotube material: aerosol release during the handling of unrefined single-walled carbon nanotube material. J Toxicol Environ Health A, 2004. 67(1): p. 87-107.
230. Donaldson, K. and C.L. Tran, An introduction to the short-term toxicology of respirable industrial fibres. Mutat Res, 2004. 553(1-2): p. 5-9.
231. Cherukuri, P., et al., Near-infrared fluorescence microscopy of single-walled carbon nanotubes in phagocytic cells. J Am Chem Soc, 2004. 126(48): p. 15638-9.
232. Cui, D., et al., Effect of single wall carbon nanotubes on human HEK293 cells. Toxicol Lett, 2005. 155(1): p. 73-85.
233. Jia, G., et al., Cytotoxicity of carbon nanomaterials: single-wall nanotube, multi-wall nanotube, and fullerene. Environ Sci Technol, 2005. 39(5): p. 1378-83.
234. Bottini, M., et al., Multi-walled carbon nanotubes induce T lymphocyte apoptosis. Toxicol Lett, 2006. 160(2): p. 121-6.
235. Poland, C.A., et al., Carbon nanotubes introduced into the abdominal cavity of mice show asbestos-like pathogenicity in a pilot study. Nat Nanotechnol, 2008. 3(7): p. 423-8.
236. Chusuei, C.C., et al., Cytotoxicity in the age of nano: the role of fourth period transition metal oxide nanoparticle physicochemical properties. Chem Biol Interact, 2013. 206(2): p. 319-26.
237. Baek, M., et al., Effect of different forms of anionic nanoclays on cytotoxicity. J Nanosci Nanotechnol, 2011. 11(2): p. 1803-6.
238. Bhattacharjee, S., et al., Role of surface charge and oxidative stress in cytotoxicity of organic monolayer-coated silicon nanoparticles towards macrophage NR8383 cells. Part Fibre Toxicol, 2010. 7: p. 25.
239. Goodman, C.M., et al., Toxicity of gold nanoparticles functionalized with cationic and anionic side chains. Bioconjug Chem, 2004. 15(4): p. 897-900.

240. Yin, H., H.P. Too, and G.M. Chow, The effects of particle size and surface coating on the cytotoxicity of nickel ferrite. Biomaterials, 2005. 26(29): p. 5818-26.
241. Onuma, K., et al., Nano-scaled particles of titanium dioxide convert benign mouse fibrosarcoma cells into aggressive tumor cells. Am J Pathol, 2009. 175(5): p. 2171-83.
242. Xia, T., et al., Comparison of the abilities of ambient and manufactured nanoparticles to induce cellular toxicity according to an oxidative stress paradigm. Nano Lett, 2006. 6(8): p. 1794-807.
243. Pujalte, I., et al., Toxicokinetics of titanium dioxide (TiO2) nanoparticles after inhalation in rats. Toxicol Lett, 2017. 265: p. 77-85.
244. Miller, M.R., et al., Correction to"Inhaled Nanoparticles Accumulate at Sites of Vascular Disease". ACS Nano, 2017. 11(10): p. 10623-10624.
245. Xue, C., et al., Nano titanium dioxide induces the generation of ROS and potential damage in HaCaT cells under UVA irradiation. J Nanosci Nanotechnol, 2010. 10(12): p. 8500-7.
246. Sung, J.H., et al., Subchronic inhalation toxicity of silver nanoparticles. Toxicol Sci, 2009. 108(2): p. 452-61.
247. Powell, J.J., et al., Origin and fate of dietary nanoparticles and microparticles in the gastrointestinal tract. J Autoimmun, 2010. 34(3): p. J226-33.
248. Yoshida, T., et al., Intestinal absorption and biological effects of orally administered amorphous silica particles. Nanoscale Res Lett, 2014. 9(1): p. 532.
249. Loeschner, K., et al., Distribution of silver in rats following 28 days of repeated oral exposure to silver nanoparticles or silver acetate. Part Fibre Toxicol, 2011. 8: p. 18.
250. Hadrup, N. and H.R. Lam, Oral toxicity of silver ions, silver nanoparticles and colloidal silver--a review. Regul Toxicol Pharmacol, 2014. 68(1): p. 1-7.
251. van der Zande, M., et al., Distribution, elimination, and toxicity of silver nanoparticles and silver ions in rats after 28-day oral exposure. ACS Nano, 2012. 6(8): p. 7427-42.
252. Tak, Y.K., et al., Shape-Dependent Skin Penetration of Silver Nanoparticles: Does It Really Matter? Sci Rep, 2015. 5: p. 16908.
253. Rissler, J., et al., Deposition efficiency of inhaled particles (15-5000 nm) related to breathing pattern and lung function: an experimental study in healthy children and adults. Part Fibre Toxicol, 2017. 14(1): p. 10.
254. Bakand, S. and A. Hayes, Toxicological Considerations, Toxicity Assessment, and Risk Management of Inhaled Nanoparticles. Int J Mol Sci, 2016. 17(6).
255. Kreyling, W.G., et al., Size dependence of the translocation of inhaled iridium and carbon nanoparticle aggregates from the lung of rats to the blood and secondary target organs. Inhal Toxicol, 2009. 21 Suppl 1: p. 55-60.
256. Seipenbusch, M., A. Binder, and G. Kasper, Temporal evolution of nanoparticle aerosols in workplace exposure. Ann Occup Hyg, 2008. 52(8): p. 707-16.
257. Donaldson, K., C.A. Poland, and R.P. Schins, Possible genotoxic mechanisms of nanoparticles: criteria for improved test strategies. Nanotoxicology, 2010. 4: p. 414-20.
258. Mercer, R.R., et al., Distribution and fibrotic response following inhalation exposure to multi-walled carbon nanotubes. Part Fibre Toxicol, 2013. 10: p. 33.
259. Mercer, R.R., et al., Extrapulmonary transport of MWCNT following inhalation exposure. Part Fibre Toxicol, 2013. 10: p. 38.
260. Ryman-Rasmussen, J.P., et al., Inhaled carbon nanotubes reach the subpleural tissue in mice. Nat Nanotechnol, 2009. 4(11): p. 747-51.
261. Ryman-Rasmussen, J.P., et al., Inhaled multiwalled carbon nanotubes potentiate airway fibrosis in murine allergic asthma. Am J Respir Cell Mol Biol, 2009. 40(3): p. 349-58.
262. Bergin, I.L. and F.A. Witzmann, Nanoparticle toxicity by the gastrointestinal route: evidence and knowledge gaps. Int J Biomed Nanosci Nanotechnol, 2013. 3(1-2).

263. Pietroiusti, A., Health implications of engineered nanomaterials. Nanoscale, 2012. 4(4): p. 1231-47.
264. Geiser, M. and W.G. Kreyling, Deposition and biokinetics of inhaled nanoparticles. Part Fibre Toxicol, 2010. 7: p. 2.
265. Powell, J.J., V. Thoree, and L.C. Pele, Dietary microparticles and their impact on tolerance and immune responsiveness of the gastrointestinal tract. Br J Nutr, 2007. 98 Suppl 1: p. S59-63.
266. Lomer, M.C., R.P. Thompson, and J.J. Powell, Fine and ultrafine particles of the diet: influence on the mucosal immune response and association with Crohn's disease. Proc Nutr Soc, 2002. 61(1): p. 123-30.
267. Nguyen, T.H., M. Lin, and A. Mustapha, Toxicity of graphene oxide on intestinal bacteria and Caco-2 cells. J Food Prot, 2015. 78(5): p. 996-1002.
268. Pietroiusti, A., A. Magrini, and L. Campagnolo, New frontiers in nanotoxicology: Gut microbiota/microbiome-mediated effects of engineered nanomaterials. Toxicol Appl Pharmacol, 2016. 299: p. 90-5.
269. Hansson, G.C., Role of mucus layers in gut infection and inflammation. Curr Opin Microbiol, 2012. 15(1): p. 57-62.
270. Bellmann, S., et al., Mammalian gastrointestinal tract parameters modulating the integrity, surface properties, and absorption of food-relevant nanomaterials. Wiley Interdiscip Rev Nanomed Nanobiotechnol, 2015. 7(5): p. 609-22.
271. McConnell, E.L., A.W. Basit, and S. Murdan, Measurements of rat and mouse gastrointestinal pH, fluid and lymphoid tissue, and implications for in-vivo experiments. J Pharm Pharmacol, 2008. 60(1): p. 63-70.
272. Kraehenbuhl, J.P. and M.R. Neutra, Epithelial M cells: differentiation and function. Annu Rev Cell Dev Biol, 2000. 16: p. 301-32.
273. Ahamed, M., M.S. Alsalhi, and M.K. Siddiqui, Silver nanoparticle applications and human health. Clin Chim Acta, 2010. 411(23-24): p. 1841-8.
274. Elder, A., S. Vidyasagar, and L. DeLouise, Physicochemical factors that affect metal and metal oxide nanoparticle passage across epithelial barriers. Wiley Interdiscip Rev Nanomed Nanobiotechnol, 2009. 1(4): p. 434-50.
275. Bouwstra, J.A. and P.L. Honeywell-Nguyen, Skin structure and mode of action of vesicles. Adv Drug Deliv Rev, 2002. 54 Suppl 1: p. S41-55.
276. Christophers, E., The architecture of stratum corneum after wounding. J Invest Dermatol, 1971. 57(4): p. 241-6.
277. Christophers, E., Cellular architecture of the stratum corneum. J Invest Dermatol, 1971. 56(3): p. 165-9.
278. Naik, A., Y.N. Kalia, and R.H. Guy, Transdermal drug delivery: overcoming the skin's barrier function. Pharm Sci Technolo Today, 2000. 3(9): p. 318-326.
279. Van Duuren-Stuurman, B., et al., A structured observational method to assess dermal exposure to manufactured nanoparticles DREAM as an initial assessment tool. Int J Occup Environ Health, 2010. 16(4): p. 399-405.
280. Niska, K., et al., Metal nanoparticles in dermatology and cosmetology: Interactions with human skin cells. Chem Biol Interact, 2017.
281. Alkilany, A.M. and C.J. Murphy, Toxicity and cellular uptake of gold nanoparticles: what we have learned so far? J Nanopart Res, 2010. 12(7): p. 2313-2333.
282. Gulson, B., et al., Small amounts of zinc from zinc oxide particles in sunscreens applied outdoors are absorbed through human skin. Toxicol Sci, 2010. 118(1): p. 140-9.
283. Hillaireau, H. and P. Couvreur, Nanocarriers' entry into the cell: relevance to drug delivery. Cell Mol Life Sci, 2009. 66(17): p. 2873-96.

284. Muhlfeld, C., P. Gehr, and B. Rothen-Rutishauser, Translocation and cellular entering mechanisms of nanoparticles in the respiratory tract. Swiss Med Wkly, 2008. 138(27-28): p. 387-91.
285. Beddoes, C.M., C.P. Case, and W.H. Briscoe, Understanding nanoparticle cellular entry: A physicochemical perspective. Adv Colloid Interface Sci, 2015. 218: p. 48-68.
286. Kuhn, D.A., et al., Different endocytotic uptake mechanisms for nanoparticles in epithelial cells and macrophages. Beilstein J Nanotechnol, 2014. 5: p. 1625-36.
287. Mahmoudi, M., et al., Cell "vision": complementary factor of protein corona in nanotoxicology. Nanoscale, 2012. 4(17): p. 5461-8.
288. Ding, H.M. and Y.Q. Ma, Theoretical and computational investigations of nanoparticle-biomembrane interactions in cellular delivery. Small, 2015. 11(9-10): p. 1055-71.
289. Conner, S.D. and S.L. Schmid, Regulated portals of entry into the cell. Nature, 2003. 422(6927): p. 37-44.
290. Greulich, C., et al., Uptake and intracellular distribution of silver nanoparticles in human mesenchymal stem cells. Acta Biomater, 2011. 7(1): p. 347-54.
291. Dausend, J., et al., Uptake mechanism of oppositely charged fluorescent nanoparticles in HeLa cells. Macromol Biosci, 2008. 8(12): p. 1135-43.
292. Falcone, S., et al., Macropinocytosis: regulated coordination of endocytic and exocytic membrane traffic events. J Cell Sci, 2006. 119(Pt 22): p. 4758-69.
293. Shukla, R., et al., Biocompatibility of gold nanoparticles and their endocytotic fate inside the cellular compartment: a microscopic overview. Langmuir, 2005. 21(23): p. 10644-54.
294. Li, W., et al., The translocation of fullerenic nanoparticles into lysosome via the pathway of clathrin-mediated endocytosis. Nanotechnology, 2008. 19(14): p. 145102.
295. Harush-Frenkel, O., et al., Targeting of nanoparticles to the clathrin-mediated endocytic pathway. Biochem Biophys Res Commun, 2007. 353(1): p. 26-32.
296. Harush-Frenkel, O., et al., Surface charge of nanoparticles determines their endocytic and transcytotic pathway in polarized MDCK cells. Biomacromolecules, 2008. 9(2): p. 435-43.
297. Jiang, X., et al., Endo- and exocytosis of zwitterionic quantum dot nanoparticles by live HeLa cells. ACS Nano, 2010. 4(11): p. 6787-97.
298. Kam, N.W., Z. Liu, and H. Dai, Carbon nanotubes as intracellular transporters for proteins and DNA: an investigation of the uptake mechanism and pathway. Angew Chem Int Ed Engl, 2006. 45(4): p. 577-81.
299. Zhang, L.W., et al., Endocytic mechanisms and toxicity of a functionalized fullerene in human cells. Toxicol Lett, 2009. 191(2-3): p. 149-57.
300. Rejman, J., et al., Size-dependent internalization of particles via the pathways of clathrin- and caveolae-mediated endocytosis. Biochem J, 2004. 377(Pt 1): p. 159-69.
301. Wang, Z., et al., Size and dynamics of caveolae studied using nanoparticles in living endothelial cells. ACS Nano, 2009. 3(12): p. 4110-6.
302. Contreras, J., et al., Intracellular uptake and trafficking of difluoroboron dibenzoylmethane-polylactide nanoparticles in HeLa cells. ACS Nano, 2010. 4(5): p. 2735-47.
303. Partlow, K.C., G.M. Lanza, and S.A. Wickline, Exploiting lipid raft transport with membrane targeted nanoparticles: a strategy for cytosolic drug delivery. Biomaterials, 2008. 29(23): p. 3367-75.
304. Geiser, M., et al., Ultrafine particles cross cellular membranes by nonphagocytic mechanisms in lungs and in cultured cells. Environ Health Perspect, 2005. 113(11): p. 1555-60.
305. Mu, Q., et al., Mechanism of cellular uptake of genotoxic silica nanoparticles. Part Fibre Toxicol, 2012. 9: p. 29.

306. Lesniak, W., et al., Silver/dendrimer nanocomposites as biomarkers: fabrication, characterization, in vitro toxicity, and intracellular detection. Nano Lett, 2005. 5(11): p. 2123-30.
307. Rothen-Rutishauser, B.M., et al., Interaction of fine particles and nanoparticles with red blood cells visualized with advanced microscopic techniques. Environ Sci Technol, 2006. 40(14): p. 4353-9.
308. Christianson, H.C. and M. Belting, Heparan sulfate proteoglycan as a cell-surface endocytosis receptor. Matrix Biol, 2014. 35: p. 51-5.
309. Favretto, M.E., et al., Glycosaminoglycans in the cellular uptake of drug delivery vectors - bystanders or active players? J Control Release, 2014. 180: p. 81-90.
310. Siegel, G., M. Malmsten, and E. Ermilov, Anionic biopolyelectrolytes of the syndecan/perlecan superfamily: physicochemical properties and medical significance. Adv Colloid Interface Sci, 2014. 205: p. 275-318.
311. Carmona-Ribeiro, A.M. and L.D. de Melo Carrasco, Cationic antimicrobial polymers and their assemblies. Int J Mol Sci, 2013. 14(5): p. 9906-46.
312. Teixeira, V., M.J. Feio, and M. Bastos, Role of lipids in the interaction of antimicrobial peptides with membranes. Prog Lipid Res, 2012. 51(2): p. 149-77.
313. Zeng, Z., et al., Synthetic polymer nanoparticle-polysaccharide interactions: a systematic study. J Am Chem Soc, 2012. 134(5): p. 2681-90.
314. Porter, A.E., et al., Uptake of C60 by human monocyte macrophages, its localization and implications for toxicity: studied by high resolution electron microscopy and electron tomography. Acta Biomater, 2006. 2(4): p. 409-19.
315. Mecke, A., et al., Lipid bilayer disruption by polycationic polymers: the roles of size and chemical functional group. Langmuir, 2005. 21(23): p. 10348-54.
316. Shimizu, K., H. Nakamura, and S. Watano, MD simulation study of direct permeation of a nanoparticle across the cell membrane under an external electric field. Nanoscale, 2016. 8(23): p. 11897-906.
317. Su, J. and H. Guo, Translocation of a charged nanoparticle through a fluidic nanochannel: the interplay of nanoparticle and ions. J Phys Chem B, 2013. 117(39): p. 11772-9.
318. Lin, J., et al., Penetration of lipid membranes by gold nanoparticles: insights into cellular uptake, cytotoxicity, and their relationship. ACS Nano, 2010. 4(9): p. 5421-9.
319. Lin, J. and A. Alexander-Katz, Cell membranes open "doors" for cationic nanoparticles/biomolecules: insights into uptake kinetics. ACS Nano, 2013. 7(12): p. 10799-808.
320. Li, Y., X. Zhang, and D. Cao, A spontaneous penetration mechanism of patterned nanoparticles across a biomembrane. Soft Matter, 2014. 10(35): p. 6844-56.
321. Song, B., et al., Nanoparticle permeation induces water penetration, ion transport, and lipid flip-flop. Langmuir, 2012. 28(49): p. 16989-7000.
322. Choe, S., et al., Molecular dynamics simulation study of a pulmonary surfactant film interacting with a carbonaceous nanoparticle. Biophys J, 2008. 95(9): p. 4102-14.
323. Ding, H.M. and Y.Q. Ma, Computer simulation of the role of protein corona in cellular delivery of nanoparticles. Biomaterials, 2014. 35(30): p. 8703-10.
324. Moghadam, B.Y., et al., Role of nanoparticle surface functionality in the disruption of model cell membranes. Langmuir, 2012. 28(47): p. 16318-26.
325. Negoda, A., et al., Polystyrene nanoparticle exposure induces ion-selective pores in lipid bilayers. Biochim Biophys Acta, 2013. 1828(9): p. 2215-22.
326. Santhosh, P.B., et al., Influence of iron oxide nanoparticles on bending elasticity and bilayer fluidity of phosphotidylcholine liposomal membranes. Colloids and Surfaces A: Physicochemical and Engineering Aspects, 2014. 460: p. 248-253.

327. Santhosh, P.B., et al., Influence of nanoparticle-membrane electrostatic interactions on membrane fluidity and bending elasticity. Chem Phys Lipids, 2014. 178: p. 52-62.
328. Drasler, B., et al., Effects of magnetic cobalt ferrite nanoparticles on biological and artificial lipid membranes. Int J Nanomedicine, 2014. 9: p. 1559-81.
329. de Planque, M.R., et al., Electrophysiological characterization of membrane disruption by nanoparticles. ACS Nano, 2011. 5(5): p. 3599-606.
330. Le Bihan, O., et al., Cryo-electron tomography of nanoparticle transmigration into liposome. J Struct Biol, 2009. 168(3): p. 419-25.
331. Alkhammash, H.I., et al., Native silica nanoparticles are powerful membrane disruptors. Phys Chem Chem Phys, 2015. 17(24): p. 15547-60.
332. Peetla, C. and V. Labhasetwar, Biophysical characterization of nanoparticle-endothelial model cell membrane interactions. Mol Pharm, 2008. 5(3): p. 418-29.
333. Chen, J., et al., Cationic nanoparticles induce nanoscale disruption in living cell plasma membranes. J Phys Chem B, 2009. 113(32): p. 11179-85.
334. Wang, T., et al., Cellular uptake of nanoparticles by membrane penetration: a study combining confocal microscopy with FTIR spectroelectrochemistry. ACS Nano, 2012. 6(2): p. 1251-9.
335. Warren, E.A. and C.K. Payne, Cellular binding of nanoparticles disrupts the membrane potential. RSC Adv, 2015. 5(18): p. 13660-13666.
336. Zhao, Y., et al., Interaction of mesoporous silica nanoparticles with human red blood cell membranes: size and surface effects. ACS Nano, 2011. 5(2): p. 1366-75.
337. Guarnieri, D., et al., Transport across the cell-membrane dictates nanoparticle fate and toxicity: a new paradigm in nanotoxicology. Nanoscale, 2014. 6(17): p. 10264-73.
338. Shin, E.H., et al., Membrane potential mediates the cellular binding of nanoparticles. Nanoscale, 2013. 5(13): p. 5879-86.
339. Gornati, R., et al., Zerovalent Fe, Co and Ni nanoparticle toxicity evaluated on SKOV-3 and U87 cell lines. J Appl Toxicol, 2016. 36(3): p. 385-93.
340. Bernareggi, A., et al., Xenopus laevis Oocytes as a Model System for Studying the Interaction Between Asbestos Fibres and Cell Membranes. Toxicol Sci, 2015. 145(2): p. 263-72.
341. T. Masui, T. Ozaki, K.-i. Machida, G.-y. Adachi, Preparation of ceria–zirconia sub-catalysts for automotive exhaust cleaning, J. Alloys Compd. 303 (2000)49–55.
342. Stratakis E, Kymakis E. Nanoparticle-based plasmonic organic photovoltaic devices. Mater Today. 2013;16(4):133-146. doi:10.1016/j.mattod.2013.04.006.
343. A. Arnida, H. Ghandehari Malugin, Cellular uptake and toxicity of gold nanoparticles in prostate cancer cells: a comparative study of rods and spheres, J. Appl. Toxicol.: JAT 30 (3) (2010) 212–217.
344. Shinde PV, Campbell CJ, Yun YH, Slack SM, Goetz DJ. Particle diameter influences adhesion under flow. Biophys J. 2001;80(4):1733–1743.
345. Kango S, Kalia S, Celli A, Njuguna J, Habibi Y, Kumar R (2013) Surface modification of inorganic nanoparticles for development of organic–inorganic nanocomposites—a review. Prog Polym Sci 38(8):1232–1261
346. J. Xie, C. Xu, N. Kohler, Y. Hou, S. Sun, Controlled PEGylation of monodisperse Fe3O4 nanoparticles for reduced non-specific uptake by macrophage cells, Adv. Mater. 19 (20) (2007) 3163–3166.
347. D.L. Feldheim, A. Colby, J. Foss, Metal Nanoparticles: Synthesis, Characterization, and Applications, Marcel Dekker Inc., New York, 2002.
348. T. Pradeep, Noble metal nanoparticles for water purification: a critical review, Thin Solid Films 517 (2009) 6441–6478.
349. Qiang JL. The surface properties and photocatalytic activities of ZnO ultrafine particles. Appl Surf Sci 2001;180:308–14.

350. Bernardini G, Cattaneo AG, Sabbioni E, et al. Toxicology of Engineered Metal Nanoparticles. In: General, Applied and Systems Toxicology. Chichester, UK: John Wiley & Sons, Ltd; 2011. doi:10.1002/9780470744307.gat240.
351. Isa Karimzadeh MA, Taher Doroudi MR, Ganjali, Peir Hossein Kolivand (2017) Superparamagnetic iron Oxide (Fe3O4) nanoparticles coated with PEG/PEI for biomedical applications: a facile and scalable preparation route based on the cathodic electrochemical deposition method. Adv Phys Chem 2017:1–7. https ://doi.org/10.1155/2017/9437487
352. H. Cuizhu, Q. Song, W. Xinzhen, L. Jiurong, L. Liqiang, L. Wei, I. Masahiro, K.Machida, Facile synthesis of hollow porous cobalt spheres and their enhancedelectromagnetic properties, J. Mater. Chem. 22 (2012) 22160–22166.
353. N.T.K. Thanha, L.A.W. Green, Functionalisation of nanoparticles for biomedicalapplications, Nano Today 119 (2015) 503–516.[2]
354. J.K. Lim, S.A. Majetich, Composite magnetic-plasmonic nanoparticles forbiomedicine, Nano Today 8 (2013) 98–113.[4]
355. Q.A. Pankhurst, N.T.K. Thanh, S.K. Jones, J. Dobson, Progress in applications ofmagnetic nanoparticles in biomedicine, J. Phys. D: Appl. Phys. 42 (2009)224001–224015.
356. S.M. Ansari et al, Cobalt nanoparticles for biomedical applications: Facile synthesis, physiochemical characterization, cytotoxicity behavior and biocompatibility – 2017 - http://dx.doi.org/10.1016/j.apsusc.2017.03.002
357. Liu X, Qiu G, and Li X. Shape-controlled synthesis and properties of uniform spinel cobalt oxide nanocubes. Nanotechnology 2005; 12: 3035.
358. Salimi A, Hallaj R, Mamkhezri H, et al. Electrochemical properties and electrocatalytic activity of FAD immobilized onto cobalt oxide nanoparticles: application to nitrite detection. J Electroanal Chem 2008: 31–38.
359. Larese F, Crosera M, Timeus E, et al. Human skin penetration of cobalt nanoparticles through intact and damaged skin. Toxicol In Vitro 2013; 1: 121–127.
360. Morozov YG, Belousova O V., Kuznetsov M V. Preparation of nickel nanoparticles for catalytic applications. Inorg Mater. 2011;47(1):36-40. doi:10.1134/S0020168510121027.
361. Del Pino P, Pelaz B, Zhang Q, Maffre P, Nienhaus GU, Parak WJ. Protein corona formation around nanoparticles - from the past to the future. Mater Horiz 2014, 1:301–313. https://doi.org/10.1039/c3mh00106g.
362. Panessa-Warren B, Warren J, Wong S, Misewich J. Biological cellular response to carbon nanoparticle toxicity. J Phys Condens Matter. 2006;18(33):S2185.
363. Ryabchikova E, Mazurkova N, Shikina N, Ismagilov Z. The crystalline forms of titanium dioxide nanoparticles affect their interactions with individual cells. J Med Chem Biol Radiol Def. 2010:8.
364. Soenen SJ, Rivera-Gil P, Montenegro J-M, ParakWJ, De Smedt SC, Braeckmans K (2011) Cellular toxicity of inorganic nanoparticles: common aspects and guidelines for improved nanotoxicity evaluation. Nano Today 6(5):446–465
365. Kamata H, Zinchenko A, Murata S. Effects of cationic and anionic nanoparticles on the stability of the secondary structure of DNA. Colloid Polymer Sci. 2011;289(12):1329–1335.
366. Takagi A, Hirose A, Nishimura T, et al. Induction of mesothelioma in p53+/- mouse by intraperitoneal application of multi-wall carbon nanotube. J Toxicol Sci. 2008;33(1):105–116.
367. Sayes, C. M.; Fortner, J. D.; Guo, W.; Lyon, D.; Boyd, A. M.; Ausman, K. D.; Tao, Y. J.; Sitharaman, B.; Wilson, L. J.; Hughes, J. B.; West, J. L.; Colvin, V. L. Nano Lett. 2004, 4, 1881–1887. doi:10.1021/nl0489586
368. Ruizendaal L, Bhattacharjee S, Pournazari K, et al. Synthesis and cytotoxicity of silicon nanoparticles with covalently attached organic monolayers. Nanotoxicology. 2009;3(4):339–347.

369. Sung, J.H.; Ji, J.H.; Yoon, J.U.; Kim, D.S.; Song, M.Y.; Jeong, J.; Han, B.S.; Han, J.H.; Chung, Y.H.; Kim, J.; et al. Lung function changes in Sprague-Dawley rats after prolonged inhalation exposure to silver nanoparticles. Inhal. Toxicol. 2008, 20, 567–574.
370. Park, Y.H.; Bae, H.C.; Jang, Y.; Jeong, S.H.; Lee, H.N.; Ryu,W.I.; Yoo, M.G.; Kim, Y.R.; Kim, M.K.; Lee, J.K.; et al. Effect of the size and surface charge of silica nanoparticles on cutaneous toxicity. Mol. Cell. Toxicol. 2013, 9, 67–74.
371. Siegmann, K.; Scherrer, L.; Siegmann, H.C. Physical and chemical properties of airborne nanoscale particles and how to measure the impact on human health. J. Mol. Struct. 1999, 458, 191–201.
372. Wickett, R.R.; Visscher, M.O. Structure and function of the epidermal barrier. Am. J. Infect. Control 2006, 34, s98–s110.
373. Seipenbusch, M., Yu, M., Aschbach, C., Rating, U., Kuhlbusch, T., & Lidén, G. (2014). From source to emission, transport dynamics and dose assessment for workplace aerosol exposure. In U. Vogel, K. Savolainen, Q. Wu, M. van Tongeren, D. Brouwer, & M. Berges (Eds.), Handbook of nanosafety. Measurement, exposure and toxicology (p. 135). London, England: Elsevier.
374. Blank, F.; Gehr, P.; Rutishauser, R.R. In Vitro Human Lung Cell Culture Models to Study the Toxic Potential of Nanoparticles; JohnWily & Sons Ltd.: Chichester, UK, 2009.
375. Monteiro-Riviere, N.A. Structure and Function of Skin; In Toxicology of the Skin—Target Organ Series; Monteiro-Riviere, N.A., Ed.; Informa Healthcare: Raleigh, NC, USA, 2010; pp. 1–18, ISBN 9781420079173.
376. Piccinno, F.; Gottschalk, F.; Seeger, S.; Nowack, B. Industrial production quantities and uses of ten engineered nanomaterials in Europe and the world. J. Nanopart. Res. 2012, 14, 1109.
377. T. G. Iversen, T. Skotland, K. Sandvig, Nano Today 2011, 6, 176.
378. Schmidtchen A, Malmsten M. Peptide interactions with bacterial lipopolysaccharides. Curr Opin Colloid Interface Sci 2013;18:381–92.
379. Hong S, Hessler J, Banaszak Holl M, Leroueil P, Mecke A, Orr B. Physical interactions of nanoparticles with biological membranes: the observation of nanoscale hole formation. Chem Health Saf. 2006;13(3): 16–20.
380. Borm, P., et al., Research strategies for safety evaluation of nanomaterials, part V: role of dissolution in biological fate and effects of nanoscale particles. Toxicol Sci, 2006. 90(1): p. 23-32
381. Misra, S.K., et al., The complexity of nanoparticle dissolution and its importance in nanotoxicological studies. Sci Total Environ, 2012. 438: p. 225-32.
382. Sabbioni, E., et al., Interaction with culture medium components, cellular uptake and intracellular distribution of cobalt nanoparticles, microparticles and ions in Balb/3T3 mouse fibroblasts. Nanotoxicology, 2014. 8(1): p. 88-99.
383. Gornati, R., et al., Zerovalent Fe, Co and Ni nanoparticle toxicity evaluated on SKOV-3 and U87 cell lines. J Appl Toxicol, 2016. 36(3): p. 385-93.
384. Shi, M., et al., The roles of surface chemistry, dissolution rate, and delivered dose in the cytotoxicity of copper nanoparticles. Nanoscale, 2017. 9(14): p. 4739-4750.
385. Crowe, T.P., et al., Mechanism of intranasal drug delivery directly to the brain. Life Sci, 2018. 195: p. 44-52.
386. Pires, P.C. and A.O. Santos, Nanosystems in nose-to-brain drug delivery: A review of non-clinical brain targeting studies. J Control Release, 2018. 270: p. 89-100.
387. Calderon-Garciduenas, L., et al., Air pollution and brain damage. Toxicol Pathol, 2002. 30(3): p. 373-89.
388. Calderon-Garciduenas, L., et al., DNA damage in nasal and brain tissues of canines exposed to air pollutants is associated with evidence of chronic brain inflammation and neurodegeneration. Toxicol Pathol, 2003. 31(5): p. 524-38.

389. Oberdorster, G., et al., Translocation of inhaled ultrafine particles to the brain. Inhal Toxicol, 2004. 16(6-7): p. 437-45.
390. Block, M.L. and L. Calderon-Garciduenas, Air pollution: mechanisms of neuroinflammation and CNS disease. Trends Neurosci, 2009. 32(9): p. 506-16.
391. Gartziandia, O., et al., Nanoparticle transport across in vitro olfactory cell monolayers. Int J Pharm, 2016. 499(1-2): p. 81-89.
392. Khan, A.R., et al., Progress in brain targeting drug delivery system by nasal route. J Control Release, 2017. 268: p. 364-389.

Sitography

1S http://calteches.library.caltech.edu/1976/
2S http://ec.europa.eu/health/scientific_committees/opinions_layman /en/nanotechnologies/about-nanotechnologies.htm#6
3S Taniguchi, N. (1974) On the Basic Concept of Nanotechnology. Proceedings of the International Conference on Production Engineering, Tokyo, 18-23.
4S Nobbmann, U.L. Polydispersity–What Does It Mean for DLS and Chromatography. 2014. Available online: http: //www.materials-talks.com/blog/2014/10/23/polydispersity-what-does-it-mean-for-dls-and-chromatography/ (accessed on 14 March 2018).
5S Bera, B. Nanoporous silicon prepared by vapour phase strain etch and sacrificial technique. In Proceedings of the International Conference on Microelectronic Circuit and System (Micro), Kolkata, India, 11–12 July 2015; pp. 42–45.
6S International Commission on Radiological Protection (ICRP). (1994). Human respiratory tract model for radiological protection. A report of a task Group of the International Commission on radiological protection. ICRP publication 66. Annals of the ICRP, 24(1–3), 1–482.

Chapter 2

Cobalt oxide nanoparticles can enter inside the cells by crossing plasma membranes

Originally published in Scientific Reports (2016)

Elena Bossi[1,2], Daniele Zanella[1], Rosalba Gornati[1,2] and Giovanni Bernardini[1,2]

[1]Department of Biotechnology and Life Sciences, University of Insubria; Via Dunant 3, Varese, Italy

[2]Interuniversity Center "The Protein Factory", Politecnico di Milano and Università dell'Insubria, Via Mancinelli 7, I-20131 Milan, Italy

Abstract

The ability of nanoparticles (NPs) to be promptly uptaken by the cells makes them both dangerous and useful to human health. It was recently postulated that some NPs might cross the plasma membrane also by a non-endocytotic pathway gaining access to the cytoplasm. To this aim, after having filled mature *Xenopus* oocytes with Calcein, whose fluorescence is strongly quenched by divalent metal ions, we have exposed them to different cobalt NPs quantifying quenching as evidence of the increase of the concentration of Co^{2+} released by the NPs that entered into the cytoplasm. We demonstrated that cobalt oxide NPs, but not cobalt nor cobalt oxide NPs that were surrounded by a protein corona, can indeed cross plasma membranes.

Introduction

It is well known that nanoparticles (NPs) readily enter cells [1] by different endocytotic mechanisms [2-6]. The capability of NPs to be promptly uptaken by the cells, as well as that of crossing biological barriers [7-9], makes them at the same time potentially dangerous and useful to human health. Dangerous, as NPs might exert their toxicity, once inside

the cell, very close to target organelles as nuclei and mitochondria, a phenomenon which is referred to as Trojan horse effect [10-12]. Useful, as they can be directed to exert their toxicity toward cancer cells, used for drug delivery, injected as a contrast agent for diagnostic and even for theranostic purposes [13], and assumed for food supplementation.
Recently, it has been considered the possibility that some NPs might also cross the plasma membrane by a non-endocytotic pathway [14-19] gaining a direct access to the cytoplasm. This pathway is usually poorly considered as it challenges the idea of non-permeability of membranes to large hydrophilic molecules. To verify this possibility, we have set up a new protocol that has proved capable to follow the NP-plasma membrane dynamics and we have demonstrated that cobalt oxide NPs, but not cobalt nor cobalt oxide NPs that were surrounded by a protein corona, can cross plasma membranes.
Cobalt NPs have a large use in industrial and biomedical applications. They efficiently catalyse the combustion of various hydrocarbons[20] and the degradation of water pollutants[21] providing a cheap candidate to replace noble metals. Cobalt NPs are also used in electrocatalysis for the oxygen evolution reaction[22], important in hydrogen generation. Recently, it has been shown that cobalt NPs can self-assemble to constitute photonic hyper-crystals[23], which might have a strong potential in biological and chemical sensing. Moreover, cobalt NPs are magnetic and this property allows to manipulate them in a chemical or biological system using an external magnet. Moreover, magnetic NPs can be easily conjugated to biologically important constituents such as DNA, peptides, antibodies[24] as well as enzymes[25,26] and sugars[27,28] to construct versatile bio-nano hybrids.

Results and Discussion

Calcein as "Metal Detector" in *Xenopus laevis* oocytes.

As a preliminary step, we have tested the ability of Calcein to detect cobalt uptake in fully grown *Xenopus laevis* oocytes. Oocytes are naturally arrested for prolonged period of time at prophase of meiosis I during which time the oocyte grows and stores macromolecular

components that are necessary for future development. They exhibit different sizes that reflect different stages of growth. Fully grown oocytes, which have been used in the present paper, have a diameter of about 1.2 mm and provide a simple system for membrane transport characterization. For this purpose, we firstly needed to set up a system capable to consistently transport divalent metal ions across the plasma membrane from the extracellular milieu to the cytoplasm. We have, therefore, prepared transfected *Xenopus* oocytes by injecting them with the cRNA of the Divalent Metal ion Transporter 1 from rat (rDMT1). This membrane protein is a proton and voltage dependent transporter of divalent metal ions such as $Fe^{2+}$and Mn^{2+}, as well as Co^{2+}, Ni^{2+} and Cd^{2+} [29-32]. In mammals, it is mostly expressed in duodenum enterocytes, but it can be also found in kidney, brain, testis and placenta. By a two electrode voltage-clamp with a holding potential of -40 mV, we have recorded the currents generated by the exposure to manganese, iron and cobalt ions at pH 5.5. In non transfected (i.e., not injected with DMT1 cRNA) *Xenopus laevis* oocytes, the perfusion of ions in the bath solution did not elicit currents indicating the absence of electrogenic endogenous transporters in their plasma membrane. Conversely, in rDMT1 transfected oocytes, all the three substrates elicited, as expected [33], inward currents in the range of -40 to -50 nA (Figure 1 A and B). As shown in Figure 1 B, iron, the physiological substrate, resulted slightly more efficiently transported than cobalt and manganese. With these experiments, we have confirmed that rDMT1 transfected oocytes, but not non-transfected ones, were able to transport iron, cobalt and manganese ions across their plasma membrane.

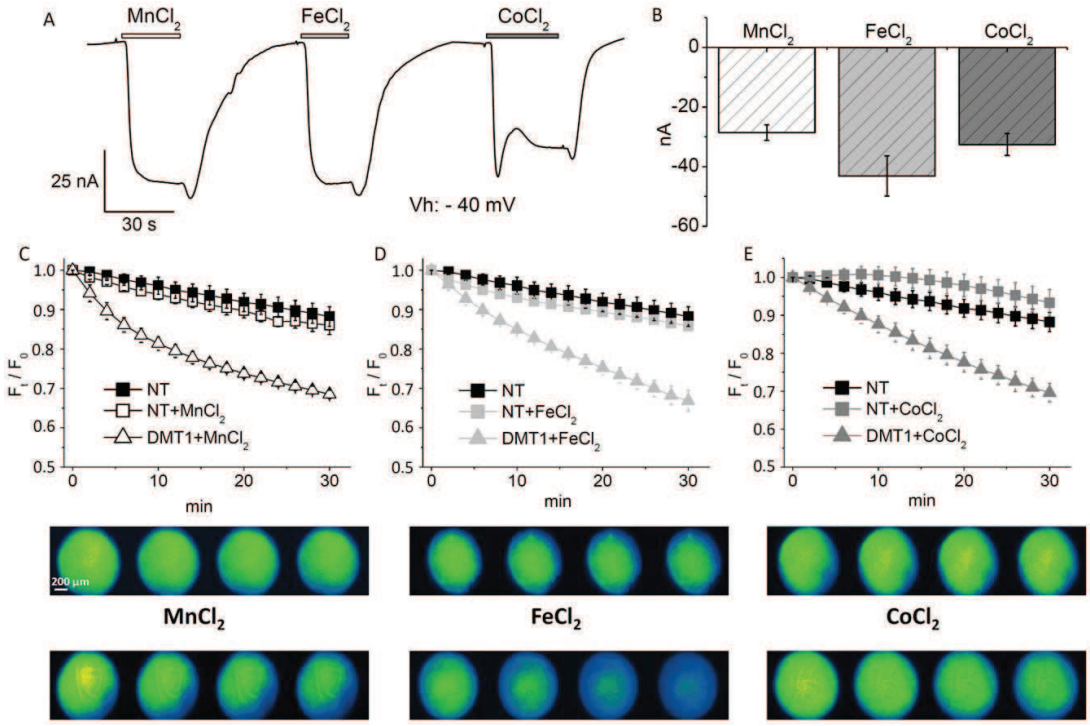

Figure 1 Calcein as a cytoplasmic "metal detector". *A: two electrode voltage clamp of a representative rDMT1 transfected oocyte; inward currents are induced by 100 µM $MnCl_2$, $FeCl_2$ and $CoCl_2$ (V_h= -40 mV, pH 5.5). B: means and standard errors of the transport currents obtained from 40 oocytes, five batches. C, D and E: Plots of fluorescence decay (F_t/F_0) with corresponding images of Calcein-injected oocytes (upper series: non-transfected (NT) and lower series: rDMT1 transfected) exposed to 100 µM $MnCl_2$ (C), $FeCl_2$ (D), and $CoCl_2$ (E) at pH 5.5 from 3 to 10 oocytes, from 2 to 4 oocytes batches.*

We have, then, filled transfected and not transfected oocytes with Calcein and monitored their fluorescence decay with an inverted fluorescence microscope. We have controlled that, before Calcein injection and at the used wavelengths, oocytes were not fluorescent (data not shown). We have also monitored the decay of the fluorescence signal in non-transfected Calcein-injected oocytes. Fluorescence decreased about 11.8% ± 2.5% in a 30 min interval (Fig. 1 C, D, and E, black squares) and, in the pH range 5.5 - 7.6, the decrease was pH-independent. Therefore, at our experimental conditions, only minimal photo-bleaching phenomena occurred. Similarly, non-transfected Calcein-injected oocytes which were exposed to 100 µM $MnCl_2$, $FeCl_2$,

and $CoCl_2$ (Fig. 1 C, D, and E, squares) underwent a moderate fluorescence decay not dissimilar to that occurring in the absence of the tested divalent metal ions.

Fluorescence decay was, instead, evident in transfected oocytes, i.e., in oocytes expressing rDMT1. We measured a 31.5% ± 1.1% decay for Mn^{2+} (empty triangles), a 33.2% ± 2.7% decay for Fe^{2+} (light grey triangles) and a 30.4% ± 2.4% for Co^{2+} (grey triangles). This indicates that the entry of the divalent metal ions into the cell caused the quenching of Calcein and, consequently, that Calcein can be used to monitor divalent metal ion concentration changes in the cytoplasm of *Xenopus* oocytes.

In this context, we further investigated metal-Calcein interactions by spectrofluorimetry measuring quenching in cuvettes at pH 7.6, close to the intracellular value, and at pH 5.5, value at which rDMT1 performs optimally. Values at the emission peak wavelength (i.e., 512 nm) were recorded for each concentration of Fe^{2+}, Mn^{2+} and Co^{2+}. The data revealed that Calcein quenching is higher for Co^{2+} and Fe^{2+}, with $K_{0.5}$ of 7.6 ± 0.7 and 5.3 ± 0.4 μM at pH 5.5 and 9 ± 3 and 0.9 ± 0.04 μM at pH 7.6. Quenching is lower for Mn^{2+} with a $K_{0.5}$ of 53.6 ± 27 μM at pH 5.5 and of 21 ± 5.7 μM at pH 7.6. These spectrofluorometric data confirm that Calcein can be used to evaluate changes in the intracellular concentration of Mn^{2+}, Fe^{2+} and Co^{2+}.

NPs cross the plasma membrane of *Xenopus laevis* oocytes

After having verified that we were able to detect an increase of divalent metal ions in the cytoplasm of *Xenopus* oocytes filled with Calcein, we have used them to reveal the possible permeation of NPs inside the cell. To this aim, we have chosen cobalt NPs in two different forms, metallic (Co^0) and oxide (Co_3O_4). Both NP forms undergo dissolution [1,11,34,35] releasing cobalt ions that can be detected by Calcein quenching. Therefore, we have exposed Calcein-filled oocytes to cobalt NPs and, as a control, to the corresponding ion.

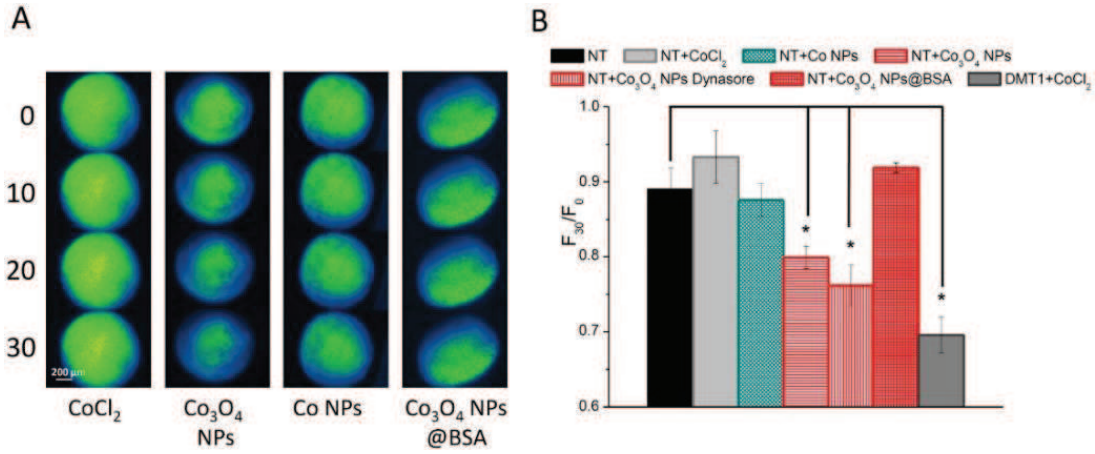

Figure 2. Calcein quenching in oocytes exposed to cobalt NPs. *A: Representative image series of non-transfected (NT) Calcein-injected oocytes exposed to $CoCl_2$ or different cobalt NPs for 0, 10, 20 and 30 min. B: Means of the fluorescence decay of 5 to 25 oocytes (obtained from 2 to 5 different batches). Decay is expressed as the fluorescence intensity at time 30 min over fluorescence intensity at time 0 (F_{30}/F_0). Note that quenching is statistically significant in NT oocytes exposed to bare Co_3O_4 NPs and in rDMT1 expressing oocytes exposed to $CoCl_2$ (positive control); moreover, the endocytosis blocker Dynasore does not change the quenching effect of Co_3O_4 NPs. Bars are ± SE; stars indicate a statistically significant (One-way ANOVA, $P<0.05$) difference with non exposed oocytes.*

In oocytes from different batches, Co_3O_4 NPs consistently induced a quenching of Calcein fluorescence (Fig. 2). This fluorescence decrease, although lower than that occurring in rDMT1 expressing oocytes exposed to $CoCl_2$ (Fig. 2 B), was significantly higher than that occurring in non-transfected oocytes either exposed or not exposed to $CoCl_2$. These results suggest that Co_3O_4 NPs interact with the plasma membrane of the oocyte, succeed in crossing it and, once in the cytoplasm, their partial dissolution causes the observed quenching activity. Indeed, cobalt ions and not NPs are able to interact with Calcein and quench its fluorescence. Co NPs, instead, did not cause a reduction of fluorescence (Fig. 2 B) suggesting to be unable to pass through the plasma membrane of the oocyte. This different behavior of cobalt and cobalt oxide NPs could be ascribed to different chemical and physical

characteristics of their surfaces. The importance of the surface structure of NPs in their interactions with cell membranes has been demonstrated comparing membrane penetration of two NPs that were coated with the same molecules, but arranged differently [19]. In our case, the normal spinel structure Co^{2+} Co_2^{3+} O_2^{2-} of Co_3O_4 NPs [36] might present a surface charge distribution capable to electrostatically interact with the negative charges which are present on the plasma membrane surface; indeed, Co_3O_4 NPs firmly bind, through electrostatic interactions, to negatively charged biomolecules such as heparin and carboxymethylchitosan [27,28]. Different cationic NPs have been shown to interact with lipid bilayers and cause their disruption [37], cationic gold NPs can enter cells by a non-endocytotic, energy-independent pathway [16] and cationic polystyrene NPs electrostatically interact with lipid bilayers causing deformation and poration, while anionic polystyrene NPs do not [14,38]. In this context, Lin and Alexander-Katz [18], with a coarse-grained simulation, have described the dynamics of cationic NP translocation through cell membranes and Nolte and colleagues [15] have modelled the transport of spherical metal oxide NPs across a lipid bilayer.

Protein corona impedes plasma membrane crossing

The importance of the surface characteristics of NPs in their interactions with the biological matter is well documented and is cardinal for their toxicity as well as for their use in nanomedicine. We have, therefore, modified the surface characteristics of Co_3O_4 NPs by letting them to adsorb bovine serum albumin (BSA). This is known to create, around the NP, a protein corona, which is capable to modify NP-membrane interaction [39,40] as also suggested by computer simulations [17]. In our experiments, BSA coated Co_3O_4 NPs (Co_3O_4 NP@BSA) do not cause fluorescence quenching (Fig. 2).

These results suggest that a "protein corona" effect can prevent or significantly reduce the interactions between NPs and the oocyte membrane blocking or limiting the passage of NPs into the cytoplasm. These findings are in agreement with experiments where the interaction of cationic polystirene NPs with artificial lipid bilayers were eliminated

with serum proteins [38]. Alternatively, rather than impeding NP entry into the oocytes, the protein corona could have stabilized NPs against dissolution, preventing them, once in the cytoplasm, from releasing Calcein-quenching ions. To rule out this possibility, we have performed *in vitro* experiments where NPs, which were previously exposed to BSA, were tested for their ability to quench Calcein. Since no significant differences were observed, we think that BSA treatment of NPs, although capable to generate a protein corona, was not able to prevent dissolution.

Endocytosis does not seem to be responsible of Co_3O_4 NP entry

Some of our results could also be explained by endocytosis followed by NP escape from the endosomal compartment to the cytoplasm. To exclude this possibility, we have used two different approaches: in the first one, we have repeated quenching experiments on oocytes treated with Dynasore, an endocytosis inhibitor that has been used several times to block membrane recycle in *Xenopus* oocytes[41]; in the second one, we have verified whether or not NP exposure might have elicited endocytosis by optical and electron microscopy.

Dynasore is a cell-permeable molecule that inhibits the GTPase activity of dynamin which in turn blocks dynamin-dependent endocytosis [42]. Quenching experiments were repeated in oocytes that were previously incubated for 24 h in 40 μM Dynasore. As shown in Fig. 2 B, there are no significant differences in the quenching activity of Co_3O_4 NPs between oocytes that were treated with Dynasore and oocytes that were not.

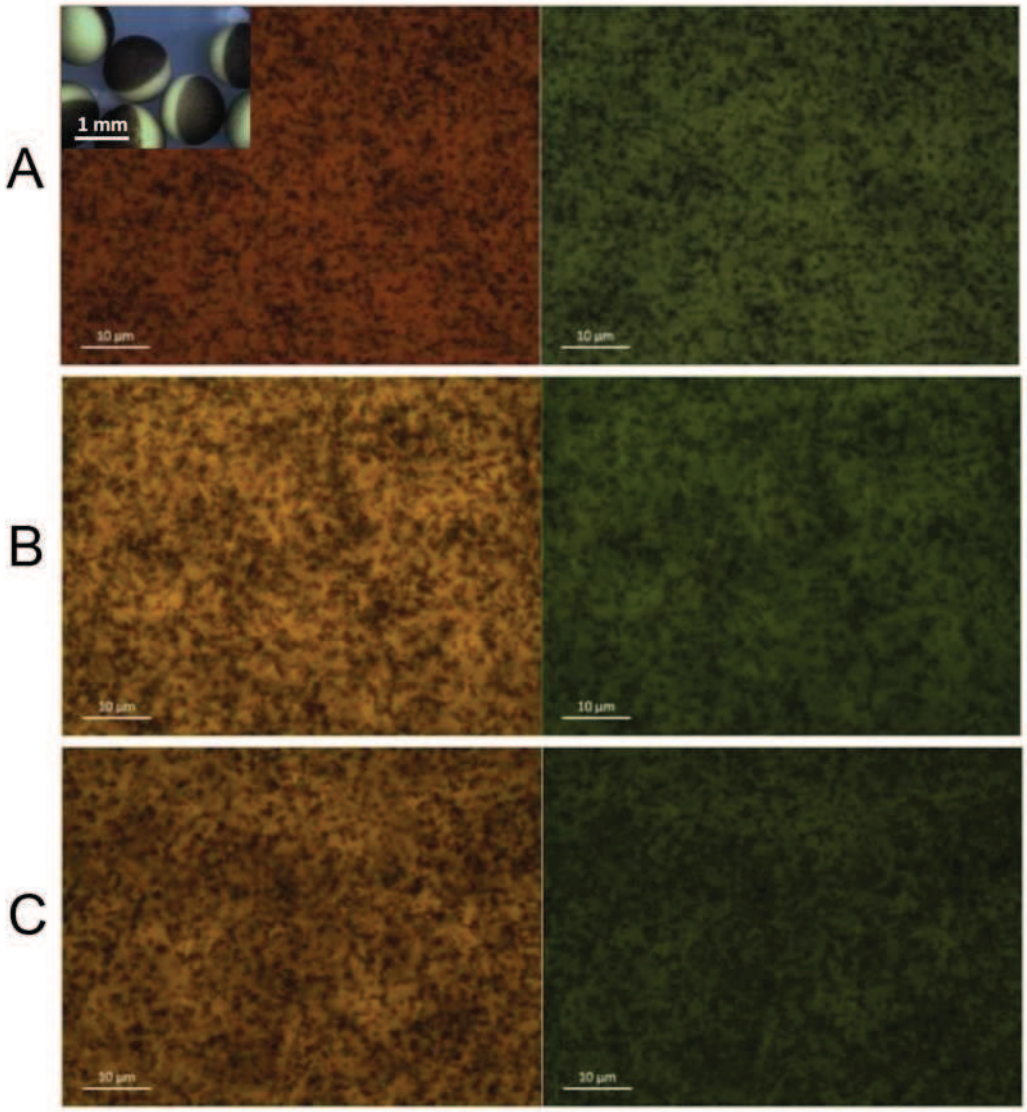

Figure 3. Endocytosis is not involved in NP quenching activity. *In the inset, few fully grown oocytes are visible; note the presence of a pigmented pole (denominated animal pole) and of an unpigmented one (denominated vegetal pole). After fixation, a spherical cap is hand sliced with a razor blade, placed on a glass slide under a coverslip and observed with a 63X oil immersion objective from above. A, B, and C: Bright field (left) and the corresponding FITC filter (right) images of oocytes exposed to 1 mg/mL Lucifer Yellow CH. (A) control oocyte; (B) oocyte exposed to 0.1 mg/mL Co_3O_4 NPs and (C) oocyte incubated 24 h with 40 µM Dynasore and exposed to 0.1 mg/mL Co_3O_4 NPs. In bright field images, pigment granules, which are present in the cortex of the oocyte, are clearly visible as dark brown dots indicating that we are observing the*

oocyte animal pole. In the corresponding FITC filter images, no fluorescent vesicles are visible indicating no endocytotic activity.

Dynasore, however, does not halt all the endocytotic routes. Therefore, to reveal the possible formation of endocytotic vesicles after NP exposure, we have used Lucifer Yellow CH, a water-soluble and membrane-impermeable fluorescent dye; it contains a carbohydrazide (CH) group that allows it to be covalently linked to the surrounding biomolecules by aldehyde fixation. Fully grown oocytes were exposed to the tracer dye in presence and in absence of NPs for 30 min, fixed and observed under a fluorescence microscope with a 63X oil immersion objective. As shown in Figure 3 A, B and C, no fluorescent vesicles are visible indicating that there is minimal or no endocytosis in the tested conditions. Lucifer Yellow CH had been previously shown to be effective in tracing endocytosis occurring immediately after cortical granule exocytosis during *Xenopus* egg fertilization [43,44]. Likewise, treated samples were prepared also for transmission electron microscopy and, notwithstanding a careful observation of the oocyte cortex, we could not find any NP carrying endocytotic vesicle among the pigment granules and the tightly packed cortical granules which characterise the oocyte cortex (data not shown).

No endogenous divalent metal ion transporters are present on the oocyte plasma membrane

To better characterize our system, and also to rule out possible unpredicted artefacts, we have performed further experiments which are shown in Figure 4. We have confirmed by electrophysiology that no endogenous divalent metal ion transporters are present on the oocyte plasma membrane. Indeed, as shown in Figure 4 A, with two electrode voltage clamp no currents were recorded in the presence of $CoCl_2$, $MnCl_2$; similarly, no currents were recorded also in the presence of Co_3O_4 and Co NPs, which are known to readily dissolve releasing ions. This is in agreement with the results shown in Figure 2 where there was not fluorescence reduction in non-transfected oocytes placed in solution containing $CoCl_2$.

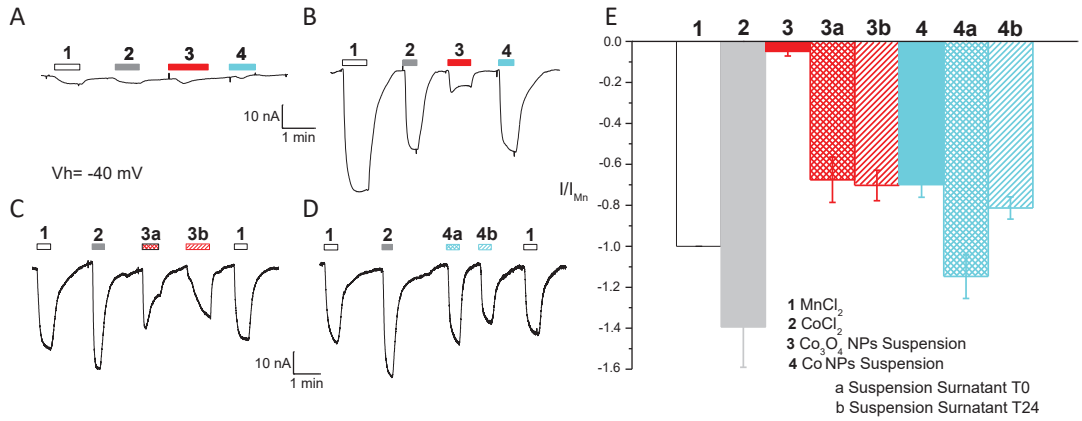

Figure 4. Two electrode voltage-clamp of Xenopus oocytes*. Inward currents elicited by solutions and NP suspensions in NT (A) and rDMT1 transfected (B, C and D) representative oocytes. Oocytes were clamped at a holding potential of -40 mV and exposed to $MnCl_2$ (1) and $CoCl_2$ (2) solutions, to Co_3O_4 (3) and Co (4) NP suspensions and to their surnatants obtained at time 0 h (a) and 24 h (b). E: Current mean values (± SE) obtained by subtracting from the current in the presence of the substrate, the current in its absence and normalizing to the Mn^{2+} current, a reference for divalent metal transporters in electrophysiological studies 6 to 12 oocytes from 4 batches.*

Co, Co_3O_4 and BSA coated Co_3O_4 NPs release ions

Conversely, when rDMT1 transfected oocytes were tested in the presence of $CoCl_2$ and $MnCl_2$, inward currents were recorded (Fig. 4 B), indicating an electrogenic transport of ions across the plasma membrane. Similarly, inward currents were recorded also in the presence of Co_3O_4 and Co NPs, indicating that both NPs, although in a different amount, were releasing ions. To confirm the release of Co ions from NPs, we have performed a set of experiments (Fig. 4 C and D) exposing rDMT1 transfected oocytes to the surnatants of suspensions of Co_3O_4 and Co NPs and obtaining the expected inward currents. Moreover, we added BSA exposed NPs to rDMT1 expressing oocytes and, in all the tested conditions, we observed a current similar to that evoked by the same NPs that were not exposed to BSA (data not shown). These data rule out the possibility that BSA might have a role in preventing dissolution in our experiments.

NPs do not impair oocyte plasma membrane integrity

To understand whether or not Co_3O_4 NPs damage oocyte plasma membrane, we have measured membrane resistence by two electrode voltage clamp. If the NPs damaged the oocyte membrane, we would expect a change in membrane permeability and the entrance of Ca^{2+} ions that, in *Xenopus* oocytes, activate Ca^{2+}-gated chloride channels [45] which, at potentials more positive than the chloride reversal potential, give rise to an outward current [46]. As shown in Figure 5, we applyed a voltage ramp to oocytes which were previously exposed to Co_3O_4 NPs for 30 min and we did not observe a change in membrane resistance. Conversely, after A23187 ionophore addition [45,47], a large chloride current appeared, expecially at more positive potentials, due to the activation of the Ca^{2+}-gated chloride channels. Therefore, we think that NP entry does not cause injury to the plasma membrane.

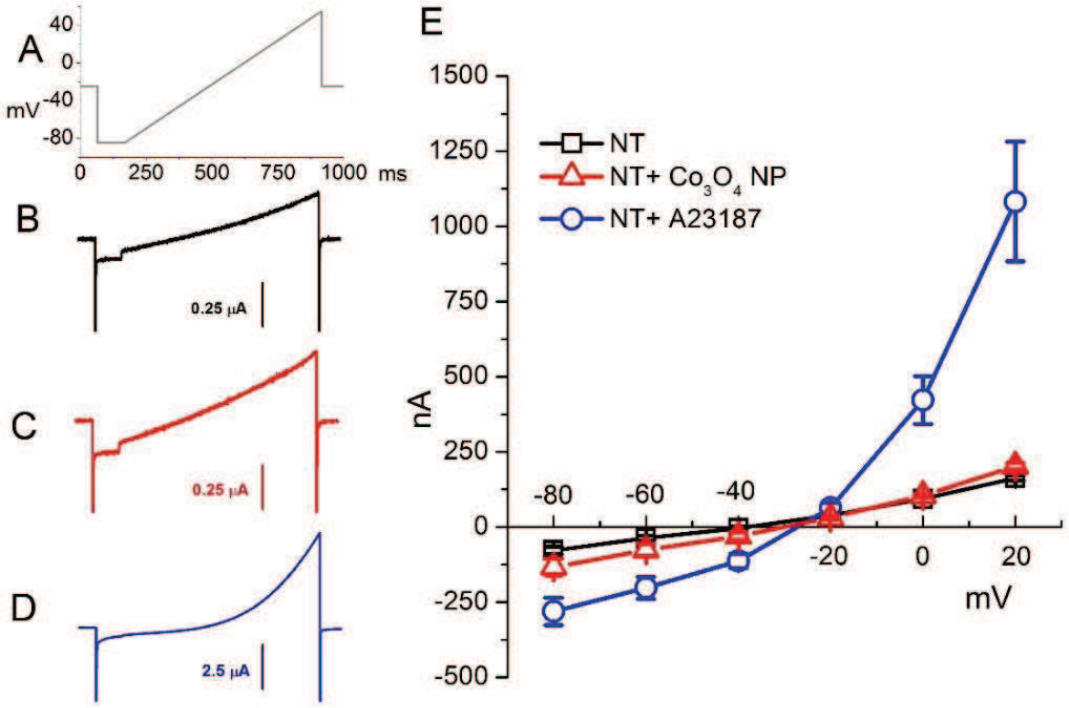

Figure 5. Measure of membrane resistence of Xenopus oocytes*. Ramp (from - 85 to + 25 mV) protocols (A) were applied in non transfected oocytes starting from the holding potential of -25 mV. Representative currents elicited by the protocol in not-exposed oocytes (black line in B), exposed to* Co_3O_4 *NP*

suspensions (red line in C) and perfused with ionophore A23187 (blue line in D). Current mean values at -80, -60, -40, -20, 0 and + 20 mV (± SE) obtained from at least 12 oocytes (from 2 different batches) are plotted in E.

In conclusion, we have demonstrated that NPs can cross cytomembranes with no evident damage to cell integrity. The canonical way of NPs to be uptaken by cells is endocytosis that makes NPs to gain access to the endosomal compartment. The NP capability to cross lipid bilayers exposes further cellular compartments to NPs. We have learned that the capability of Co_3O_4 NPs to cross the oocyte plasma membrane is not paralleled by that of Co NPs and that the crossing of Co_3O_4 NPs can be prevented by a protein corona. Moreover, we have set up a system that can be of help in evaluating the effects of different functionalizations on NP ability to cross cytomembranes. Finally, we have confirmed that Co NPs and, to a less extent, Co_3O_4 NPs release ions in the environment where they are present, i.e., in the extracellular solution as well as in the cytoplasm. Dissolution, indeed, is a phenomenon one should take into account not only for nanotoxicological studies, but also in nanomedicine or in food and feed fortification.

Materials and Methods

Solutions

ND96 solution had the following composition (in mM): NaCl 96, KCl 2, $MgCl_2$ 1, HEPES 5, pH 7.6; modified Barth's saline (MBS) solution had the following composition (in mM): NaCl 88, KCl 1, $NaHCO_3$ 2.4, HEPES 15, $Ca(NO_3)_2$ 0.30, $CaCl_2$ 0.41, $MgSO_4$ 0.82, sodium penicillin 10 μg/mL, streptomycin sulphate 10 μg/mL, gentamycin sulphate 100 μg/mL, pH 7.6; external control solution contained (in mM): NaCl 98; $MgCl_2$, 1; $CaCl_2$, 1.8, HEPES or MES 5, pH 7.6 or 5.5; intracellular solution contained (in mM): KCl 130, NaCl 4, $MgCl_2$ 1.6, EGTA 5, HEPES 10, glucose 5, pH 7.6. The final pH values of 5.5 or 7.6 were adjusted with HCl and NaOH.

Oocyte collection and preparation

Oocytes were obtained from adult *Xenopus laevis* females. Animals were anaesthetised in 0.1 % (w/v) MS222 (tricaine methansulfonate) solution in tap water and portions of the ovary were removed through an incision on the abdomen. The oocytes were treated with 1 mg/mL collagenase (Sigma Type IA) in ND96 calcium free for at least 1 h at 18 °C. Healthy and fully grown oocytes were selected and stored at 18°C in MBS solution[48]. The oocytes to be transfected with the cDNA coding for rDMT1 were injected with 25 ng of cRNA in 50 nl of water, the day after the removal, using a manual microinjection system (Drummond Scientific Company, Broomall, PA) and incubated at 18 °C for 3-4 days before electrophysiological or fluorescence experiments. The experiments were carried out according to the institutional and national ethical guidelines (permit nr. 05/12).

NP preparation

Oocytes were exposed to zerovalent (Co, 28 nm, IOLITEC, Salzstrasse 184, D-74076 Heilbronn) and oxide (Co_3O_4, < 50 nm TEM determined, Sigma-Aldrich) cobalt NPs. 1 mg/mL Stock suspensions were prepared in deionised water. 0.1 mL of stock suspension was added to the test chamber containing 0.9 mL of external control solution (pH 7.6). Suspensions were carefully sonicated before addition to the test chamber.

For dissolution experiments, stock suspensions of Co and Co_3O_4 NPs were prepared to have a 10 mM concentration in terms of cobalt (i.e., 5.9 mg / 10 mL for Co NPs and 8 mg / 10 mL for Co_3O_4 NPs). Stock suspensions were sonicated for 15 min and 0.5 mL of each suspension was added to a Petri dish containing 24.5 mL of deionised water or of 1 mg/mL BSA to reach a final cobalt concentration of 200 μM.

After 1 and 24 h, 15 mL were collected from each Petri dish and centrifuged for 5 min at 8000 g at 10 °C. The surnatant was transferred in a new tube and the procedure was repeated for 4 times. Finally, 8 mL of surnatant from the last centrifugation were ultracentrifuged at 300 000 g at 4 °C for 2 h. The surnatant was collected and filtered (0.22 μm

syringe filter). The resulting surnatant was diluted 1:1 in a 2X external control solution at pH 5.5 and used in electrophysiological experiments.

Single Oocyte Fluorescence Assay (SOFA)

Untransfected oocytes and oocytes transfected with cRNA encoding rDMT1 were injected with a 50 nL drop of a 25 μM Calcein in intracellular solution. The nominal volume of a 1.2 mm diameter oocyte is 1 μL; therefore, a 50 nL injected drop will be diluted 20 times. The exact dilution factor is, however, difficult to establish, since not all the theoretical volume may be available for free diffusion [49]. Following Calcein injection, the oocytes were placed in external control solution solution at pH 5.5 or 7.6 containing or not, divalent metals at a final concentration of 0.1 mM.

For NP experiments, Co NPs and Co_3O_4 NPs were added to the testing solution to a final concentration of 0.1 mg/mL (pH 7.6). All experiments were carried out at room temperature. To block the endocytotic pathway, oocytes were incubated in 40 μM Dynasore (Sigma-Aldrich) for 24 h before the experiment.

Images of single oocytes were acquired every 2 min for 30 min with a fluorescence microscope (AxioVert 200, Carl Zeiss with a 4x objective, COLIBRI fluorescence filters, 470 nm excitation - 515 to 565 nm emission) equipped with CCD camera (Axiocam ICM1, Carl Zeiss).

Fluorescence and transmission electron microscopy

To assess endocytosis, oocytes were incubated for 30 min in external control solution at pH 7.6 with 1 mg/mL Lucifer Yellow CH (Sigma-Aldrich). Negative controls, oocytes exposed to 0.1 mg/mL Co_3O_4 NP, and oocytes pretreated with Dynasore and exposed to 0.1 mg/mL Co_3O_4 NPs were washed 3 times in cold (4°C) external control solution at pH 7.6 and fixed in 4% paraformaldehyde for two days. Oocytes were washed 3 times in cold external control solution, cut in 2 halves which were placed on a slide and covered with slips. Samples were observed with a fluorescence microscope (Axiophot, Carl Zeiss) with a 63x oil

ojective. Bright field and FITC filter images were taken using a CCD camera (Discovery C30, TiEsselab).
For TEM, oocytes were fixed in 4% paraformaldehide and 2% glutaraldehide in 0.1 M sodium cacodylate buffer (pH 7.4) for 24h at 4°C and stored in 0.1 M sodium cacodylate buffer (pH 7.4) at 4°C. Specimens were postfixed in 1% OsO_4 in 0.1M sodium cacodylate buffer (pH 7.4), dehydrated in ethanol and embedded in Epon-Araldite. For ultrastructural studies, thin sections were cut using a Reichert Ultracut-S-Ultratome ultramicrotome (Leica, Nussloch, Germany), collected on 300 mesh copper grids, counterstained with uranyl acetate and lead citrate and examined under a Jeol 1010 electron microscope operating at 90 KV (Jeol, Tokyo, Japan).

Spectrofluorometry

Calcein quenching by divalent metal ions were measured in external control solution at pH 5.5 and 7.6 using a Jasco FP-750 fluorometer with excitation at 470 nm. The spectra of 2.5 μM Calcein alone or mixed with iron, manganese and cobalt ions at different concentrations were acquired in the 490 to 560 nm range. Experiments at pH 7.6 with $FeCl_2$ were performed in presence of 1 mM ascorbic acid to maintain iron in a reduced form.

Electrophysiology

The two-electrode voltage-clamp technique was performed with an Oocyte Clamp OC-725B (Warner Instruments, Hamden, CT, USA). Intracellular glass microelectrodes, filled with 3 M KCl, had tip resistances in the 0.5 - 4 MΩ range. Agar bridges (3% agar in 3 M KCl) connected the bath electrodes to the experimental chamber. The holding potential (V_h) was - 40 mV for the recording of transport currents and - 25 mV for the measurements of membrane resistance. Currents associated to membrane transport of divalent ions were recorded in oocytes perfused with external control solution at pH 5.5 in the absence or in the presence of the indicated divalent metal ions, NPs and NP surnatants. To check for the possible presence of membrane damage,

the oocyte conductances were tested applying a 1-s long protocol with a voltage ramp from - 85 to + 55 mV. Positive controls of membrane conductance alteration were obtained perfusing oocytes with 10 μM ionophore A-23187 (Sigma-Aldrich). WinWCP version 4.4.6 (J. Dempster, University of Strathclyde, UK) or Clampex 10.2 (Molecular Devices, Sunnyvale, CA, USA, www.moleculardevices.com) were used to run the experiments.

Data analysis

Data were analysed using Clampfit 10.2 software (Molecular Devices, Sunnyvale, CA, USA, www.moleculardevices.com) while OriginPro 8.0 (OriginLab Corp., Northampton, MA, USA, www.originlab.com) was used for statistics and figure preparation. Transport currents were determined by subtracting the records in the absence of a substrate from the corresponding ones in its presence. Fluorescence decay images were analysed with ImageJ (Rasband, W.S., ImageJ, U. S. National Institutes of Health, Bethesda, Maryland, USA, http://imagej.nih.gov/ij/, 1997-2015). For F_t/F_0 quantification, the fluorescence intensity at time 0 (F_0) and at subsequent times (F_t) was calculated in the entire area of the oocyte.

Acknowledgements

This work was supported by Fondazione Cariplo (2013-1052). We thank Dr. Raffella Cinquetti and Ms Arianna Parnigoni for their help in performing experiments.

Additional information

Competing financial interests.

The authors declare no competing financial interests.

Authors contribution

E.B. and R.G planned and designed the experiments, D.Z. performed the experiments and prepared the figures, E.B. and G.B. wrote the manuscript. All authors reviewed the manuscript.

References

1 Papis, E. et al. Engineered cobalt oxide nanoparticles readily enter cells. Toxicology letters 189, 253-259, doi:10.1016/j.toxlet.2009.06.851 (2009).

2 Contreras, J. et al. Intracellular Uptake and Trafficking of Difluoroboron Dibenzoylmethane-Polylactide Nanoparticles in HeLa Cells. Acs Nano 4, 2735-2747, doi:DOI 10.1021/nn901385y (2010).

3 Bregar, V. B., Lojk, J., Sustar, V., Veranic, P. & Pavlin, M. Visualization of internalization of functionalized cobalt ferrite nanoparticles and their intracellular fate. Int J Nanomedicine 8, 919-931, doi:10.2147/IJN.S38749 (2013).

4 Shang, L., Nienhaus, K. & Nienhaus, G. U. Engineered nanoparticles interacting with cells: size matters. Journal of nanobiotechnology 12, 5-5, doi:10.1186/1477-3155-12-5 (2014).

5 Fröhlich, E. The role of surface charge in cellular uptake and cytotoxicity of medical nanoparticles. International journal of nanomedicine 7, 5577-5591, doi:10.2147/IJN.S36111 (2012).

6 Mickler, F. M. et al. Tuning Nanoparticle Uptake: Live-Cell Imaging Reveals Two Distinct Endocytosis Mechanisms Mediated by Natural and Artificial EGFR Targeting Ligand. Nano Letters 12, 3417-3423, doi:DOI 10.1021/nl300395q (2012).

7 Castellini, C. et al. Long-term effects of silver nanoparticles on reproductive activity of rabbit buck. Systems biology in reproductive medicine 60, 143-150, doi:10.3109/19396368.2014.891163 (2014).

8 Coccini, T. et al. Gene Expression Changes in Rat Liver and Testes after Lung Instillation of a Low Dose of Silver Nanoparticles. Journal of Nanomedicine & Nanotechnology 5, doi:10.4172/2157-7439.1000227 (2014).

9 Ye, D. et al. Nanoparticle accumulation and transcytosis in brain endothelial cell layers. Nanoscale 5, 11153-11165, doi:10.1039/c3nr02905k (2013).

10 Gliga, A. R., Skoglund, S., Wallinder, I. O., Fadeel, B. & Karlsson, H. L. Size-dependent cytotoxicity of silver nanoparticles in human lung cells: the role of cellular uptake, agglomeration and

Ag release. Part Fibre Toxicol 11, 11, doi:10.1186/1743-8977-11-11 (2014).
11 Ortega, R. et al. Low-solubility particles and a Trojan-horse type mechanism of toxicity: the case of cobalt oxide on human lung cells. Particle and fibre toxicology 11, 14-14, doi:10.1186/1743-8977-11-14 (2014).
12 Sabella, S. et al. A general mechanism for intracellular toxicity of metal-containing nanoparticles. Nanoscale 6, 7052-7061, doi:10.1039/c4nr01234h (2014).
13 Cattaneo, A. G. et al. Nanotechnology and human health: risks and benefits. Journal of applied toxicology : JAT 30, 730-744, doi:10.1002/jat.1609 (2010).
14 Li, S. & Malmstadt, N. Deformation and poration of lipid bilayer membranes by cationic nanoparticles. Soft Matter 9, 4969-4976, doi:DOI 10.1039/c3sm27578g (2013).
15 Nolte, T. M., Kettler, K., Meesters, J. A., Hendriks, A. J. & van de Meent, D. A semi-empirical model for transport of inorganic nanoparticles across a lipid bilayer: implications for uptake by living cells. Environmental toxicology and chemistry / SETAC 34, 488-496, doi:10.1002/etc.2812 (2015).
16 Taylor, U. et al. Nonendosomal cellular uptake of ligand-free, positively charged gold nanoparticles. Cytometry. Part A : the journal of the International Society for Analytical Cytology 77, 439-446, doi:10.1002/cyto.a.20846 (2010).
17 Ding, H.-m. & Ma, Y.-q. Computer simulation of the role of protein corona in cellular delivery of nanoparticles. Biomaterials 35, 8703-8710, doi:10.1016/j.biomaterials.2014.06.033 (2014).
18 Lin, J. Q. & Alexander-Katz, A. Cell Membranes Open "Doors" for Cationic Nanoparticles/Biomolecules: Insights into Uptake Kinetics. Acs Nano 7, 10799-10808, doi:DOI 10.1021/nn4040553 (2013).
19 Verma, A. et al. Surface-structure-regulated cell-membrane penetration by monolayer-protected nanoparticles. Nat Mater 7, 588-595, doi:10.1038/nmat2202 (2008).
20 Wang, H. et al. In situ oxidation of carbon-encapsulated cobalt nanocapsules creates highly active cobalt oxide catalysts for hydrocarbon combustion. Nature Communications 6 (2015).

21 Mondal, A., Adhikary, B. & Mukherjee, D. Room-temperature synthesis of air stable cobalt nanoparticles and their use as catalyst for methyl orange dye degradation. Colloid Surface A 482, 248-257 (2015).

22 Wu, L. H. et al. Stable Cobalt Nanoparticles and Their Monolayer Array as an Efficient Electrocatalyst for Oxygen Evolution Reaction. Journal of the American Chemical Society 137, 7071-7074 (2015).

23 Smolyaninova, V. N., Yost, B., Lahneman, D., Narimanov, E. E. & Smolyaninov, I. I. Self-assembled tunable photonic hyper-crystals. Scientific Reports 4 (2014).

24 Jun, Y.-W., Seo, J.-W. & Cheon, J. Nanoscaling laws of magnetic nanoparticles and their applicabilities in biomedical sciences. Accounts of chemical research 41, 179-189 (2008).

25 Bava, A. et al. D-amino acid oxidase-nanoparticle system: a potential novel approach for cancer enzymatic therapy. Nanomedicine (London, England) 8, 1797-1806, doi:10.2217/nnm.12.187 (2013).

26 Cappellini, F. et al. New synthesis and biodistribution of the D-amino acid oxidase-magnetic nanoparticle system. Future Science OA, doi:10.4155/fso.15.67 (2015).

27 Bava, A. et al. Heparin and carboxymethylchitosan metal nanoparticles: an evaluation of their cytotoxicity. BioMed research international 2013, 314091-314091, doi:10.1155/2013/314091 (2013).

28 Vismara, E. et al. Non-covalent synthesis of metal oxide nanoparticle-heparin hybrid systems: a new approach to bioactive nanoparticles. Int J Mol Sci 14, 13463-13481, doi:10.3390/ijms140713463 (2013).

29 Gunshin, H. et al. Cloning and characterization of a mammalian proton-coupled metal-ion transporter. Nature 388, 482-488, doi:Doi 10.1038/41343 (1997).

30 Au, C., Benedetto, A. & Aschner, M. Manganese transport in eukaryotes: The role of DMT1. Neurotoxicology 29, 569-576, doi:DOI 10.1016/j.neuro.2008.04.022 (2008).

31 Mackenzie, B. & Hediger, M. A. SLC11 family of H+-coupled metal-ion transporters NRAMP1 and DMT1. Pflug Arch Eur J Phy 447, 571-579, doi:DOI 10.1007/s00424-003-1141-9 (2004).

32 Bressler, J. P., Olivi, L., Cheong, J. H., Kim, Y. & Bannon, D. Divalent metal transporter 1 in lead and cadmium transport. Ann Ny Acad Sci 1012, 142-152, doi:DOI 10.1196/annals.1306.011 (2004).

33 Buracco, S. et al. Dictyostelium Nramp1, which is structurally and functionally similar to mammalian DMT1 transporter, mediates phagosomal iron efflux. J Cell Sci 128, 3304-3316, doi:10.1242/jcs.173153 (2015).

34 Sabbioni, E. et al. Interaction with culture medium components, cellular uptake and intracellular distribution of cobalt nanoparticles, microparticles and ions in Balb/3T3 mouse fibroblasts. Nanotoxicology 8, 88-99, doi:10.3109/17435390.2012.752051 (2014).

35 Gornati, R. et al. Zerovalent Fe, Co and Ni nanoparticle toxicity evaluated on SKOV-3 and U87 cell lines. Journal of applied toxicology : JAT, doi:10.1002/jat.3220 (2015).

36 Xiao, J. et al. Surface structure dependent electrocatalytic activity of Co(3)O(4) anchored on graphene sheets toward oxygen reduction reaction. Sci Rep 3, 2300, doi:10.1038/srep02300 (2013).

37 Leroueil, P. R. et al. Wide varieties of cationic nanoparticles induce defects in supported lipid bilayers. Nano Lett 8, 420-424, doi:10.1021/nl0722929 (2008).

38 Lu, B., Smith, T. & Schmidt, J. J. Nanoparticle-lipid bilayer interactions studied with lipid bilayer arrays. Nanoscale 7, 7858-7866, doi:10.1039/c4nr06892k (2015).

39 Chen, R. et al. Interaction of lipid vesicle with silver nanoparticle-serum albumin protein corona. Appl Phys Lett 100, 13703-137034, doi:10.1063/1.3672035 (2012).

40 Lesniak, A. et al. Effects of the presence or absence of a protein corona on silica nanoparticle uptake and impact on cells. ACS Nano 6, 5845-5857, doi:10.1021/nn300223w (2012).

41 Rousset, M. et al. Regulation of neuronal high-voltage activated Ca(V)2 Ca(2+) channels by the small GTPase RhoA.

Neuropharmacology 97, 201-209, doi:10.1016/j.neuropharm.2015.05.019 (2015).
42 Kirchhausen, T., Macia, E. & Pelish, H. E. Use of dynasore, the small molecule inhibitor of dynamin, in the regulation of endocytosis. Methods Enzymol 438, 77-93, doi:10.1016/S0076-6879(07)38006-3 (2008).
43 Peres, A. & Bernardini, G. The effective membrane capacity of Xenopus eggs: Its relations with membrane conductance and cortical granule exocytosis. Pflugers Archiv European Journal of Physiology 404, 266-272 (1985).
44 Bernardini, G., Ferraguti, M. & Stipani, R. Fertilization induces endocytosis in Xenopus eggs. Cell differentiation 21, 255-260 (1987).
45 Centinaio, E., Bossi, E. & Peres, A. Properties of the Ca(2+)-activated Cl- current of Xenopus oocytes. Cell Mol Life Sci 53, 604-610 (1997).
46 Bertram, S., Cherubino, F., Bossi, E., Castagna, M. & Peres, A. GABA reverse transport by the neuronal cotransporter GAT1: influence of internal chloride depletion. American journal of physiology Cell physiology 301, C1064-1073 (2011).
47 Boton, R., Dascal, N., Gillo, B. & Lass, Y. Two calcium-activated chloride conductances in Xenopus laevis oocytes permeabilized with the ionophore A23187. The Journal of physiology 408, 511-534 (1989).
48 Bossi, E., Fabbrini, M. S. & Ceriotti, A. Exogenous protein expression in Xenopus oocytes: basic procedures. Methods in molecular biology 375, 107-131, doi:10.1007/978-1-59745-388-2_6 (2007).
49 Zeuthen, T., Zeuthen, E. & Klaerke, D. A. Mobility of ions, sugar, and water in the cytoplasm of Xenopus oocytes expressing Na(+)-coupled sugar transporters (SGLT1). The Journal of physiology 542, 71-87 (2002).

Chapter 3

Iron oxide nanoparticles can cross plasma membranes

Originally published in Scientific Reports (2017)

Daniele Zanella[1], Elena Bossi[1,2]*, Rosalba Gornati[1,2], Carlos Bastos[3], Nuno Faria[3] and Giovanni Bernardini[1,2]

[1]Department of Biotechnology and Life Sciences, University of Insubria; Via Dunant 3, I-21100 Varese, Italy

[2]Interuniversity Center "The Protein Factory", Politecnico di Milano and Università dell'Insubria, Via Mancinelli 7, I-20131 Milan, Italy

[3]Department of Veterinary Medicine, University of Cambridge, Madingley Road, Cambridge CB3 OES, UK

Abstract

Iron deficiency is a major global public health problem despite decades of efforts with iron supplementation and fortification. The issue lies on the poor tolerability of the standard of care soluble iron salts, leading to non-compliance and ineffective correction of iron-deficiency anaemia. Iron nanoformulations have been proposed to fortify food and feed to address these issues. Since it was just postulated that some nanoparticles (NPs) might cross the plasma membrane also by a non-endocytotic pathway gaining direct access to the cytoplasm, we have studied iron NP uptake under this perspective. To this aim, we have used a recently tested protocol that has proven to be capable of following the cytoplasmic changes of iron concentration dynamics and we have demonstrated that iron oxide NPs, but not zerovalent iron NPs nor iron oxide NPs that were surrounded by a protein corona, can cross plasma membranes. By electrophysiology, we have also shown that a

small and transient increase of membrane conductance parallels NP crossing of plasma membrane.

Introduction

Iron deficiency is a major global public health problem, common in adolescence, in menstruating women and in elderly, and particularly evident in developing countries. In addition, several diseases cause iron deficiency, including intestinal parasite infections, malaria, gastric and duodenal ulcers, gastrointestinal cancer and rare mutations in genes encoding ion transporters[1,2]. Iron deficiency can be efficaciously controlled by iron supplementation or food fortification. Unfortunately, the water-soluble and bioavailable ferrous sulphate, fumarate or gluconate, that are currently used therapeutically, affect the gastrointestinal tract with significant side effects such as constipation, diarrhoea and nausea[3]; moreover, iron salts cause unacceptable changes in the colour and taste of foods[4]. In contrast, poorly water-soluble compounds cause fewer sensory changes, but present limited bioavailability. Recently, the use of NPs in iron supplementation and fortification has been suggested since their use may combine high bioavailability, good product stability, limited side effects and absence of changes of taste and colour of the fortified foods[5-8]. Moreover, *in vitro* and *in vivo* experiments have shown that iron NPs can be considered safe[9,10]. Nanoformulations have also found their way into the fortification of animal feeds[11-13]. Ferritin, which is well absorbed[14], is itself composed of an iron oxide nanocore surrounded by a protein shell and, recently, a nanoparticulate mimetic of the ferritin core was proposed as a potentially side effect-free form of cheap supplemental iron[15].

In the gut lumen, dietary iron is present as heme and non-heme (inorganic) iron; inorganic iron can be found in two oxidation states: ferrous (Fe^{2+}) iron and, predominantly, as ferric (Fe^{3+}) iron. Ferric iron is

reduced to ferrous iron by duodenal cytochrome b, an enzyme present on the plasma membrane of the enterocyte brush border; Fe^{2+} is eventually transported into the cytoplasm by means of the divalent metal transporter DMT1[1,16] Nanoparticulate iron might follow a different route to access enterocyte cytoplasm. Powell and colleagues[15,17-19] have suggested that nanoparticulate iron, like ferritin[20], enters cells by endocytosis reaching the cytoplasm by lysosomal escape. Endocytosis is, indeed, the canonical mechanism by which NPs are known to be up-taken[21], but it might not be the only one. The work on ferritin core mimetics focused on highly disperse NPs with an outer layer of charged short-chain carboxylates[15], however, poorly charged or 'naked' (i.e. lacking an outer coating) NPs may behave differently. In effect, it has been recently postulated that some metal NPs might also cross the plasma membrane by a non-endocytotic pathway[22-28] gaining a direct access to the cytoplasm. Indeed, we have recently confirmed this pathway for cobalt oxide NPs. This pathway, which involves perforation of the lipid bilayer, is usually poorly considered and challenges the idea of non-permeability of membranes to hydrophilic molecules or supramolecular structures.

To verify this possibility, we have studied commercially available iron based NPs that do not comprise a dispersing outer layer. We have characterized their size and surface charge and, through a recently developed protocol, we have followed the cytoplasmic concentration dynamics of iron, demonstrating that iron oxide NPs, but not zerovalent iron NPs, were up-taken. We have also shown that the NP crossing of the plasma membrane is accompanied by a transient increase of membrane conductance, but this crossing did not occur when the iron oxide NPs were aggregated or surrounded by a protein corona.

Results and Discussion

Calcein and *Xenopus laevis* oocytes for monitoring intracellular iron increase

As a preliminary step, we have tested the ability of Calcein to detect intracellular iron concentration increase in fully-grown *Xenopus laevis* oocytes. Fully-grown oocytes are large cells arrested at prophase of meiosis I, which provide a simple system for the study of membrane transport. Calcein is a divalent metal ion chelating fluorochrome whose fluorescence, at physiological pH, is strongly quenched by cobalt, nickel, copper, iron and manganese divalent cations.

To this aim, we have prepared transfected *Xenopus* oocytes expressing the Divalent Metal ion Transporter 1 from rat (rDMT1). This membrane protein is a proton dependent transporter of divalent metal ions such as Fe^{2+}, Mn^{2+}, Co^{2+}, Ni^{2+} and Cd^{2+} [29-32]. We have performed voltage-clamp experiments in transfected (i.e., injected with DMT1 cRNA) and in non-transfected (control) oocytes exposed to $FeCl_2$, both at pH 5.5 and 7.6. We have calculated transport currents as the difference between the currents recorded in the presence and in the absence of 100 μM $FeCl_2$ in the external solution. As shown by the current-voltage (I-V) relationship (Figure 1A), no transport currents were recorded in non-transfected (control) oocytes when exposed to iron ions confirming the absence of endogenous electrogenic Fe^{2+} transporters in the oocyte plasma membrane. Conversely, in rDMT1 transfected oocytes, at pH 5.5, but not at pH 7.6, the presence of $FeCl_2$ in the extracellular solution elicited large inward currents at negative potentials. This indicates that, at pH 5.5, a transmembrane transport of iron ions occurs in rDMT1 transfected oocytes.

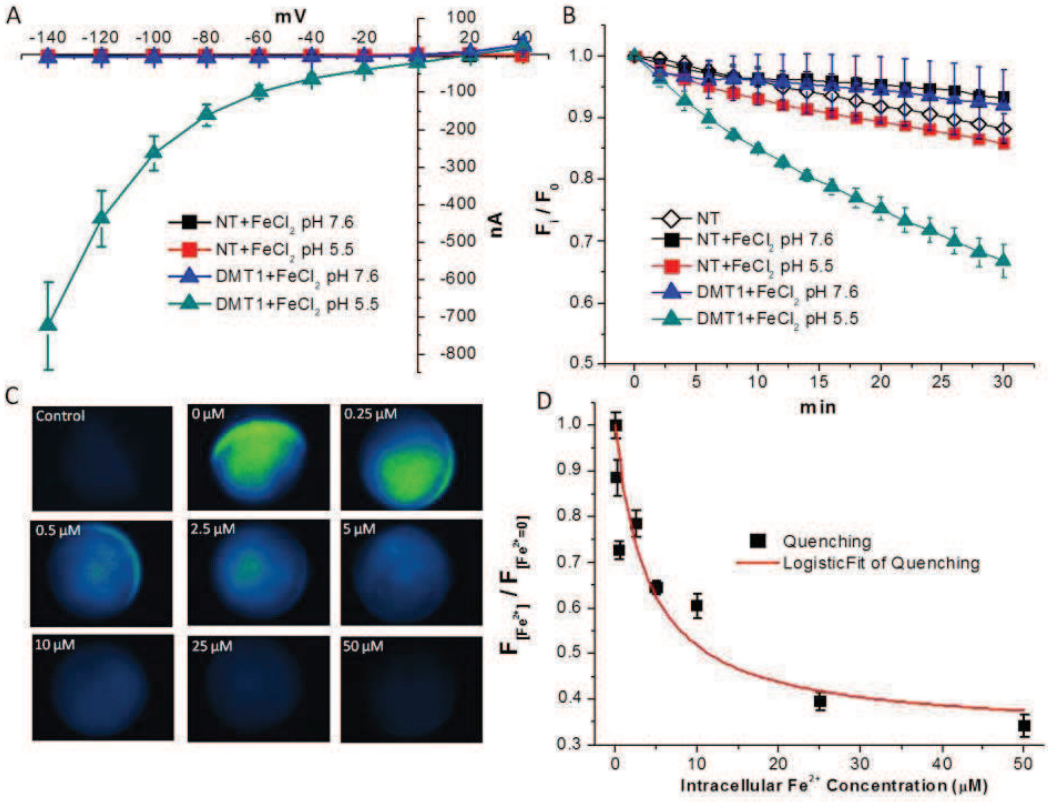

Figure 1: Calcein as iron detector. *A) Current-voltage (I-V) relationships of Non-Transfected (NT) oocytes and DMT1-expressing oocytes at pH 5.5 and 7.6; note that only DMT1-transfected oocytes at pH 5.5 are able to transport iron ions causing large inward currents. B) Calcein quenching is plotted versus time as the ratio of the fluorescence (F_I) and the fluorescence recorded at time 0 (F_0); again only DMT1-transfected oocytes at pH 5.5 are able to transport iron ions causing the increase of their intracellular concentration. C) Representative images of oocytes injected with Calcein and increasing amount of iron ions to obtain the standard curve of panel D. D) The mean values of fluorescence, normalized to the mean values of fluorescence measured in oocytes injected with Calcein alone are plotted versus intracellular iron concentration; (from 60 to 80 from 3 batches for each concentration) of oocytes for each iron concentrations; data were fitted with a logistic curve ($K_{0.5}$ = 3.97 ± 2.09 µM).*

We repeated the same experimental plan in oocytes previously injected with Calcein (25 µM) to demonstrate that Calcein was able to detect an

intracellular increase of Fe^{2+} concentration. As shown in Figure 1B, we monitored the reduction of Calcein fluorescence for 30 min in transfected and in non-transfected oocytes exposed to 100 μM $FeCl_2$ at pH 5.5 and 7.6. The results clearly show that a significant quenching of the fluorescence occurred only in DMT1 expressing oocytes at pH 5.5. It has to be noted that in DMT1 expressing oocytes at pH 7.6 no current (Figure 1A) and no Calcein quenching (Figure 1B) was recorded, according to the transporter pH dependence. These experiments, taken together, demonstrate that Calcein can detect an increase in the concentration of intracellular iron ions, and that oocytes are devoid of endogenous iron transporters.

To define the sensitivity of the method, we have injected oocytes with a fixed amount of Calcein together with increasing amounts of $FeCl_2$. We have then measured the residual fluorescence for each iron concentration and we have recorded a dose dependent reduction of the emission values (Figure 1C) that we have fitted with a logistic equation (Figure 1D). Given an oocyte volume of about 1 μl, the $K_{0,5}$ resulted 3.97 ± 2.09 (SE) μM. By means of this curve, we can estimate the concentrations of iron ions in the cytoplasm of *Xenopus* oocytes. Indeed, Figure 1B shows that DMT1 transfected oocytes reach, 30 min after exposure to $FeCl_2$, quenching values corresponding to concentrations of about the 5 μM.

After 30 min of exposure of *Xenopus* oocytes to radioactive iron, Marciani and colleagues[33] reported concentrations slightly higher. Their experimental approach based on radioactive $^{55}Fe^{2+}$, however, considered the total amount of iron that entered the cytoplasm through DMT1. Since a large amount of iron might become protein-bound, they estimated the total concentration of the iron ions.

Iron oxide NPs cross the plasma membrane of *Xenopus laevis* oocytes

After having verified that we were able to detect an increase of iron ions in the cytoplasm of *Xenopus* oocytes that were filled with Calcein, we have used them to reveal the possible permeation of iron NPs inside the cell. To this aim, we have chosen iron NPs in two different forms, zerovalent (Fe) and oxide (Fe_3O_4). Similarly to other metal NPs[10,21,34], iron[35] and iron oxide[36,37] NPs undergo dissolution releasing iron ions that, as we have here demonstrated, can be detected by Calcein quenching. As such, we exposed Calcein-filled oocytes to iron NPs. In oocytes obtained from different batches, iron oxide NPs constantly induced a quenching of Calcein fluorescence (Figure 2, blue column). This fluorescence decrease, although lower than that occurring in rDMT1 expressing oocytes exposed to 100 μM $FeCl_2$ (Figure 2, dark blue column), was significantly greater than that occurring in non-transfected oocytes either exposed (Figure 1B, black squares) or not exposed (Figure 1B, white diamond and Figure 2, white bar) to $FeCl_2$. These results suggest that Fe_3O_4 NPs interact with the plasma membrane of the oocyte, cross it and, once in the cytoplasm, dissolve causing the observed Calcein quenching. Zerovalent iron NPs, instead, did not cause a reduction of fluorescence (Figure 2, dark cyan column) suggesting that, in this case, NPs do not cross the plasma membrane of the oocyte.

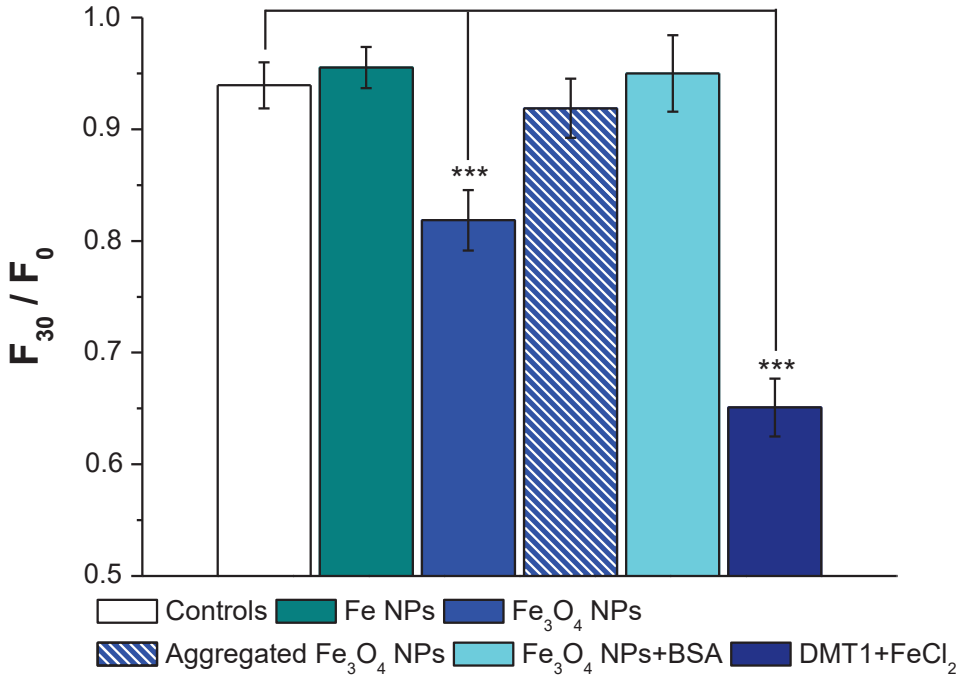

Figure 2: Iron oxide NPs induce intracellular iron increase. *Histogram of the means of the F_{30}/F_0 values calculated as the fluorescence values at time 30 min normalized for the fluorescence values at time 0. Fe_3O_4 NPs (blue column) caused a statistically significant quenching of Calcein compared to the controls, i.e., Calcein injected oocytes exposed to external control solution at pH 7.6 (white column). Conversely, Fe NPs (green column), aggregated Fe_3O_4 NPs (blue barred column) and BSA modified Fe_3O_4 NPs (cyan column) did not induce quenching; rDMT1 transfected oocytes exposed to iron chloride were used as positive controls (dark blue column). Bars represent ± SEM; from 10 to 40 oocytes for each column deriving from 2 to 8 batches were used. Statistical analysis was performed with One-way ANOVA and orthogonal comparisons with Holm-Bonferroni post hoc test (***=p<0.005).*

In a previous paper, we attributed the different biological behaviour (capacity to cross cell membranes) between metal oxide and zerovalent metal NPs to the chemical and physical characteristics of their surfaces. To better understand the causes of these differences, in this paper, we have measured z-potentials and described the aggregation dynamics of both NPs. The z-potentials, as determined by Laser Doppler Micro-

electrophoresis (Figure 3, top), were -5.0 ±0.2 mV and -2.2 ± 0.1 mV for zerovalent iron and iron oxide NPs, respectively. Thus, both types of NPs are poorly charged when suspended in external control solution and this does not explain the difference in capacity to cross cell membranes, but explains why both NPs rapidly aggregate into micronized assemblies when added to media (Figure 3, bottom) despite prior ultrasonication. Indeed, z-potentials above 30 mV or below -30 mV are generally required to maintain NPs disperse in solution through electrostatic repulsion. However, the rate of aggregation, as determined by Static Light Scattering (Figure 3, bottom), differed between zerovalent NPs, which aggregated very rapidly, and iron oxide NPs, which retained a sub-micron population for at least 5 min (Figure 3, insets of bottom graphs).

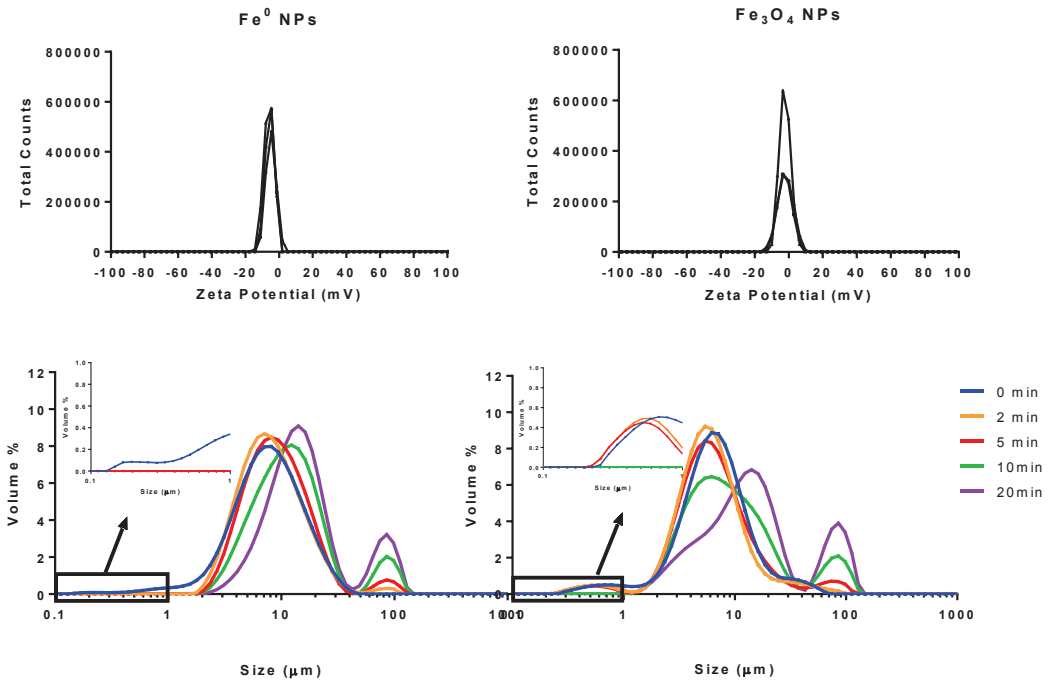

Figure 3: Characterisation charge and hydrodynamic size of zerovalent iron (Fe^0) and iron oxide (Fe_3O_4) NPs in external control solution (0.1 mg/mL). *Zeta potential (top graphs) was determined by Laser Doppler Micro-electrophoresis as -5.0 ± 0.2 mV and -2.2 ± 0.1 mV for zerovalent iron and iron*

oxide NPs, respectively (N=3). Hydrodynamic size was determined over time by Static Light Scattering (bottom graphs).

We think that the NPs that constitute this sub-micron population are those that can cross the plasma membrane possibly because these remained below a not yet determined upper particle size limit for plasma permeation. Physical penetration of lipid bilayer membranes by NPs has been demonstrated to possibly occur by dissipative particle dynamics simulations for single NPs and for very small clusters. Aggregated NPs, instead, are likely too large to penetrate the lipid bilayer[28]. Indeed, when the oocytes were exposed to aggregated NPs, we did not record Calcein quenching (Figure 2, blue barred column).

NPs do not impair oocyte plasma membrane integrity, but open a transient conductance

To learn more about the interactions of NPs with the plasma membrane of the oocytes, we have followed possible changes of its integrity due to exposure to Fe_3O_4 NPs by Two Electrodes Voltage Clamp (TEVC). With a similar approach, Bernareggi and colleagues[38] have recently evaluated the effects of asbestos fibres on *Xenopus* oocyte membrane.

We have measured membrane capacitance, resting potential and resistance during a 30 min period of exposure to Fe_3O_4 NPs. Since we have noticed that the alterations of membrane parameters occur within the first 5 min, we have decided to perform the electrophysiological measurements after 5 and 20 min of exposure; we have also exposed oocytes to NPs that, after sonication, were left undisturbed for 30 min. A statistically significant decrease of membrane resistance, as shown in Figure 4, occurs only in oocytes exposed for 5 min and disappears completely in oocytes exposed for 20 min. A slight decrease of resting potential, statistically significant, accompanied the decrease of membrane resistance. Membrane capacitance, instead, remained unaffected by Fe_3O_4 NPs treatment.

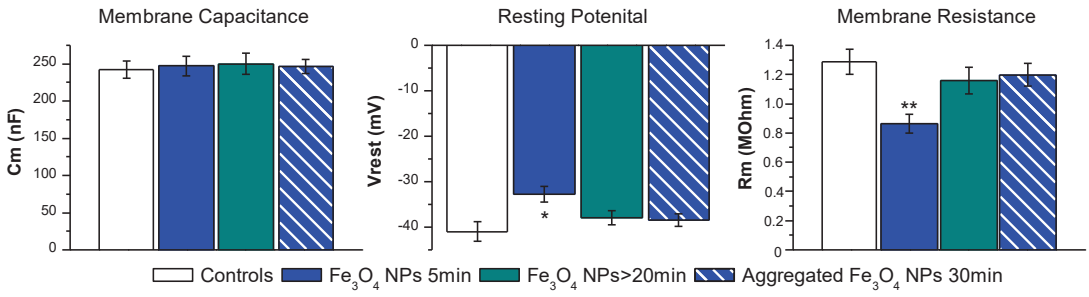

Figure 4: Effects of Fe_3O_4 NPs on oocyte membrane electrical properties. *Mean values of membrane electrical parameters registered from oocytes exposed to control conditions (white columns), to a Fe_3O_4 NP suspension for 5 min (blue columns) or for more than 20 min (green columns), and to NPs that after sonication, were left undisturbed for 30 min, blue barred columns). Membrane capacitance of control and treated oocytes showed no significant differences at any incubation times. Resting potential and Membrane resistance significantly diminishes in oocytes treated 5 min with Fe_3O_4 NPs compared to their controls; the difference disappears in oocytes treated for 20 min and in oocyte treated with aggregated NPS. Bars represent mean ± SEM; 14 to 30 oocytes from 2 oocyte batches were used. Statistical analysis was performed with one-way ANOVA and orthogonal comparisons with Holm-Bonferroni post hoc test (*=p<0.05 - **=p<0.01).*

The decrease of membrane resistance can be attributed to the opening of a small transient conductance. On the other hand, the constancy of membrane capacitance is an indication that no large endocytosis phenomena occur after exposure to iron oxide NPs[39], while the small reduction of the resting potential proves that the membrane has maintained its integrity[40], notwithstanding a small increase of ion permeability.

To investigate further this transient conductance, we have performed a protocol to obtain I-V curves. Figure 5A shows representative current traces recorded after imposing voltage steps in a control oocyte and in an oocyte exposed to Fe_3O_4 NPs for 5 min. We have calculated the

average currents at each potential and reported these data in the I-V curves of Figure 5D.

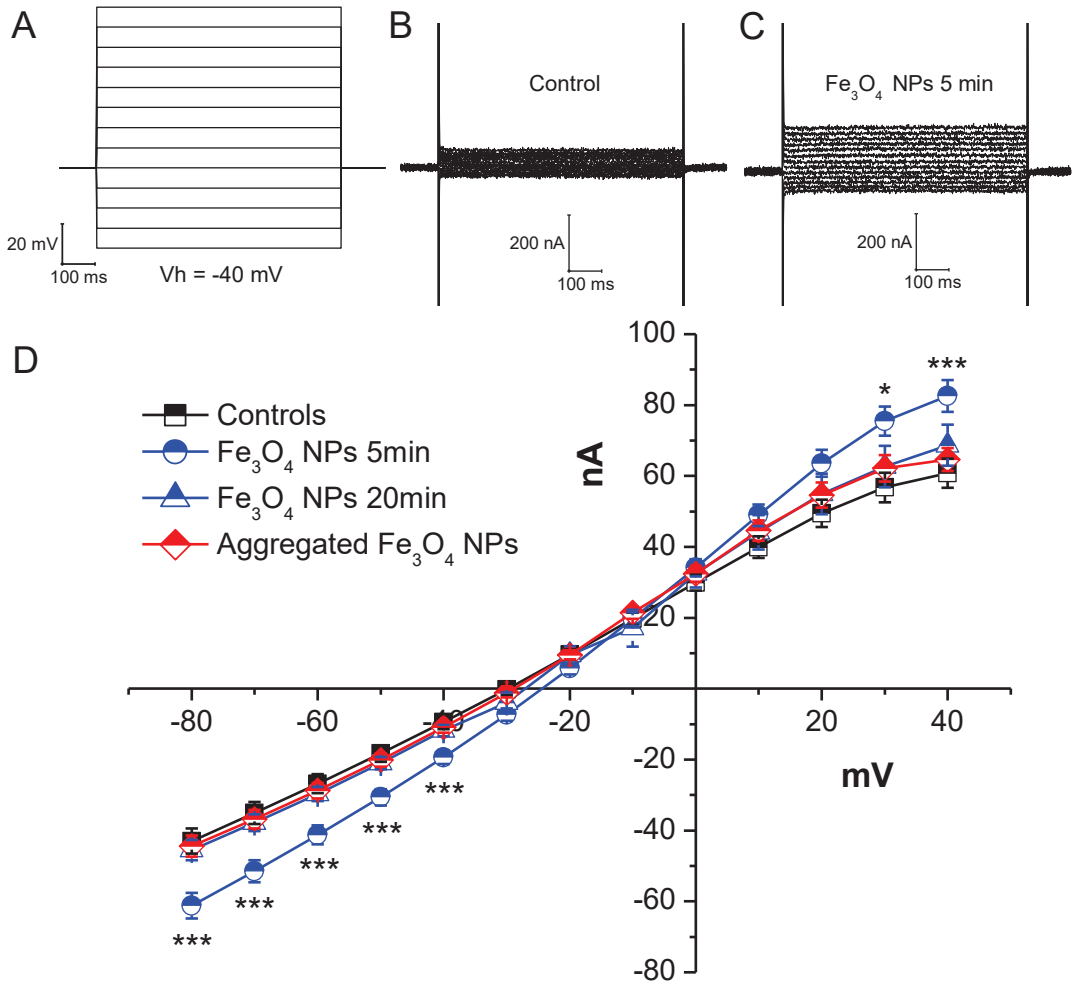

Figure 5: Membrane currents recorded in oocyte exposed or not to Fe_3O_4 NPs. *A) Voltage Protocol: from holding potential of -40 mV, 10 mV steps of 1 s were applied from -80 mV to +50 mV. Representative traces recorded from oocytes not exposed (B) or (C) exposed for 5 min to Fe_3O_4 NPs. In D, the averages of steady state membrane currents are reported as I-V relationships.*

After 5 min of NP exposure (blue circles), a slight, but statistically significant current increase is recorded at the curve extremes; after 20 min (blue triangles), no more statistically significant differences can be appreciated. Aggregated NP treatment generated in oocytes currents (red diamonds) almost overlapping with controls (black squares) and 20 min treatment currents, and that is an

indication of the inefficacy of this treatment (=p<0.05, ***=p<0.005; one-way ANOVA, Holm-Bonferroni post hoc orthogonal comparison; 14 to 30 oocytes from 2 batches).*

At potentials more negative than -40 mV and more positive than +30 mV, a slight increase of the currents obtained in exposed oocytes, compared to those in the control condition, is evident. This current increase is statistically significant only in oocytes tested within 5 min of the NPs treatment and it tends to disappear in oocytes exposed for more than 20 min and is not present in oocytes exposed to NPs that, after sonication, were left undisturbed for 30 min. The I-V curves confirm the onset of a conductance caused by the exposure to Fe_3O_4 NPs for 5 min and its transient nature.

Protein corona impedes plasma membrane crossing and the opening of the transient conductance

To verify our hypothesis concerning the role of the interactions between NPs and plasma membrane, we tested uptake of Fe_3O_4 NPs in bovine serum albumin (BSA) containing media. These molecules create a coating around the NPs, referred to as protein corona. This corona is highly dynamic and its formation and stability depends on NP characteristics and environmental variables[41]. BSA is negatively charged in water, but not in this media (Supp Figure S1) presumably due to the presence of positively charged calcium and magnesium ions. Consequently, the addition of BSA did not alter the surface charge of the iron oxide NPs (zeta potential was -1.3 ± 0.2 mV; Figure 6 top).

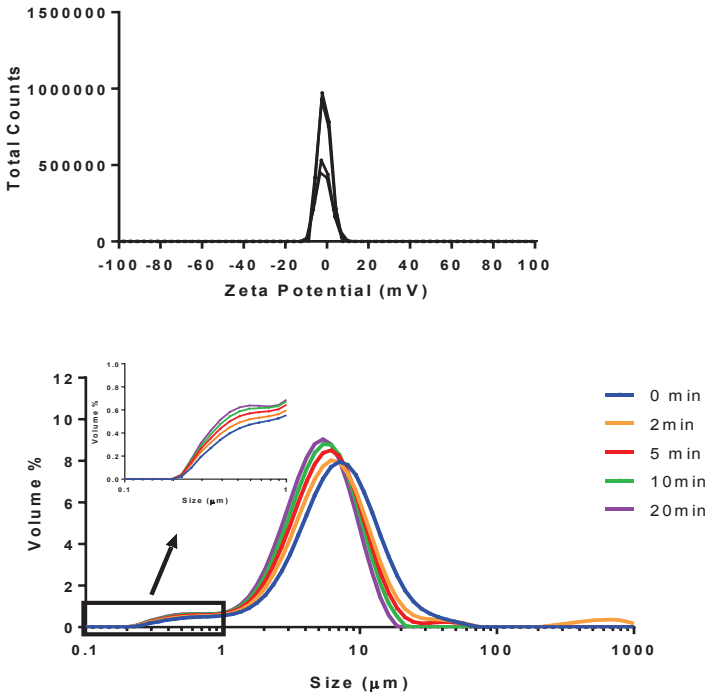

Figure 6: Zeta potential distribution (top) and particle size distribution over time (bottom) of a suspension of Fe_3O_4 NPs (0.1 mg/mL) in external control solution with 1 mg/mL BSA. *Zeta potential was determined by Laser Doppler Micro-electrophoresis as -1.3 ± 0.2 mV (N=4).*

However, the addition of BSA did increase dispersibility as determined by the presence of the sub-micron fraction for the duration of the assay (Figure 6). As shown above, plasma membrane crossing occurs in the presence of disperse colloids; however, exposure to BSA-coated Fe_3O_4 NPs did not cause fluorescence quenching (Figure 2, cyan column). Therefore, protein corona prevents or significantly reduces the interactions between NPs and the oocyte plasma membrane blocking or limiting the passage of NPs into the cytoplasm. These findings are also in agreement with experiments where the interaction of cationic polystyrene NPs with artificial lipid bilayers were eliminated with serum proteins [42].

To confirm this hypothesis, we have performed TEVC experiments to obtain I-V curves (Figure 7).

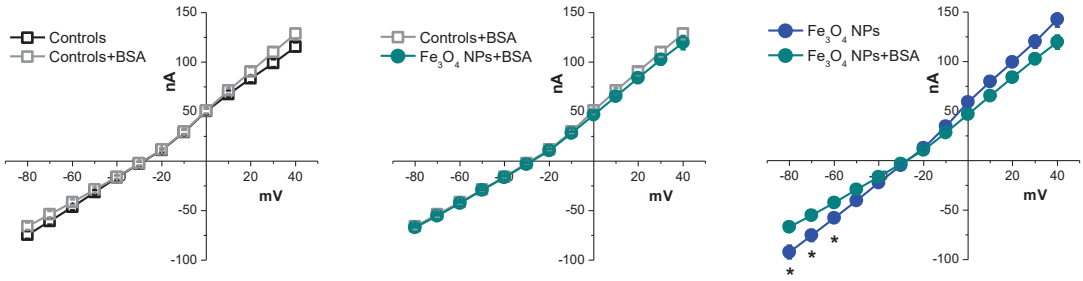

Figure 7: Protein corona affects NP capacity to elicit membrane currents. *I-V relationships of control oocytes and oocytes treated for 5 min with BSA are compared in the left panel and no statistically significant differences are present, indicating that BSA does not affect per se membrane resistance. In the central panel, it is shown that Fe_3O_4 NPs that were coated with a BSA corona do not cause a decrease of the membrane resistance suspension. In the right panel, the I-V relationships of oocytes treated for 5 min with Fe_3O_4 NPs and BSA coated Fe_3O_4 NPs are compared. Their difference is statistically significant, indicating that the presence of a protein corona around Fe_3O_4 NPs diminishes their capacity to elicit membrane currents. Statistical analysis was performed with one-way ANOVA and orthogonal comparisons with Holm-Bonferroni post hoc test (*=p<0.05); 27 to 61 oocytes for each condition from 3 to 4 batches were used.*

After having verified that BSA *per se* does not affect membrane conductance, we have compared oocytes exposed to BSA-modified Fe_3O_4 NPs with unexposed oocytes, and to oocytes exposed to Fe_3O_4 NPs. These experiments suggest that, when NPs are surrounded by a protein corona, they become unable to modify membrane resistance.

Conclusions

In conclusion, we have added further evidence to the possibility of cytomembranes being permeable to uncoated NPs. Endocytosis is the typical mechanism cells use to uptake NPs that, in this way, gain access

to the endosomal compartment. Conversely, by directly crossing lipid bilayers, NPs enter cytoplasm and other cellular compartments. Moreover, we have shown that the penetration by NPs of the lipid bilayer opens a transient conductance that does not impair plasma membrane integrity.

Whether we should favour NP presence in the cytoplasm or avoid it, we have to understand the mechanisms that regulate their uptake and consider how physicochemical properties of NPs impact on their fate. In this work, we have also learned that, unlike iron oxide NPs, zerovalent iron NPs do not cross plasma membranes. We have explained this different behaviour with the very fast aggregation rate of zerovalent iron NPs. In addition, we have shown that the crossing of metal oxide NPs can be impeded by a protein corona. Indeed, proteins are abundant in the tissue fluids, but NPs could be functionalized to become corona-free[43], thus potentially enabling the non-endocytic pathway. For example, superparamagnetic iron oxide NPs can be induced to rotate around their axes by a remote magnetic field[44] and have been used to kill cancer cells through mechanical rupture[45]. Understanding the mechanisms that regulate NP uptake or their interactions with the cellular membrane could help in potentiating the anticancer properties of such NPs.

We also understand that the conditions iron NPs find in the gastrointestinal tract greatly differ from those of the simple model system we have used. In particular, the intestinal millieu comprises a diverse group of soluble species, ranging from small carboxylates throught bile acids to high molecular weight mucins[46-48], many of which may interact with the surface of uncoated NPs and, in doing so, may alter their behaviour. This now merits assessment in future studies using conditions that are representative of the complex gastrointestinal environment.

Materials and Methods

Solutions

ND96 solution had the following composition (in mM): NaCl 96, KCl 2, $CaCl_2$ 1.8, $MgCl_2$ 1, HEPES 5, pH 7.6; NDE solution was composed of ND96 plus 2.5mM pyruvate and 50 μg/mL Gentamycin sulphate; external control solution contained (in mM): NaCl 98; $MgCl_2$, 1; $CaCl_2$, 1.8, HEPES or MES 5, pH 7.6 or 5.5; intracellular solution contained (in mM): KCl 130, NaCl 4, $MgCl_2$ 1.6, EGTA 5, HEPES 10, glucose 5, pH 7.6. The final pH values of 5.5 or 7.6 were adjusted with HCl and NaOH.

Oocytes collection and preparation

Oocytes were obtained from adult *Xenopus laevis* females. Animals were anaesthetised in 0.1 % (w/v) MS222 (tricaine methansulfonate) solution in tap water; after carefully cleaning the frog abdomen with an antiseptic agent (Povidone-iodine 10%)[49], laparotomy was performed and portions of the ovary were collected. The oocytes were treated with 0,5 mg/mL collagenase (Sigma Type IA) in ND96 calcium free for at least 30 min at 18 °C. Healthy and fully grown oocytes were selected and stored at 18°C in NDE solution[50]. The oocytes to be transfected with the cRNA coding for rDMT1 were injected with 25 ng of cRNA in 50 nL of water, the day after the removal, using a manual microinjection system (Drummond Scientific Company, Broomall, PA) and incubated at 18 °C for 3-4 days before electrophysiological or fluorescence experiments. The experimental protocol was approved locally by the Committee of the "Organismo Preposto al Benessere degli Animali" of the University of Insubria (OPBA-permit #02_15) and nationally by Ministero della Salute (permit nr. 1011/2015).

NP preparation and incubation conditions

Zerovalent (Fe, 25 nm, IOLITEC, Salzstrasse 184, D-74076 Heilbronn) and oxide (Fe_3O_4, < 50 nm TEM determined, Sigma-Aldrich) iron NPs

were prepared as 10 mg/mL stock suspensions in deionised water and sonicated before addition of 10 μL to the test chamber (4 wells plate) containing 990 μL of external control solution (pH 7.6). Oocytes were then added to the chamber.

For electrophysiological experiments, the oocytes were transferred to the TEVC recording chamber within 5 min or after 20 min from the beginning of the exposure. For the fluorescence assay, recordings start immediately after oocytes addition to the test chamber. Treatments with the aggregated NPs were performed adding oocytes to the suspension of NPs that were let to aggregate in the test chamber for 30 min after sonication.
All experiments were carried out at room temperature.

Fluorescence Assay

Oocytes were injected with a 50 nL drop of intracellular solution containing 25 μM Calcein. In dose-response evaluation experiments (Fig. 1C and D), solutions containing Calcein and increasing amounts of $FeCl_2$ were co-injected in oocytes. Effective intracellular metal concentrations were calculated using the nominal oocyte volume of 1 μL[51]. Images were acquired for every oocyte at fixed acquisition parameters, calculated on control oocytes.
In experiments with NPs, images of single oocytes were acquired every 2 min for 30 min with a fluorescence microscope (AxioVert 200, Carl Zeiss with a 4x objective, COLIBRI fluorescence filters, 470 nm excitation - 515 to 565 nm emission) equipped with CCD camera (Axiocam ICM1, Carl Zeiss).

Electrophysiology

The two-electrode voltage clamp was performed with an Oocyte Clamp OC-725B (Warner Instruments, Hamden, CT, USA) that was controlled by Clampex 10.2 (Molecular Devices, Sunnyvale, CA, USA,

www.moleculardevices.com). Intracellular glass microelectrodes, filled with 3 M KCl, had tip resistances in the 0.5 - 4 MΩ range. Agar bridges (3% agar in 3 M KCl) connected the bath electrodes to the experimental chamber. The holding potential applied (V_h) was -40 mV for all the experiments performed. The I-V curves of Figure 1A were obtained applying 20 mV steps of 200 ms from -140 to + 40 mV.

Oocytes were transferred in the recording chamber (Warner- RC-1Z) (warneronline.com) and impaled with microelectrodes; to recover from possible damage they were left for 2 min in a continuous solution flux. Only oocytes with resting potential equal or lower than -20 mV were used for the experiments. The number of discarded oocytes was not significantly different between treated and controls.

The capacitance and resistance values that were reported in Figure 4 were obtained applying 10 mV steps of 20 ms every 200 ms in voltage clamp conditions. The protocol for the I-V curves of Figure 1 was previously described[52] and for Figures 5 and 7 is shown in Figure 5A (10 mV steps of 750 ms from -80 to +40 mV).

Data analysis

Data were analysed using Clampfit 10.2 software (Molecular Devices, Sunnyvale, CA, USA, www.moleculardevices.com) while OriginPro 8.0 (OriginLab Corp., Northampton, MA, USA, www.originlab.com) was used for statistics and figure preparation. For the Voltage Step protocol, current values were measured for every voltage step at the steady state condition; mean values at every voltage were calculated and plotted.

Fluorescence decay images were analysed with ImageJ (Rasband, W.S., ImageJ, U. S. National Institutes of Health, Bethesda, Maryland, USA, http://imagej.nih.gov/ij/, 1997-2015). For F_{30}/F_0 quantification, the fluorescence intensity at time 0 (F_0) and at time 30 min (F_t) was calculated in the entire area of the oocyte. In dose-response experiments, images were analysed calculating fluorescence intensity on the entire

area of oocytes and normalized to the control oocytes. Mean values were calculated for every condition and used to determine through a non-linear fitting (Logistic Fitting, OriginPro8) the $K_{0.5}$, relating residual fluorescence to metal concentration.

Static light scattering (SLS)

SLS was performed on a Mastersizer 2000 with a Hydro 2000μP Micro Precision sample dispersion unit (Malvern Instruments Limited). Baseline correction was carried out with fresh external control solution (prepared as described above). Next, 200 μL of 10 mg/mL stock suspension was added to the 20mL dispersion cell to achieve a final concentration of 0.1 mg/mL (as per Oocyte assays). The dispersion unit was run at 1000 rpm and care was taken to prevent bubble formation. The stock suspension was carefully sonicated prior to introduction to the dispersion cell, after which data acquisition was immediately initiated. Size measurements then were carried out over a period of 60 min (refractive index: 2.42; absorption 1.0; dispersant refractive index: 1.33).

Zeta potential

The zeta potential of suspensions of iron NPs was determined by Laser Doppler Micro-electrophoresis (Zetasizer NanoZS, Malvern Instruments Ltd) using disposable folded capillary cells (DTS1070). Measurements (N=3) were carried out using the diffusion barrier as per instrument manufacturer instructions. Briefly, the zeta cell was filled with 1 mM NaCl solution and then 100 μL sample (0.1 mg/mL suspension of NPs in external control solution) was gently injected to the bottom of the cell with a gel-loading tip. Electrophoretic mobility of particles was converted into zeta potentials by Dispersion Technology Software 7.11 using the Smoluchowski approximation, and a viscosity of 0.8872cP and dielectric constant of 78.5 for the dispersant.

Acknowledgements

This work was supported by a grant of Fondazione Cariplo (2013-1052) to R.G. We thank Dr Raffella Cinquetti for her help in performing experiments.

Additional information

Competing financial interests.

The authors declare no competing financial interests.

Authors' contribution

All authors designed the experiments and reviewed the manuscript. D.Z., E.B. and C.B. performed the experiments and prepared the figures, E.B., N.F. and G.B. wrote the manuscript.

Supplementary figure

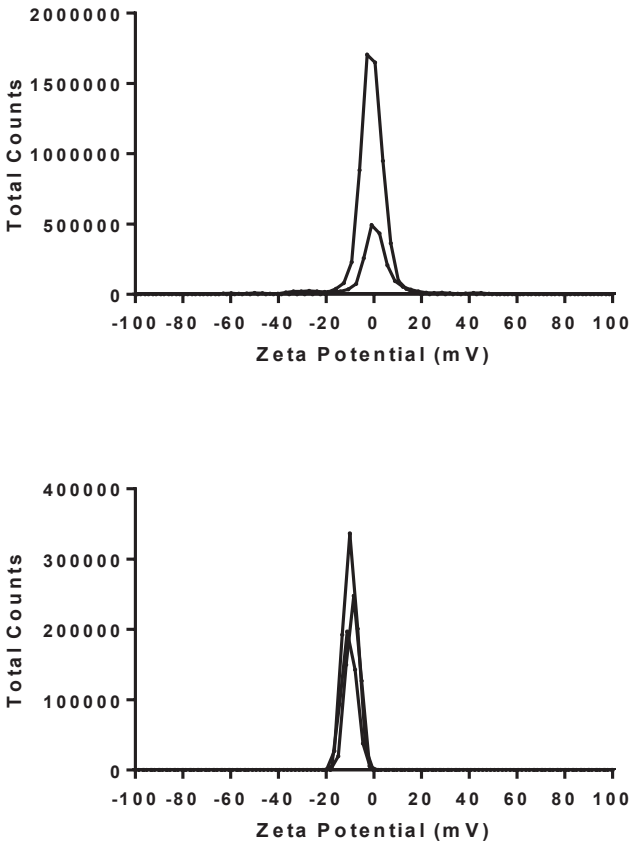

Figure S1. *Zeta potential distribution of a BSA solution (40 mg/mL) in external control solution (Top; N=2) and in water (Bottom, n=3).*

Bibliography

1 Gulec, S., Anderson, G. J. & Collins, J. F. Mechanistic and regulatory aspects of intestinal iron absorption. *Am J Physiol Gastrointest Liver Physiol* **307**, G397-409 (2014).

2 Gozzelino, R. & Arosio, P. Iron Homeostasis in Health and Disease. *International journal of molecular sciences* **17** (2016).

3 Tolkien, Z., Stecher, L., Mander, A. P., Pereira, D. I. & Powell, J. J. Ferrous sulfate supplementation causes significant gastrointestinal side-effects in adults: a systematic review and meta-analysis. *PloS one* **10**, e0117383, doi:10.1371/journal.pone.0117383 (2015).

4 Hurrell, R. F. Fortification: overcoming technical and practical barriers. *J Nutr* **132**, 806S-812S (2002).

5 Rohner, F. *et al.* Synthesis, characterization, and bioavailability in rats of ferric phosphate nanoparticles. *J Nutr* **137**, 614-619 (2007).

6 Zimmermann, M. B., Biebinger, R., Egli, I., Zeder, C. & Hurrell, R. F. Iron deficiency up-regulates iron absorption from ferrous sulphate but not ferric pyrophosphate and consequently food fortification with ferrous sulphate has relatively greater efficacy in iron-deficient individuals. *Br J Nutr* **105**, 1245-1250, doi:10.1017/S0007114510004903 (2011).

7 Hilty, F. M. *et al.* Iron from nanocompounds containing iron and zinc is highly bioavailable in rats without tissue accumulation. *Nat Nanotechnol* **5**, 374-380, doi:10.1038/nnano.2010.79 (2010).

8 Hosny, K. M., Banjar, Z. M., Hariri, A. H. & Hassan, A. H. Solid lipid nanoparticles loaded with iron to overcome barriers for treatment of iron deficiency anemia. *Drug Des Devel Ther* **9**, 313-320, doi:10.2147/DDDT.S77702 (2015).

9 Cappellini, F. *et al.* New synthesis and biodistribution of the D-amino acid oxidase-magnetic nanoparticle system. *Future Science OA*, doi:10.4155/fso.15.67 (2015).

10 Gornati, R. *et al.* Zerovalent Fe, Co and Ni nanoparticle toxicity evaluated on SKOV-3 and U87 cell lines. *Journal of applied toxicology : JAT*, doi:10.1002/jat.3220 (2015).

11 Sekhon, B. S. Nanotechnology in agri-food production: an overview. *Nanotechnol Sci Appl* **7**, 31-53, doi:10.2147/NSA.S39406 (2014).

12 Nikonov, I. N. *et al.* Iron nanoparticles as a food additive for poultry. *Dokl Biol Sci* **440**, 328-331 (2011).

13 Izquierdo, M. S. *et al.* Organic, inorganic and nanoparticles of Se, Zn and Mn in early weaning diets for gilthead seabream (Sparus aurata; Linnaeus, 1758). *Aquaculture Research*, n/a-n/a, doi:10.1111/are.13119 (2016).

14 Lonnerdal, B., Bryant, A., Liu, X. & Theil, E. C. Iron absorption from soybean ferritin in nonanemic women. *Am J Clin Nutr* **83**, 103-107 (2006).

15 Powell, J. J. *et al.* A nano-disperse ferritin-core mimetic that efficiently corrects anemia without luminal iron redox activity. *Nanomedicine : nanotechnology, biology, and medicine* **10**, 1529-1538 (2014).

16 Montalbetti, N., Simonin, A., Kovacs, G. & Hediger, M. A. Mammalian iron transporters: families SLC11 and SLC40. *Mol Aspects Med* **34**, 270-287, doi:10.1016/j.mam.2013.01.002 (2013).

17 Latunde-Dada, G. O. *et al.* A nanoparticulate ferritin-core mimetic is well taken up by HuTu 80 duodenal cells and its absorption in mice is regulated by body iron. *J Nutr* **144**, 1896-1902 (2014).

18 Pereira, D. I. A. *et al.* Nanoparticulate iron(III) oxo-hydroxide delivers safe iron that is well absorbed and utilised in humans. *Nanomedicine : nanotechnology, biology, and medicine* **10**, 1877-1886 (2014).

19 Pereira, D. I. A. *et al.* Caco-2 cell acquisition of dietary iron(III) invokes a nanoparticulate endocytic pathway. *PloS one* **8**, e81250 (2013).

20 Kalgaonkar, S. & Lonnerdal, B. Receptor-mediated uptake of ferritin-bound iron by human intestinal Caco-2 cells. *The Journal of*

nutritional biochemistry **20**, 304-311, doi:10.1016/j.jnutbio.2008.04.003 (2009).

21 Papis, E. *et al.* Engineered cobalt oxide nanoparticles readily enter cells. *Toxicology letters* **189**, 253-259, doi:10.1016/j.toxlet.2009.06.851 (2009).

22 Li, S. & Malmstadt, N. Deformation and poration of lipid bilayer membranes by cationic nanoparticles. *Soft Matter* **9**, 4969-4976, doi:DOI 10.1039/c3sm27578g (2013).

23 Nolte, T. M., Kettler, K., Meesters, J. A., Hendriks, A. J. & van de Meent, D. A semi-empirical model for transport of inorganic nanoparticles across a lipid bilayer: implications for uptake by living cells. *Environmental toxicology and chemistry / SETAC* **34**, 488-496, doi:10.1002/etc.2812 (2015).

24 Taylor, U. *et al.* Nonendosomal cellular uptake of ligand-free, positively charged gold nanoparticles. *Cytometry. Part A : the journal of the International Society for Analytical Cytology* **77**, 439-446, doi:10.1002/cyto.a.20846 (2010).

25 Ding, H.-m. & Ma, Y.-q. Computer simulation of the role of protein corona in cellular delivery of nanoparticles. *Biomaterials* **35**, 8703-8710, doi:10.1016/j.biomaterials.2014.06.033 (2014).

26 Lin, J. Q. & Alexander-Katz, A. Cell Membranes Open "Doors" for Cationic Nanoparticles/Biomolecules: Insights into Uptake Kinetics. *Acs Nano* **7**, 10799-10808, doi:DOI 10.1021/nn4040553 (2013).

27 Verma, A. *et al.* Surface-structure-regulated cell-membrane penetration by monolayer-protected nanoparticles. *Nat Mater* **7**, 588-595, doi:10.1038/nmat2202 (2008).

28 Zhang, H. *et al.* Cooperative transmembrane penetration of nanoparticles. *Sci Rep* **5**, 10525, doi:10.1038/srep10525 (2015).

29 Gunshin, H. *et al.* Cloning and characterization of a mammalian proton-coupled metal-ion transporter. *Nature* **388**, 482-488, doi:Doi 10.1038/41343 (1997).

30 Au, C., Benedetto, A. & Aschner, M. Manganese transport in eukaryotes: The role of DMT1. *Neurotoxicology* **29**, 569-576, doi:DOI 10.1016/j.neuro.2008.04.022 (2008).

31 Mackenzie, B. & Hediger, M. A. SLC11 family of H+-coupled metal-ion transporters NRAMP1 and DMT1. *Pflug Arch Eur J Phy* **447**, 571-579, doi:DOI 10.1007/s00424-003-1141-9 (2004).

32 Bressler, J. P., Olivi, L., Cheong, J. H., Kim, Y. & Bannon, D. Divalent metal transporter 1 in lead and cadmium transport. *Ann Ny Acad Sci* **1012**, 142-152, doi:DOI 10.1196/annals.1306.011 (2004).

33 Marciani, P., Trotti, D., Hediger, M. A. & Monticelli, G. Modulation of DMT1 activity by redox compounds. *J Membr Biol* **197**, 91-99 (2004).

34 Sabbioni, E. *et al.* Interaction with culture medium components, cellular uptake and intracellular distribution of cobalt nanoparticles, microparticles and ions in Balb/3T3 mouse fibroblasts. *Nanotoxicology* **8**, 88-99, doi:10.3109/17435390.2012.752051 (2014).

35 Bae, S. & Hanna, K. Reactivity of Nanoscale Zero-Valent Iron in Unbuffered Systems: Effect of pH and Fe(II) Dissolution. *Environ Sci Technol* **49**, 10536-10543 (2015).

36 Zhu, M.-T. *et al.* Endothelial dysfunction and inflammation induced by iron oxide nanoparticle exposure: Risk factors for early atherosclerosis. *Toxicology letters* **203**, 162-171 (2011).

37 Casals, E. *et al.* Programmed iron oxide nanoparticles disintegration in anaerobic digesters boosts biogas production. *Small (Weinheim an der Bergstrasse, Germany)* **10**, 2801-2808, 2741 (2014).

38 Bernareggi, A. *et al.* Xenopus laevis Oocytes as a Model System for Studying the Interaction Between Asbestos Fibres and Cell Membranes. *Toxicological sciences : an official journal of the Society of Toxicology* **145**, 263-272 (2015).

39 Peres, A. & Bernardini, G. The effective membrane capacity of Xenopus eggs: Its relations with membrane conductance and cortical

granule exocytosis. *Pflugers Archiv European Journal of Physiology* **404**, 266-272 (1985).

40 Peres, A., Bernardini, G. & Negrini, C. Membrane potential measurements of unfertilized and fertilized Xenopus laevis eggs are affected by damage caused by the electrode. *Experimental cell research* **162**, 159-168 (1986).

41 Braun, N. J., DeBrosse, M. C., Hussain, S. M. & Comfort, K. K. Modification of the protein corona-nanoparticle complex by physiological factors. *Mater Sci Eng C Mater Biol Appl* **64**, 34-42, doi:10.1016/j.msec.2016.03.059 (2016).

42 Lu, B., Smith, T. & Schmidt, J. J. Nanoparticle-lipid bilayer interactions studied with lipid bilayer arrays. *Nanoscale* **7**, 7858-7866, doi:10.1039/c4nr06892k (2015).

43 Moyano, D. F. *et al.* Fabrication of corona-free nanoparticles with tunable hydrophobicity. *ACS nano* **8**, 6748-6755 (2014).

44 Zhang, E. *et al.* Dynamic magnetic fields remote-control apoptosis via nanoparticle rotation. *ACS nano* **8**, 3192-3201 (2014).

45 Yue, T., Zhang, X. & Huang, F. Molecular modeling of membrane responses to the adsorption of rotating nanoparticles: promoted cell uptake and mechanical membrane rupture. *Soft Matter* **11**, 456-465 (2015).

46 Powell, J. J. *et al.* Dietary minerals in the gastrointestinal tract: hydroxypolymerisation of aluminium is regulated by luminal mucins. *J Inorg Biochem* **75**, 167-180 (1999).

47 Kalantzi, L. *et al.* Characterization of the human upper gastrointestinal contents under conditions simulating bioavailability/bioequivalence studies. *Pharm Res* **23**, 165-176, doi:10.1007/s11095-005-8476-1 (2006).

48 Northfield, T. C. & McColl, I. Postprandial concentrations of free and conjugated bile acids down the length of the normal human small intestine. *Gut* **14**, 513-518 (1973).

49 Philips, B. H. *et al.* Evaluation of Presurgical Skin Preparation Agents in African Clawed Frogs (Xenopus laevis). *J Am Assoc Lab Anim Sci* **54**, 788-798 (2015).

50 Bossi, E., Fabbrini, M. S. & Ceriotti, A. Exogenous protein expression in Xenopus oocytes: basic procedures. *Methods in molecular biology* **375**, 107-131, doi:10.1007/978-1-59745-388-2_6 (2007).

51 Zeuthen, T., Zeuthen, E. & Klaerke, D. A. Mobility of ions, sugar, and water in the cytoplasm of Xenopus oocytes expressing Na(+)-coupled sugar transporters (SGLT1). *The Journal of physiology* **542**, 71-87 (2002).

52 Buracco, S. *et al.* Dictyostelium Nramp1, which is structurally and functionally similar to mammalian DMT1 transporter, mediates phagosomal iron efflux. *J Cell Sci* **128**, 3304-3316, doi:10.1242/jcs.173153 (2015).

Chapter 4

The direct permeation of nanoparticles through the plasma membrane transiently modifies its properties

Sumbitted to "Nanotoxicology"

Daniele Zanella[1], Elena Bossi[1*], Rosalba Gornati[1], Nuno Faria[2], Jonathan Powell[2] and Giovanni Bernardini[1*]

[1]Department of Biotechnology and Life Sciences, University of Insubria, Via Dunant 3, I-21100 Varese, Italy

[2]Department of Veterinary Medicine, University of Cambridge, Madingley Road, Cambridge CB3 OES, UK

Graphical Abstract

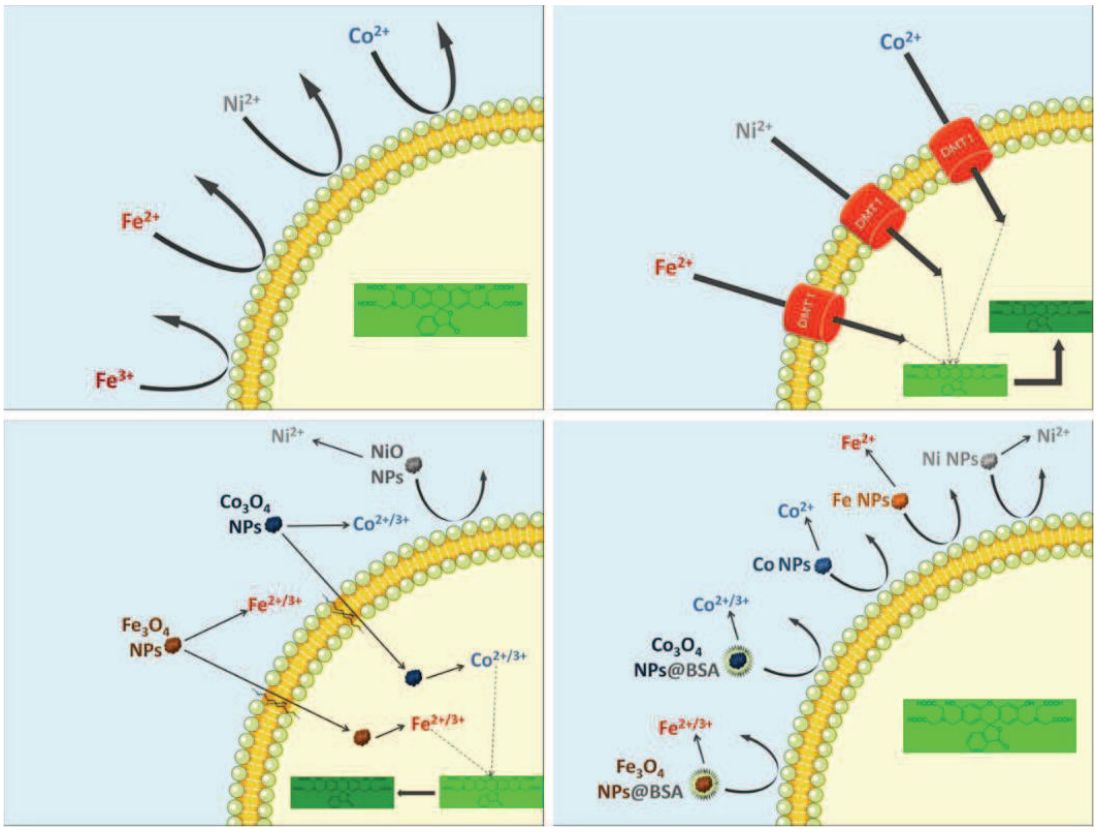

Abstract

The risk of exposure to metal nanoparticles (NPs) has increased with their widespread use in industry, research and medicine. It is well known that NPs may enter cells and that this mechanism is crucial to exert both the therapeutic and toxicity effects. The main cellular entrance route is endocytosis-based that leads to the entrapment of the internalized particles in the endosomal-lysosomal compartment. However, recent experimental studies, have reported that NPs (surface-modified or not) can also enter the cell crossing directly the plasma membrane. It is thus important to investigate on this alternative internalization mechanisms to increase the comprehension of possible NP-related cell toxicity. We have demonstrated that a direct permeation of metal oxide NPs through the lipid bilayer of the cell membrane can occur, giving direct access to the cytoplasm.

In this paper, using the powerful tool of *Xenopus laevis* oocytes and two electrode Voltage Clamp, we have investigated several parameters that can influence the direct crossing. The most significant of them is the NP hydrodynamic size as clearly shown by the comparison of the behaviour between Co_3O_4 and NiO NPs. By collecting biophysical membrane parameters in different conditions, we have shown that NPs that are able to cross the membrane share the ability to maintain a hydrodynamic size lower than 200 nm. The presence of this route of entrance must be considered for a better comprehension of the mechanism of nanotoxicity and for a safe design of engineered NPs.

Furthermore, NPs-membrane interaction studies conducted with *Xenopus laevis* oocytes proved the value of this platform to study the effects of NPs on the membrane physiology.

Introduction

The risk of exposure to nanoparticles (NPs) has increased with their widespread use in industry, research and medicine (Amde *et al.*, 2017, Bhuvaneshwari *et al.*, 2017). In most of the therapeutic applications, it is mandatory for NPs to enter the cell and reach the intracellular milieu, whereas this is considered a risk when NPs are harmful.

The main cellular entrance routes are endocytosis based, and usually these require a trigger to be activated (Bannunah *et al.*, 2014, Date *et al.*, 2016). However, recent experimental studies, have reported that NPs (surface-modified or not) can also enter the cell crossing directly the plasma membrane (Nativo *et al.*, 2008, Chen *et al.*, 2009, Brandenberger *et al.*, 2010, Lin and Alexander-Katz, 2013, Bossi *et al.*, 2016, Li *et al.*, 2017, Zanella *et al.*, 2017). This route could overcome some of the limitations related to endocytosis, giving direct access to the cytoplasm and, from there, to the intracellular organelles such as nuclei and mitochondria. It is thus important to investigate this alternative internalization mechanisms to increase the comprehension of possible NP-related cell toxicity.

It is known that size, surface chemistry, solubility and shape play a role in NP ability of entering the cell (Peters *et al.*, 2006, Cho *et al.*, 2010, Frohlich, 2012, Alkhammash *et al.*, 2015, Beddoes *et al.*, 2015, Anders *et al.*, 2018), but it is still to be elucidated how these properties act on cell membrane. Data from simulations, like molecular dynamics, may serve the purpose (Song *et al.*, 2012, Ding and Ma, 2015, Li *et al.*, 2015, Zhang *et al.*, 2015, Shimizu *et al.*, 2016), but experimental evidence is always needed to confirm simulation results. To collect data, the main approaches used were those based on cell cultures, liposomes or artificial membranes (Peetla and Labhasetwar, 2009, Moghadam *et al.*, 2012, Alkhammash *et al.*, 2015), together with fluorescent dyes able to detect the leakage of cytosolic components out of the cell or of extracellular component into cells. However, biophysical membrane

parameters were seldom considered. Shin and co-workers (Shin *et al.*, 2013) investigated the role of membrane potential in the interaction of the cell with charged NPs, demonstrating that anionic NPs, but not cationic, are influenced by cell potential in their interaction with plasma membranes. Arvizo and co-workers (Arvizo *et al.*, 2010) considered the effect of differently functionalized gold NPs on membrane potential by real-time fluorescence microscopy and voltage-sensitive fluorescent probes, while Warren and co-workers (Warren and Payne, 2015) studied the effect of differently functionalized polystyrene NPs on cell potential mainly through flow cytometry and fluorescent microscopy. However, none of these papers provide a direct measurement of membrane potential, as done by Chen and co-workers (Chen *et al.*, 2009) who, by patch clamp, recorded the effects caused by the direct access of cationic NPs to the cytoplasm.

In this paper, we have focused our attention on cobalt- and nickel-based NPs since these metals lead to cytotoxic effects that, in some cases, are caused by their degradation products (Horev-Azaria *et al.*, 2011, Frohlich, 2013, Ortega *et al.*, 2014, Sabbioni *et al.*, 2014a, Sabbioni *et al.*, 2014b, Ansari *et al.*, 2017). Nickel-based NPs induce respiratory pathologies in humans and oxidative stress in cellular models and in in vivo experiments (Horie *et al.*, 2011, Morimoto *et al.*, 2011, Ahamed *et al.*, 2013, Horie *et al.*, 2016). To define the characteristics that allow NPs to directly cross the membrane, we have measured membrane biophysical parameters of *Xenopus laevis* oocytes before and after exposure. Our data suggest a correlation between NP characteristics and resting potential, membrane resistance and current-voltage relationship. Particularly, the NP aggregation state emerged as one of the most important parameters to be considered for determining the ability of NPs of membrane direct crossing.

Results

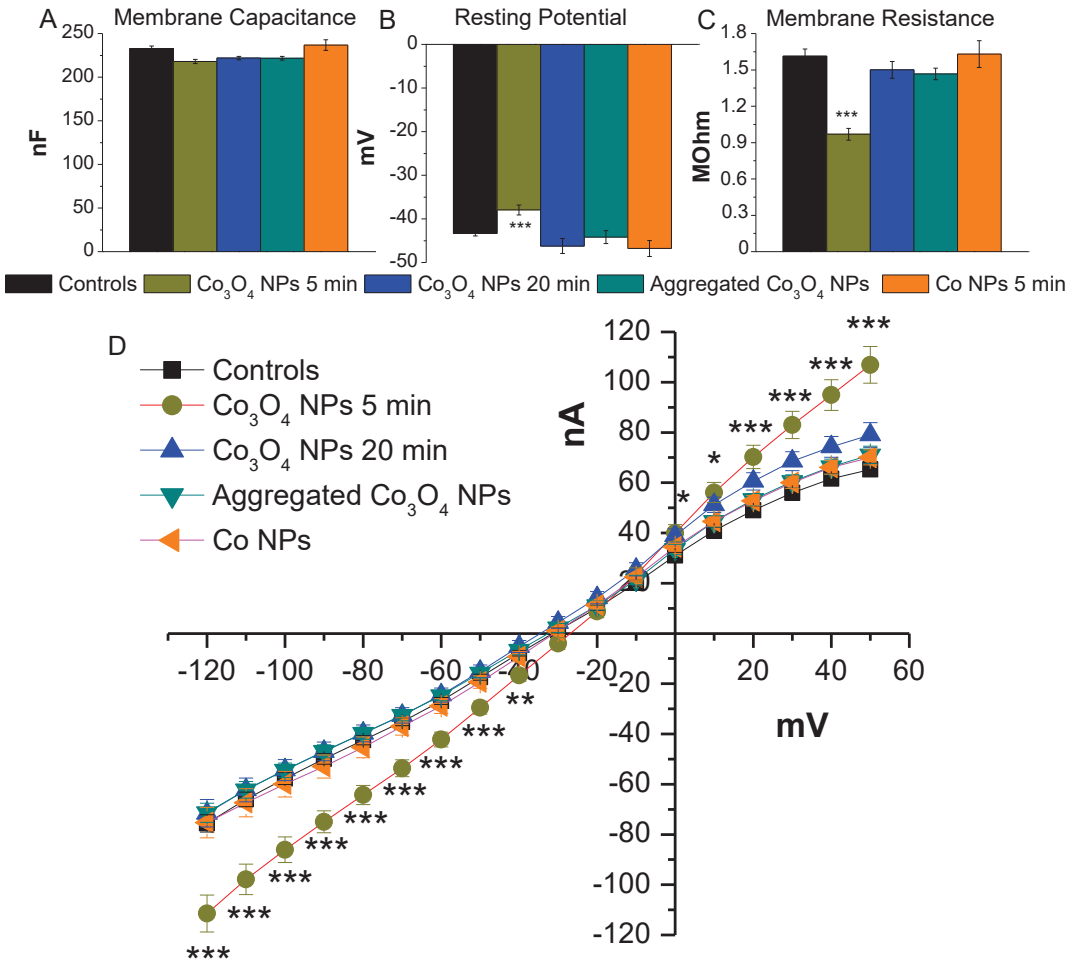

Figure 1: Effects of cobalt based NPs on plasma membrane. *Membrane capacitance, resting potential, membrane resistance, and membrane currents in oocytes treated with Co-based NPs. Histograms report membrane capacitance in A, resting potential in B and membrane resistance in C, measured from oocytes treated with 0.1 mg/ml of NPs in buffered solution, as indicated in Materials and Methods. In D, current voltage relationships (I/V) were determined for each condition applying the voltage pulse protocol described in Materials and Methods. Controls n=76 oocytes from 4 batches, Co_3O_4 NPs 5 min n=25 oocytes from 2 batches, Co_3O_4 NPs 20 min n=30 oocytes from 2 batches, Aggregated Co_3O_4 NPs n=44 oocytes from 2 batches, Co NPs n=30*

oocytes from 2 batches – statistical analysis performed with a One-Way ANOVA test with a Bonferroni-Holm post-hoc test.

Cobalt-based NP effects on oocyte membrane biophysical parameters

We have measured the effects of cobalt (Co) and cobalt oxide (Co_3O_4) NPs on the membrane biophysical parameters of *Xenopus laevis* oocytes (Figure 1) by determining membrane capacitance, resting potential, membrane resistance, membrane current reported as current-voltage (I/V) relationships as explained in Materials and Methods. Before exposing oocytes to cobalt and cobalt oxide NPs, we carefully sonicated NPs to disperse them as much as possible. We considered two time ranges in which we performed the measurements: a) within 5 min and b) after 20 min from the beginning of the exposure that occurs just after sonication. These two time ranges were selected after preliminary experiments conducted testing the oocytes every two min over 30 min (data not shown). These exposure time ranges agree with those previously observed for iron oxide NPs (Zanella *et al.*, 2017).

We first measured the biophysical membrane parameters of oocytes exposed to cobalt oxide NPs within 5 min from the beginning of the exposure and we recorded a significant reduction of resting potential and of membrane resistance. The resting potential decreased by about 5 mV (Figure 1B), a reduction that can be explained by a small flux of ions permeating the plasma membrane. Also, after 5 min exposure to cobalt oxide NPs, membrane resistance was significantly lower than that of the control oocytes (Figure 1C) and its decrease was consistent with the decrease of resting potential described above. These parameter changes are well described by the I/V curves (Figure 1D). Indeed, we recorded a marked and statistically significant increase in the slope of the I/V relationship for a broad range of potentials (-120 to +50 mV), which corresponds to an increase of membrane conductance. Moreover, it is

worth noting that the reversal potential of the I/V curve of the 5 min treatment remained the same of the control one, suggesting the presence of a non-selective conductance.

We then measured the same parameters in oocytes that were exposed to cobalt oxide NPs for more than 20 min. We noticed that they did not differ from controls (Figure 1 A, B, C) and the I/V curve overlapped with the control one, demonstrating the transient nature of the non-selective conductance**.**

Since we had previously hypothesized that aggregation was a key factor in membrane permeation, we have also tested aggregated cobalt oxide NPs. After sonication, NPs were left to aggregate for 30 min. Oocytes were exposed to the aggregated material and were tested with the same timing previously used, i.e. within 5 min and after 20 min from the NP addition. Here we did not observe any modification of the membrane parameters collected within 5 min (Figure 1) and after 20 min (data not shown). The absence of any effect of the aggregated Co_3O_4 NPs on membrane parameters was also seen with fluorescence experiments, in which intracellular calcein was not quenched (data not shown).

We have exposed oocytes also to zerovalent cobalt NPs. As for cobalt oxide NPs, zerovalent ones were sonicated just before exposure. Here again, we measured the membrane biophysical parameters within 5 min from sonication and after 20 min. As shown in Figure 1, zerovalent cobalt NPs did not modify membrane biophysical parameters. No statistically significant changes versus control oocytes were recorded for membrane resistance (Figure 1C), indicating no changes in the integrity of the plasma membrane. Similarly, the I/V curve of the oocytes exposed to zerovalent cobalt NPs did not differ from the control one (Figure 1D). We obtained similar results also for oocytes exposed for more than 20 min (data not shown). Additionally, we have measured membrane capacitance for all the tested conditions without finding any modification. Since capacitance is related to the nature and the

extension of the membrane, we think that none of the treatments caused drastic changes in membrane surface area, such as endocytosis or exocytosis.

Characterization of cobalt-based NPs

Membrane biophysical parameters of oocytes exposed to the various cobalt-based NPs changed according to the time in which the measurement occurred and to the NP type (Figure 1). Therefore, we have performed the characterization of cobalt and cobalt oxide NPs, to correlate the physico-chemical properties of the NPs with their biological outcome (Figure 2).

Both cobalt-based NPs were not stable in suspension. Indeed, in the experimental medium both NPs have a neutral z-potential (0.40 ± 0.06 mV for Co NPs, Figure 2A, and 0.52 ± 0.09 mV for Co_3O_4 NPs, Figure 2B). We have followed their aggregation dynamics by SLS (Figure 2C and D) in the time range that we used for measuring membrane biophysical parameters. The aggregation rate diverged between Co NPs, which in the experimental medium were not dispersed as sub-micron particles, and Co_3O_4 NPs, which after sonication presented a small fraction of transiently dispersed NPs. However, after 5 min, this fraction was no longer detectable due to aggregation.

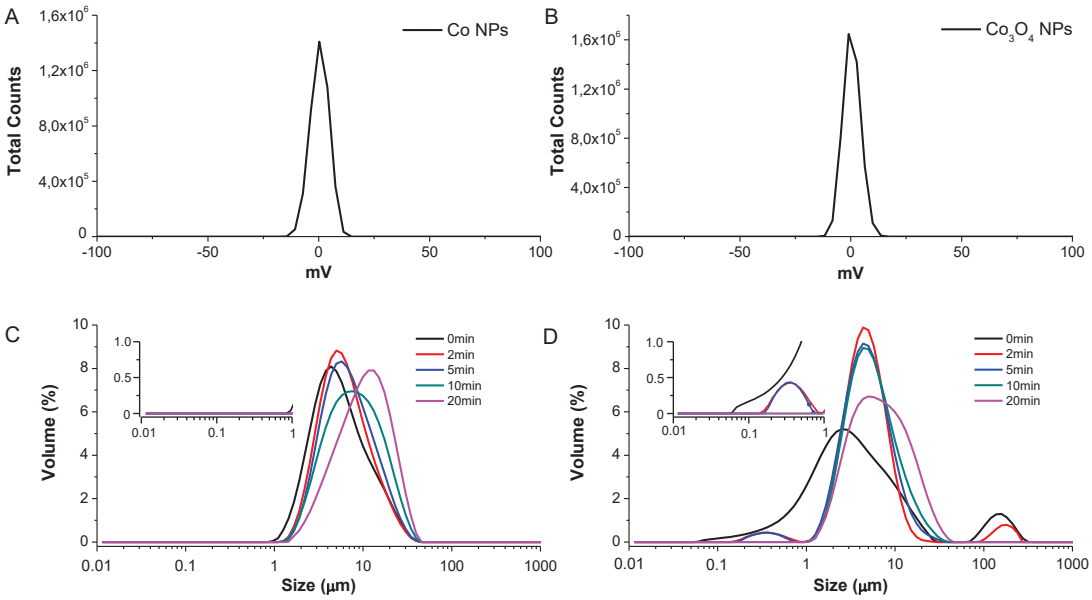

Figure 2: Co-based NPs characterization. *Charge and hydrodynamic size of zerovalent Cobalt NPs (Co NPs) in A and C and Cobalt Oxide NPs (Co_3O_4 NPs) in B and D, 0.1 mg/mL in buffered solution. Zeta potentials (A-B) were determined by Laser Doppler Micro-electrophoresis as 0.40 ± 0.06 mV for zerovalent Cobalt NPs and 0.52 ± 0.09 mV for Cobalt Oxide NPs (n=3). Hydrodynamic sizes were determined over time by Static Light Scattering and reported in C for Co NPs and in D for Co_3O_4 NPs; the insets represent an enlargement of the main graph, to highlight the NP population in the 0.01 to 1 µM range (representative experiments).*

Importance of protein corona on membrane biophysical parameters

We have treated cobalt oxide NPs with bovine serum albumin (BSA), since it interacts with the NP surface to form a protein corona. We have seen that whilst the superficial charge of NPs was not significantly modified by the presence of protein corona, their hydrodynamic size was markedly reduced (Figure 3). Indeed, the submicron population was still present after 20 min, in contrast with that for bare Co_3O_4 NPs that disappeared after 5 min (Figure 2).

Furthermore, as shown in Figure 3, BSA-coated NPs caused no significant change of the considered membrane biophysical parameters.

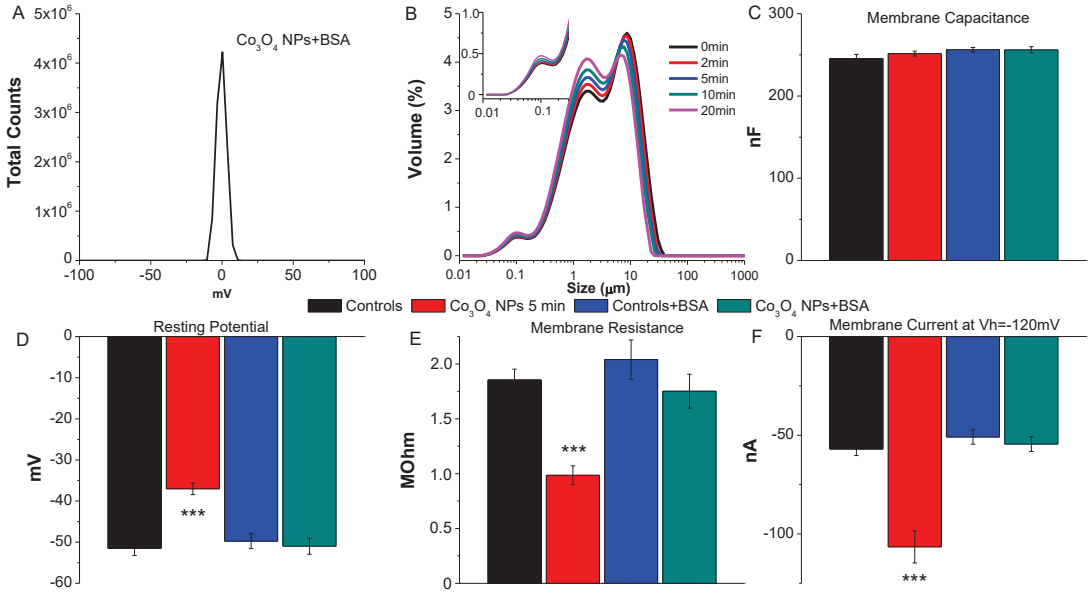

Figure 3: Co_3O_4 NPs+BSA characterization and effects on plasma membrane. *A-B) Charge and hydrodynamic size of Cobalt Oxide NPs (Co_3O_4 NPs), 0.1 mg/mL in buffered solution + 1 mg/mL BSA. Zeta potential (A) was determined by Laser Doppler Micro-electrophoresis as -0.35 ± 0.11 mV (n=3). Hydrodynamic size (B) was determined over time by Static Light Scattering (representative experiment). C-F) Membrane capacitance, resting potential, membrane resistance and membrane current at=-120mV of oocytes treated as indicated in Materials and Methods. Controls n=26 oocytes from 2 batches, Co_3O_4 NPs, 5 min, n=13 oocytes from 2 batches, Controls + BSA, n=29 oocytes from 2 batches, Co_3O_4 NPs + BSA, 5 min, n=29 oocytes from 2 batches. Statistical analysis performed with a One-Way ANOVA test with a Bonferroni-Holm post-hoc test.*

Nickel-based NPs do not cross membrane and modify its biophysical parameters

To complete the picture on transition metal-based NPs, we have performed fluorescence and electrophysiological analysis to investigate if also nickel-based NPs could cross directly the membrane. To this aim,

we tested if oxide and zerovalent nickel NPs were able to increase the cytosolic nickel content and to modify the resting potential, membrane resistance and membrane currents.

The diffusion of metal NPs through the plasma membrane into the cell would cause a cytoplasmic rise of dissolved metal ions, which could be detected by calcein quenching (Bossi *et al.*, 2016, Zanella *et al.*, 2017). To determine whether nickel-based NPs were able to cross the plasma membrane of *Xenopus* oocyte and diffuse into the cytoplasm, we first evaluated NP dissolution in the experimental buffer by measuring the amount of released nickel ions generating transport currents in oocytes expressing heterologous rDMT1 (Bossi *et al.*, 2016). These experiments confirmed that nickel-based NPs release nickel ions. We also calculated calcein affinity for Ni^{2+} that resulted suitable for detecting cytoplasmic concentration after NP exposure (7.1 ± 1.5 μM; Data not shown).

Then, we performed injection experiments as previously reported (Zanella *et al.*, 2017), to evaluate the fluorophore performance in the intracellular environment in presence of increasing nickel concentrations. As shown in Figure 4 A, the injection of $NiCl_2$ 50 μM was able to completely quench calcein fluorescence ($K_{0.5}$ determined with Logistic Fitting resulted 15.5 ± 5.9 μM), obtaining results comparable to those obtained for other metals tested in the intracellular environment. These data demonstrate that calcein is certainly able to detect Ni^{2+} ions in cytoplasm.

The fluorescence approach was then used to investigate the effect of treatment with NiO NPs or Ni NPs on intracellular presence of nickel ions. The results of these experiments showed that none of the NPs tested nor the ionic solution of $NiCl_2$ were able to quench calcein fluorescence (Figure 4B), suggesting that nickel NPs are not able to cross the cell membranes and confirming the absence of endogenous transporters for divalent cations.

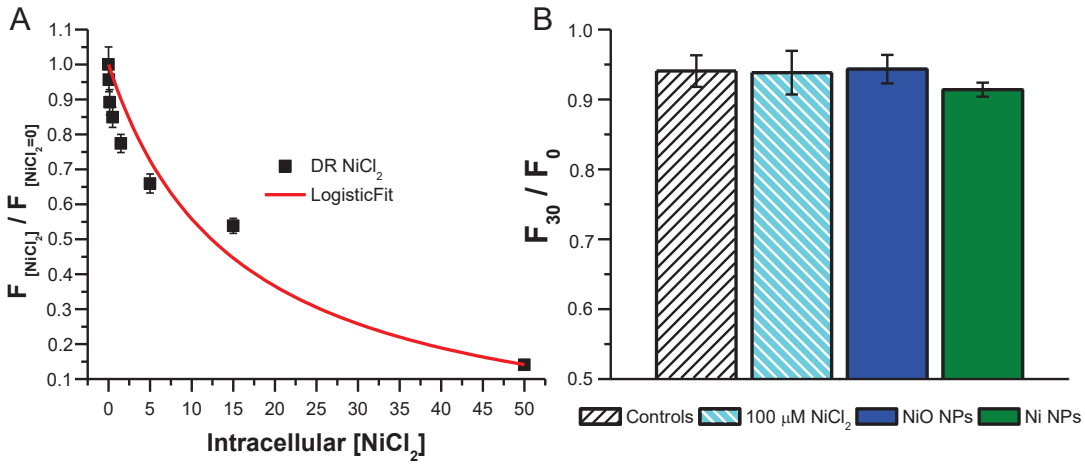

Figure 4: Effects of nickel-based NPs tested by fluorescence. *A) Residual fluorescence in presence of the indicated intracellular concentration of $NiCl_2$; the red line represents the logistic fit of the data collected from n=64 to 67 oocytes for each condition from 3 different batches. B) Normalized mean values of residual fluorescence of calcein after 30 min exposure to buffered solution, $NiCl_2$ 100μM, NiO NPs 0.1 mg/mL and Ni NPs 0.1 mg/mL. Controls n=11 oocytes from 5 batches, $NiCl_2$ 100μM n=6 oocytes from 2 batches, NiO NPs n=23 oocytes from 3 batches, Ni NPs n=10 oocytes from 2 batches – Statistical analysis performed with a One-Way ANOVA test with a Bonferroni-Holm post-hoc test.*

As shown in Figure 5, NiO NPs did not modify resting potential, membrane resistance and I/V relationship of the oocytes neither when parameters were tested within 5 min from the beginning of the treatment nor after 20 min. Similarly, we did not detect any electrophysiological changes also when oocytes were exposed to zerovalent nickel NPs.

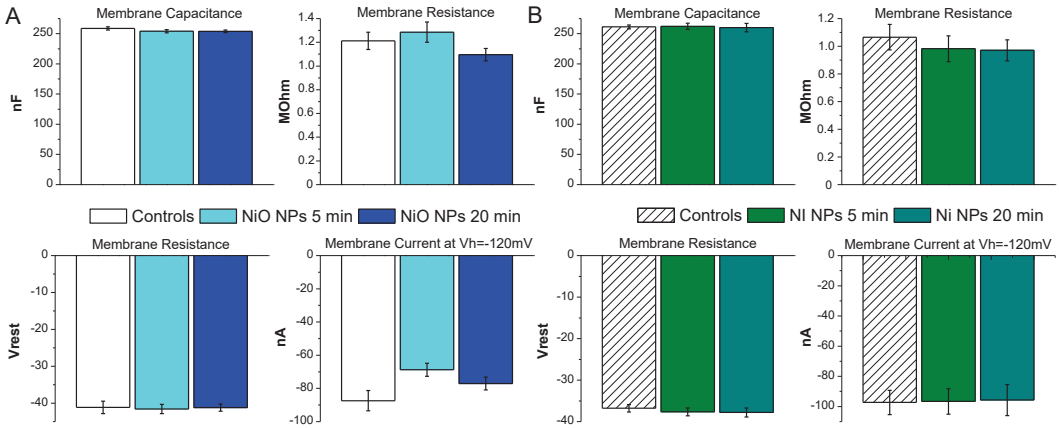

Figure 5: Effects of nickel-based NPs on plasma membrane. *Membrane capacitance, resting potential, membrane resistance and membrane current at Vm=-120 mV recorded from oocytes exposed to NiO NPs (A) and from oocytes exposed to Ni NPs (B). Controls n=53 oocytes, NiO NPs 5 min n=34 oocytes, NiO NPs 20 min n=47 oocytes from 2 batches; Controls n=25 oocytes, Ni NPs 5 min n=13 oocytes, Ni NPs 20 min n=23 from 2 batches - Statistical analysis performed with a One-Way ANOVA test with a Bonferroni-Holm post-hoc test.*

Characterization of nickel-based NPs

Nickel NPs exhibited absence of net superficial charge (Figure 6A, z-potential value of −0.17 ± 0.09 mV) and marked propensity to aggregate similarly to Co NPs. The presence of a submicron population can be recorded only immediately after NP addition to the experimental buffer, after which NPs immediately precipitated (as determined in 5 independent experiments, Figure 6C).

Conversely, NiO NPs exhibited a different behaviour from the previously studied metal oxide NPs, since the submicron population was always present in the 20 min of the hydrodynamic size experiments. Even with a neutral z-potential (Figure 6B, 0.045 ± 0.018 mV), those particles could stay in the experimental medium maintaining a population under 1 μM, the previous dimensional

"threshold" identified to explain the different biological behaviour of oxide compared to elemental NPs (Figure 6D). However, the comparison of the dimensional distributions for cobalt and nickel oxide particles highlighted a difference in the dimension of the submicron population, since Co_3O_4 NPs were able to retain for 5 min a population below 200 nm, dimension that NiO NPs never had (Figure 7).

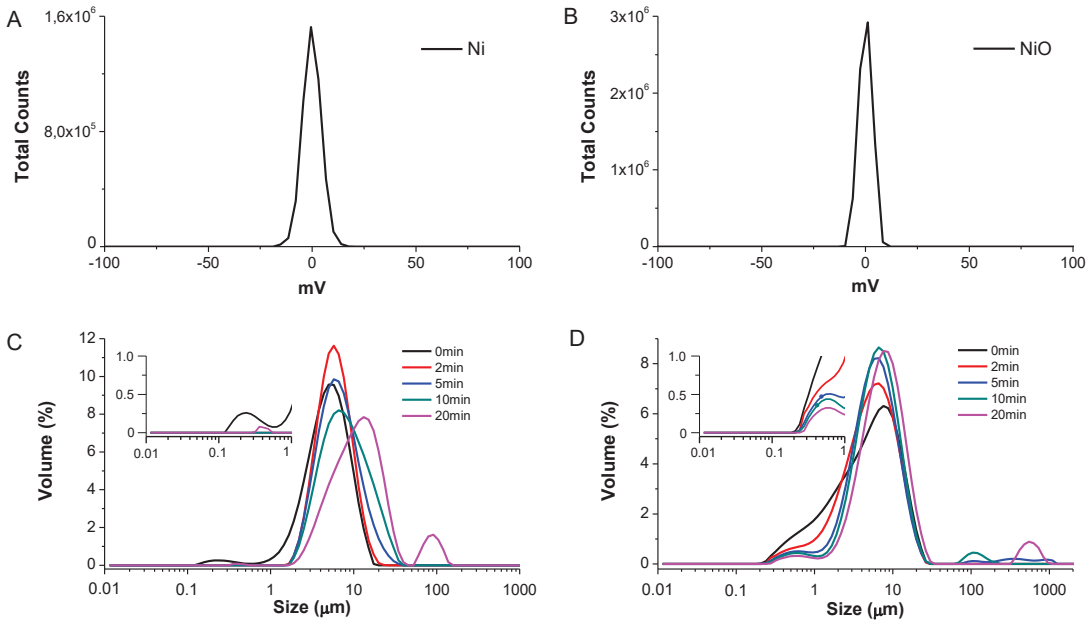

Figure 6: Ni- based NPs characterization. *Charge and hydrodynamic size of zerovalent Nickel NPs (Ni NPs - A and C) and Nickel Oxide NPs (NiO NPs – B and D), 0.1 mg/mL in buffered solution. Zeta potentials (A-B) were determined by Laser Doppler Micro-electrophoresis as −0.17 ± 0.09 mV for zerovalent Nickel NPs and 0.045 ± 0.018 mV for Nickel Oxide NPs (n=3). Hydrodynamic sizes (C-D) were determined over time by Static Light Scattering; the inset represents an enlargement of the main graph, to highlight the NP population among 0.01 to 1 μM (bottom graphs, representative experiments).*

Discussion

Endocytosis is the canonical route whereby NPs are internalized by cells (Papis *et al.*, 2009). However, an alternative mechanism has recently been suggested whereby NPs can directly cross the plasma membrane (Verma *et al.*, 2008, Taylor *et al.*, 2010, Lin and Alexander-Katz, 2013, Nolte *et al.*, 2015, Zhang *et al.*, 2015), thus bypassing the endosomal compartment. To investigate further this mechanism of NP uptake, we have made use of *Xenopus laevis* oocytes, which are large cells of approximately 1 mm in diameter, that for their characteristics, have become a convenient model for a variety of mechanistic studies (Bossi *et al.*, 2007, Cens and Charnet, 2007, Zhang and Mandato, 2007, Bernareggi *et al.*, 2015, Plautz *et al.*, 2016).

Using this model, we have been able to demonstrate that cobalt oxide NPs, but not zerovalent ones, caused an increase in cytoplasmic cobalt ion concentration (Bossi *et al.*, 2016). We explained these results hypothesizing that NPs, after having crossed plasma membrane, dissolved inside the cytoplasm, causing an increase in Co^{2+} concentration that could be detected by the quenching of the fluorescent dye that we had previously injected into the oocytes.

If this was the case, using an electrophysiological approach that monitors the integrity of the membrane, we should detect a conductance associated to the passage of the NPs. Indeed, we had measured a decrease in membrane resistance associated to the passage of iron oxide NPs (Zanella *et al.*, 2017). In the present paper, we have reinvestigated cobalt-based NPs to understand if their passage through the membrane would also cause a transient decrease of the membrane resistance. As shown in Figure 1, after exposure to cobalt oxide NPs there is a significant decrease in resting potential and membrane resistance. These results can be explained by a leakage occurring when the NPs cross the plasma membrane, causing a non-selective flux of ions. Similarly to that observed with iron oxide NPs, this conductance is present in the first 5

min after the beginning of the exposure and disappears completely after 20 min.

The resistance recovery could be explained either by an aroused unresponsiveness of the oocyte membrane to NPs or by a change in NP capability to interact with and cross the membrane. Recent experiments with iron-based NPs made us to favour the latter hypothesis. Indeed, we had demonstrated that agglomeration impeded NP diffusion through the membrane (Zanella *et al.*, 2017). To validate this hypothesis also for cobalt-based NPs, we have characterized their aggregation dynamics (Figure 2). The neutral z-potentials indicate that both NPs are unstable in our experimental medium, and SLS shows their tendency to aggregate over time. However, cobalt oxide NPs show a small (in terms of peak size of the volume-based measurement) submicron population of particles that could be those capable of diffusing through the membrane. Indeed, after 20 min this population disappears as well as the conductance in oocyte membrane. Conversely, zerovalent cobalt NPs do not present this population of dispersed NPs and are not able to cross the oocyte membrane. Hence, we have shown that the recovery of the oocyte membrane initial parameters that occurs after 20 min from the beginning of incubation is consistent with cobalt oxide NPs aggregating and no longer being able to cross the oocyte membrane.

The results of the experiments with nickel-based NPs are also consistent with this hypothesis. Here in addition to the two-electrode voltage method we also have investigated particle internalisation using a fluorescence approach. These NPs (both zerovalent and oxide) did not have any effect on the biophysical membrane parameters (Figure 5), as well as on the cytosolic Ni^{2+} concentration (Figure 4), showing that they cannot cross the plasma membrane. Their z-potentials are neutral, and their populations are polydisperse as for cobalt-based NPs (Figure 6). Ni NPs show a submicron population that precipitates too rapidly to have an impact on cell membranes. NiO NPs on the other hand show a

submicron population stable for the whole experiment length; the lack of effects could be due to the fact that, as shown in Figure 7, the submicron population hydrodynamic size is larger than that of cobalt oxide, indicating the presence bigger particles that are evidently not capable of diffusing through the membrane.

Taking all these considerations together, we propose that NPs, to diffuse though the membrane, should not be aggregated. However, dispersion is a necessary, but not sufficient, condition to allow NP membrane crossing. Our experiments with BSA-coated cobalt oxide NPs clearly show that those NPs were not able to modify oocyte membrane biophysical parameters, as bare cobalt oxide NPs did. We determined by SLS that the BSA-coated cobalt oxide NPs retain a dispersed population below 200 nm during the whole experiment, in sharp contrast with that of bare cobalt oxide NPs that start aggregating after 5 min. Notwithstanding BSA-coated NPs remaining dispersed, they do not enter inside the cells possibly because of the protein corona, which prevents particle-particle interactions as well as membrane-particle interactions.

NP coating is thus another a key factor to consider when studying the interactions of NPs with the plasma membrane. However, other factors could influence the process of NP diffusion through the membrane such as the crystalline structures of the NPs, which are different between the two metal oxide NPs (normal spinel for Co_3O_4, octahedral for NiO).

The detailed study of the interactions of NPs with membranes can be useful for designing engineered NPs as well as for a better comprehension of nanotoxicology. We could exploit this information to deliver engineered NPs functionalized with drugs, enzymes (Balzaretti *et al.*, 2017), DNA and antibiotics (Conde *et al.*, 2014, Armenia *et al.*, 2018) to the appropriate cell compartments through different cell access routes. Moreover, the possibility that NPs can transiently modify the membrane resting potential need to be considered while evaluating

their cytotoxicity or therapeutic potential. Indeed, alteration in membrane potential can act on different intracellular pathways.

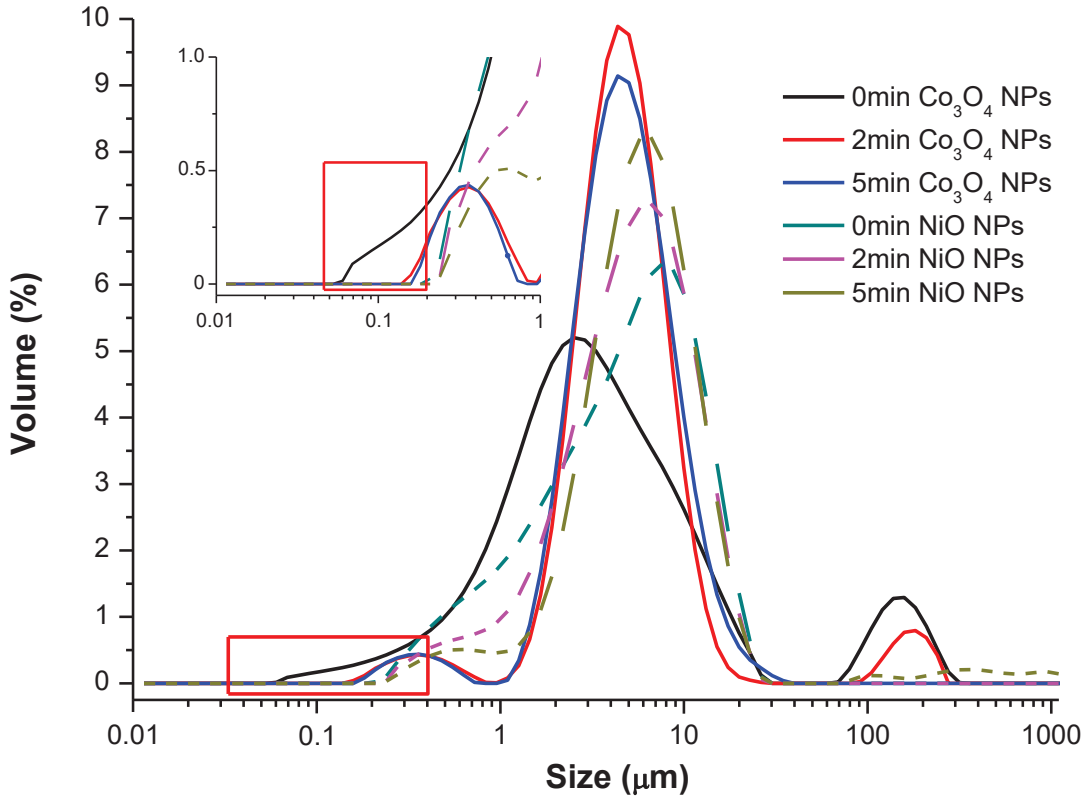

Figure 7: Hydrodynamic size distributions of Co_3O_4 and NiO NPs. *Comparison of the distributions of Co_3O_4 (continuous lines) and NiO NPs (non-continuous lines) within 5 min from the start of the measurements in the experimental medium. Submicron dimensional range in the inset, red square for the 200 nm threshold. Representative experiment.*

Materials and Methods

Solutions

Buffered solution (ND96) had the following composition (in mM): NaCl 96, KCl 2, $CaCl_2$ 1.8, $MgCl_2$ 1, HEPES 5, pH 7.6; NDE solution was composed of ND96 plus 2.5 mM pyruvate and 50 μg/mL Gentamycin sulphate; intracellular solution contained (in mM): KCl 130, NaCl 4, $MgCl_2$ 1.6, EGTA 5, HEPES 10, glucose 5, pH 7.6. The final pH values of 5.5 or 7.6 were adjusted with HCl and NaOH.

Oocytes collection and preparation

Oocytes were obtained from adult *Xenopus laevis* females. Animals were anaesthetised in 0.1 % (w/v) MS222 (tricaine methansulfonate) solution in tap water; after carefully cleaning the frog abdomen with an antiseptic agent (Povidone-iodine 10%), laparotomy was performed and portions of the ovary were collected. The oocytes were treated with 0.5 mg/mL collagenase (Sigma Type IA) in ND96 calcium free for at least 30 min at 18 °C. Healthy and fully grown oocytes were selected and stored at 18°C in NDE solution. The oocytes to be transfected with the cRNA coding for rDMT1 were injected with 25 ng of cRNA in 50 nL of water, the day after the removal, using a manual microinjection system (Drummond Scientific Company, Broomall, PA) and incubated at 18 °C for 3-4 days before electrophysiological or fluorescence experiments. The experimental protocol was approved locally by the Committee of the "Organismo Preposto al Benessere degli Animali" of the University of Insubria (OPBA-permit #02_15) and nationally by Ministero della Salute (permit nr. 1011/2015).

NP preparation and incubation conditions

The cobalt-based NPs used were Zerovalent (Co, 25 nm, IOLITEC, Salzstrasse 184, D-74076 Heilbronn) and oxide (Co_3O_4, < 50 nm TEM determined, Sigma-Aldrich). The nickel-based NPs used were

zerovalent (Ni, 25 nm, IOLITEC, Salzstrasse 184, D-74076 Heilbronn) and oxide (NiO, < 50 nm TEM determined, Sigma-Aldrich). All NPs were prepared as 10 mg/mL stock suspensions in deionised water and sonicated before the addition of 10 μL to the test chamber (4 wells plate) containing 990 μL of buffered solution (pH 7.6) where oocytes were then added. The conditions applied for oocytes NPs exposure were: Controls, oocytes exposed only to buffered solution, oocytes exposed to Co_3O_4 NPs and tested within 5 minutes from the NPs sonication, oocytes exposed to Co_3O_4 NPs and tested after 20 minutes from the NPs sonication, oocytes exposed to Co_3O_4 NPs that were let to aggregate for 30 minutes before adding them to the incubation chamber, and finally oocytes exposed to zerovalent Co NPs.

For electrophysiological experiments, the oocytes were transferred to the TEVC recording chamber within 5 min or after 20 min from the beginning of the exposure. For the fluorescence assay, recordings start immediately after oocytes addition to the test chamber. Treatments with the aggregated NPs were performed adding oocytes to the suspension of NPs that were let to aggregate in the test chamber for 30 min after sonication. Experiments with BSA were carried out using buffered containing 1 mg/mL BSA, in which were added NPs and oocytes.

All experiments were carried out at room temperature.

Fluorescence Assay

Oocytes were injected with a 50 nL drop of intracellular solution containing 25 μM calcein. In dose-response evaluation experiments, solutions containing calcein and increasing amounts of $NiCl_2$ were co-injected in oocytes. Effective intracellular metal concentrations were calculated using the nominal oocyte volume of 1 μL. Images were acquired for every oocyte at fixed acquisition parameters, calculated on control oocytes (oocytes injected only with calcein).

In experiments with NPs, images of single oocytes in each experimental condition applied were acquired every 2 min for 30 min with a fluorescence microscope (AxioVert 200, Carl Zeiss with a 4x objective, COLIBRI fluorescence filters, 470 nm excitation - 515 to 565 nm emission) equipped with CCD camera (True Chrome HD II S T EsseLab).

Electrophysiology

The two-electrode voltage clamp was performed with an Oocyte Clamp OC-725B (Warner Instruments, Hamden, CT, USA) that was controlled by Clampex 10.2 (Molecular Devices, Sunnyvale, CA, USA, www.moleculardevices.com). Intracellular glass microelectrodes, filled with 3 M KCl, had tip resistances in the 0.5 - 4 MΩ range. Agar bridges (3% agar in 3 M KCl) connected the bath electrodes to the experimental chamber. The holding potential (V_h) was -40 mV for all the experiments performed. The capacitance and resistance values reported were obtained applying 10 mV steps of 20 ms every 200 ms in voltage clamp conditions. The voltage pulses protocol, after 200 ms at the holding potential applied 10 mV voltage steps from -120 to +50 mV for 750 ms, and return to the holding potential for other 400 ms, the interval between stimuli was of 1 s.

Oocytes were transferred in the recording chamber (Warner-RC-1Z, warneronline.com) and impaled with microelectrodes; to recover from possible damage they were left for 2 min in a continuous solution flux. Only oocytes with resting potential equal or lower than -20 mV were used for the experiments. The number of discarded oocytes was not significantly different between treated and controls.

Data analysis

Data were analysed using Clampfit 10.2 software (Molecular Devices, Sunnyvale, CA, USA, www.moleculardevices.com) while OriginPro 8.0 (OriginLab Corp., Northampton, MA, USA, www.originlab.com) was

used for statistics and figure preparation. For the Voltage Step protocol, current values were measured for every voltage step at the steady state condition; mean values at every voltage were calculated and plotted. Fluorescence decay images were analysed with ImageJ (Rasband, W.S., ImageJ, U. S. National Institutes of Health, Bethesda, Maryland, USA, http://imagej.nih.gov/ij/, 1997-2015). For F_{30}/F_0 quantification, the fluorescence intensity at time 0 (F_0) and at time 30 min (F_t) was calculated in the entire area of the oocyte. In dose-response experiments, images were analysed calculating fluorescence intensity on the entire area of oocytes and normalized to the control oocytes. Mean values were calculated for every condition and used to determine through a non-linear fitting (Logistic Fitting, OriginPro8) the $K_{0.5}$, relating residual fluorescence to metal concentration.

Static light scattering (SLS)

SLS was performed on a Mastersizer 2000 with a Hydro 2000μP Micro Precision sample dispersion unit (Malvern Instruments Limited). Baseline correction was carried out with fresh buffered solution. Next, 200 μL of 10 mg/mL stock suspension was added to the 20 mL dispersion cell to achieve a final concentration of 0.1 mg/mL (as per Oocyte assays). The dispersion unit was run at 1000 rpm and care was taken to prevent bubble formation. The stock suspension was carefully sonicated prior to introduction to the dispersion cell, after which data acquisition was immediately initiated. Size measurements then were carried out over a period of 30 min (absorption 1.0; dispersant refractive index: 1.33; particles refractive index: Co_3O_4: 1.74 – Co: 2.14 – NiO: 2.18 – Ni: 1.98).

Zeta potential

The zeta potential of suspensions of iron NPs was determined by Laser Doppler Micro-electrophoresis (Zetasizer NanoZS, Malvern Instruments Ltd) using disposable folded capillary cells (DTS1070).

Measurements (n=3) were carried out using the diffusion barrier as per instrument manufacturer instructions. Briefly, the zeta cell was filled with 1 mM NaCl solution and then 100 μL sample (0.1 mg/mL suspension of NPs in buffered solution) was gently injected to the bottom of the cell with a gel-loading tip. Electrophoretic mobility of particles was converted into zeta potentials by Dispersion Technology Software 7.11 using the Smoluchowski approximation, and a viscosity of 0.8872cP and dielectric constant of 78.5 for the dispersant. Results are expressed as mean ± standard deviation.

Bibliography

Ahamed, M., Ali, D., Alhadlaq, H.A. & Akhtar, M.J., 2013. Nickel oxide nanoparticles exert cytotoxicity via oxidative stress and induce apoptotic response in human liver cells (HepG2). *Chemosphere,* 93**,** 2514-22.

Alkhammash, H.I., Li, N., Berthier, R. & De Planque, M.R., 2015. Native silica nanoparticles are powerful membrane disruptors. *Phys Chem Chem Phys,* 17**,** 15547-60.

Amde, M., Liu, J.F., Tan, Z.Q. & Bekana, D., 2017. Transformation and bioavailability of metal oxide nanoparticles in aquatic and terrestrial environments. A review. *Environmental Pollution,* 230**,** 250-267.

Anders, C.B., Eixenberger, J.E., Franco, N.A., Hermann, R.J., Rainey, K.D., Chess, J.J., Punnoose, A. & Wingett, D.G., 2018. ZnO nanoparticle preparation route influences surface reactivity, dissolution and cytotoxicity. *Environ Sci Nano,* 5**,** 572-588.

Ansari, S.M., Bhor, R.D., Pai, K.R., Sen, D., Mazumder, S., Ghosh, K., Kolekar, Y.D. & Ramana, C.V., 2017. Cobalt nanoparticles for biomedical applications: Facile synthesis, physiochemical characterization, cytotoxicity behavior and biocompatibility. *Applied Surface Science,* 414**,** 171-187.

Armenia, I., Marcone, G.L., Berini, F., Orlandi, V.T., Pirrone, C., Martegani, E., Gornati, R., Bernardini, G. & Marinelli, F., 2018. Magnetic nanoconjugated teicoplanin: a novel tool for bacterial infection site targeting. *Frontiers in Microbiology* 9.

Arvizo, R.R., Miranda, O.R., Thompson, M.A., Pabelick, C.M., Bhattacharya, R., Robertson, J.D., Rotello, V.M., Prakash, Y.S. & Mukherjee, P., 2010. Effect of nanoparticle surface charge at the plasma membrane and beyond. *Nano Lett,* 10**,** 2543-8.

Balzaretti, R., Meder, F., Monopoli, M.P., Boselli, L., Armenia, I., Pollegioni, L., Bernardini, G. & Gornati, R., 2017. Synthesis, characterization and programmable toxicity of iron oxide nanoparticles conjugated with D-amino acid oxidase. *Rsc Advances,* 7**,** 1439-1442.

Bannunah, A.M., Vllasaliu, D., Lord, J. & Stolnik, S., 2014. Mechanisms of nanoparticle internalization and transport across an intestinal epithelial cell model: effect of size and surface charge. *Molecular pharmaceutics,* 11**,** 4363-73.

Beddoes, C.M., Case, C.P. & Briscoe, W.H., 2015. Understanding nanoparticle cellular entry: A physicochemical perspective. *Advances in colloid and interface science,* 218**,** 48-68.

Bernareggi, A., Ren, E., Borelli, V., Vita, F., Constanti, A. & Zabucchi, G., 2015. Xenopus laevis Oocytes as a Model System for Studying the Interaction Between Asbestos Fibres and Cell Membranes. *Toxicol Sci,* 145**,** 263-72.

Bhuvaneshwari, M., Kumar, D., Roy, R., Chakraborty, S., Parashar, A., Mukherjee, A., Chandrasekaran, N. & Mukherjee, A., 2017. Toxicity, accumulation, and trophic transfer of chemically and biologically synthesized nano zero valent iron in a two species freshwater food chain. *Aquatic Toxicology,* 183**,** 63-75.

Bossi, E., Fabbrini, M.S. & Ceriotti, A., 2007. Exogenous protein expression in Xenopus Laevis Oocyte, Basic procedure. *In* G. Grandi (ed.) *In Vitro Transcription and translation Protocols.* 375 ed. Totowa NJ: Humana Press, 107-131.

Bossi, E., Zanella, D., Gornati, R. & Bernardini, G., 2016. Cobalt oxide nanoparticles can enter inside the cells by crossing plasma membranes. *Sci Rep,* 6**,** 22254.

Brandenberger, C., Muhlfeld, C., Ali, Z., Lenz, A.-G., Schmid, O., Parak, W.J., Gehr, P. & Rothen-Rutishauser, B., 2010. Quantitative evaluation of cellular uptake and trafficking of plain and polyethylene glycol-coated gold nanoparticles. *Small (Weinheim an der Bergstrasse, Germany),* 6**,** 1669-78.

Cens, T. & Charnet, P., 2007. Use of Xenopus oocytes to measure ionic selectivity of pore-forming peptides and ion channels. *Methods Mol Biol,* 403**,** 287-302.

Chen, J., Hessler, J.A., Putchakayala, K., Panama, B.K., Khan, D.P., Hong, S., Mullen, D.G., Dimaggio, S.C., Som, A., Tew, G.N., Lopatin, A.N., Baker, J.R., Holl, M.M. & Orr, B.G., 2009. Cationic nanoparticles induce nanoscale disruption in living cell plasma membranes. *J Phys Chem B,* 113**,** 11179-85.

Cho, E.C., Au, L., Zhang, Q. & Xia, Y., 2010. The effects of size, shape, and surface functional group of gold nanostructures on their adsorption and internalization by cells. *Small,* 6**,** 517-22.

Conde, J., Dias, J.T., Grazu, V., Moros, M., Baptista, P.V. & De La Fuente, J.M., 2014. Revisiting 30 years of biofunctionalization and surface chemistry of inorganic nanoparticles for nanomedicine. *Front Chem,* 2**,** 48.

Date, A.A., Hanes, J. & Ensign, L.M., 2016. Nanoparticles for oral delivery: Design, evaluation and state-of-the-art. *J Control Release,* 240**,** 504-526.

Ding, H.-M. & Ma, Y.-Q., 2015. Theoretical and computational investigations of nanoparticle-biomembrane interactions in cellular delivery. *Small (Weinheim an der Bergstrasse, Germany),* 11**,** 1055-71.

Frohlich, E., 2012. The role of surface charge in cellular uptake and cytotoxicity of medical nanoparticles. *International journal of nanomedicine,* 7**,** 5577-91.

Frohlich, E., 2013. Cellular targets and mechanisms in the cytotoxic action of non-biodegradable engineered nanoparticles. *Curr Drug Metab,* 14**,** 976-88.

Horev-Azaria, L., Kirkpatrick, C.J., Korenstein, R., Marche, P.N., Maimon, O., Ponti, J., Romano, R., Rossi, F., Golla-Schindler, U., Sommer, D., Uboldi, C., Unger, R.E. & Villiers, C., 2011. Predictive toxicology of cobalt nanoparticles and ions: comparative in vitro study of different cellular models using methods of knowledge discovery from data. *Toxicological sciences : an official journal of the Society of Toxicology,* 122**,** 489-501.

Horie, M., Fukui, H., Nishio, K., Endoh, S., Kato, H., Fujita, K., Miyauchi, A., Nakamura, A., Shichiri, M., Ishida, N., Kinugasa,

S., Morimoto, Y., Niki, E., Yoshida, Y. & Iwahashi, H., 2011. Evaluation of Acute Oxidative Stress Induced by NiO Nanoparticles In Vivo and In Vitro. *Journal of Occupational Health,* 53**,** 64-74.

Horie, M., Yoshiura, Y., Izumi, H., Oyabu, T., Tomonaga, T., Okada, T., Lee, B.W., Myojo, T., Kubo, M., Shimada, M. & Morimoto, Y., 2016. Comparison of the Pulmonary Oxidative Stress Caused by Intratracheal Instillation and Inhalation of NiO Nanoparticles when Equivalent Amounts of NiO Are Retained in the Lung. *Antioxidants,* 5.

Li, Y., Zhang, X. & Cao, D., 2015. Nanoparticle hardness controls the internalization pathway for drug delivery. *Nanoscale,* 7**,** 2758-69.

Li, Z., Zhang, Y., Zhu, D., Li, S., Yu, X., Zhao, Y., Ouyang, X., Xie, Z. & Li, L., 2017. Transporting carriers for intracellular targeting delivery via non-endocytic uptake pathways. *Drug Delivery,* 24**,** 45-55.

Lin, J. & Alexander-Katz, A., 2013. Cell membranes open "doors" for cationic nanoparticles/biomolecules: insights into uptake kinetics. *ACS Nano,* 7**,** 10799-808.

Moghadam, B.Y., Hou, W.C., Corredor, C., Westerhoff, P. & Posner, J.D., 2012. Role of nanoparticle surface functionality in the disruption of model cell membranes. *Langmuir,* 28**,** 16318-26.

Morimoto, Y., Hirohashi, M., Ogami, A., Oyabu, T., Myojo, T., Hashiba, M., Mizuguchi, Y., Kambara, T., Lee, B.W., Kuroda, E. & Tanaka, I., 2011. Pulmonary Toxicity Following an Intratracheal Instillation of Nickel Oxide Nanoparticle Agglomerates. *Journal of Occupational Health,* 53**,** 293-295.

Nativo, P., Prior, I.A. & Brust, M., 2008. Uptake and intracellular fate of surface-modified gold nanoparticles. *ACS Nano,* 2**,** 1639-44.

Nolte, T.M., Kettler, K., Meesters, J.A., Hendriks, A.J. & Van De Meent, D., 2015. A semi-empirical model for transport of inorganic nanoparticles across a lipid bilayer: implications for uptake by living cells. *Environ Toxicol Chem,* 34**,** 488-96.

Ortega, R., Bresson, C., Darolles, C., Gautier, C., Roudeau, S., Perrin, L., Janin, M., Floriani, M., Aloin, V., Carmona, A. & Malard, V., 2014. Low-solubility particles and a Trojan-horse type

mechanism of toxicity: the case of cobalt oxide on human lung cells. *Particle and fibre toxicology,* 11**,** 14.

Papis, E., Rossi, F., Raspanti, M., Dalle-Donne, I., Colombo, G., Milzani, A., Bernardini, G. & Gornati, R., 2009. Engineered cobalt oxide nanoparticles readily enter cells. *Toxicology Letters,* 189**,** 253-259.

Peetla, C. & Labhasetwar, V., 2009. Effect of molecular structure of cationic surfactants on biophysical interactions of surfactant-modified nanoparticles with a model membrane and cellular uptake. *Langmuir,* 25**,** 2369-77.

Peters, A., Veronesi, B., Calderon-Garciduenas, L., Gehr, P., Chen, L.C., Geiser, M., Reed, W., Rothen-Rutishauser, B., Schurch, S. & Schulz, H., 2006. Translocation and potential neurological effects of fine and ultrafine particles a critical update. *Particle and fibre toxicology,* 3**,** 13.

Plautz, C.Z., Williams, H.C. & Grainger, R.M., 2016. Functional Cloning Using a Xenopus Oocyte Expression System. *J Vis Exp***,** e53518.

Sabbioni, E., Fortaner, S., Farina, M., Del Torchio, R., Olivato, I., Petrarca, C., Bernardini, G., Mariani-Costantini, R., Perconti, S., Di Giampaolo, L., Gornati, R. & Di Gioacchino, M., 2014a. Cytotoxicity and morphological transforming potential of cobalt nanoparticles, microparticles and ions in Balb/3T3 mouse fibroblasts: an in vitro model. *Nanotoxicology,* 8**,** 455-64.

Sabbioni, E., Fortaner, S., Farina, M., Del Torchio, R., Petrarca, C., Bernardini, G., Mariani-Costantini, R., Perconti, S., Di Giampaolo, L., Gornati, R. & Di Gioacchino, M., 2014b. Interaction with culture medium components, cellular uptake and intracellular distribution of cobalt nanoparticles, microparticles and ions in Balb/3T3 mouse fibroblasts. *Nanotoxicology,* 8**,** 88-99.

Shimizu, K., Nakamura, H. & Watano, S., 2016. MD simulation study of direct permeation of a nanoparticle across the cell membrane under an external electric field. *Nanoscale,* 8**,** 11897-906.

Shin, E.H., Li, Y., Kumar, U., Sureka, H.V., Zhang, X. & Payne, C.K., 2013. Membrane potential mediates the cellular binding of nanoparticles. *Nanoscale,* 5**,** 5879-86.

Song, B., Yuan, H., Pham, S.V., Jameson, C.J. & Murad, S., 2012. Nanoparticle permeation induces water penetration, ion transport, and lipid flip-flop. *Langmuir,* 28**,** 16989-7000.

Taylor, U., Klein, S., Petersen, S., Kues, W., Barcikowski, S. & Rath, D., 2010. Nonendosomal Cellular Uptake of Ligand-Free, Positively Charged Gold Nanoparticles. *Cytometry Part A,* 77a**,** 439-446.

Verma, A., Uzun, O., Hu, Y., Hu, Y., Han, H.S., Watson, N., Chen, S., Irvine, D.J. & Stellacci, F., 2008. Surface-structure-regulated cell-membrane penetration by monolayer-protected nanoparticles. *Nat Mater,* 7**,** 588-95.

Warren, E.A. & Payne, C.K., 2015. Cellular binding of nanoparticles disrupts the membrane potential. *RSC Adv,* 5**,** 13660-13666.

Zanella, D., Bossi, E., Gornati, R., Bastos, C., Faria, N. & Bernardini, G., 2017. Iron oxide nanoparticles can cross plasma membranes. *Scientific reports,* 7**,** 11413.

Zhang, H., Ji, Q., Huang, C., Zhang, S., Yuan, B., Yang, K. & Ma, Y.Q., 2015. Cooperative transmembrane penetration of nanoparticles. *Sci Rep,* 5**,** 10525.

Zhang, T. & Mandato, C.A., 2007. Xenopus oocyte wound healing as a model system for analysis of microtubule-actin interactions. *Methods Mol.Med.,* 137**,** 181-188.

Chapter 5

Interactions of γ-Fe_2O_3 NPs and γ-Fe_2O_3 NPs functionalized with APTES with the membranes of the *Xenopus laevis* oocytes

This Chapter contains unpublished data, regarding the research conducted on γ-Fe_2O_3 NPs uncoated and functionalized with APTES, starting from the particles synthesis to their physico-chemical characterization and biological testing. The research activity production is reported starting with a brief introduction on the particles and their importance, followed by a description of the techniques used and the methods applied and by the results of the experimental activities performed.

Introduction

Iron oxide NPs, and among them Superparamagnetic Iron Oxide NPs (SPIONs) are currently utilized in biomedical applications mainly due to their biocompatibility and the large possibility of customization[1-4]. SPIONs are suitable tools for numerous applications due to their inducible high magnetization when exposed to an externally applied magnetic field, that allows heating or targeting them to the area of interest, like a specific tissue[5-7]. Specific coatings are needed to stabilize NPs in suspension and to avoid their surface oxidation and consequently partial loss of their magnetic characteristics. The coating molecules often merely act as a barrier to protect the NPs against external agents, but sometimes happen to drastically affect the electronic properties of the NPs[8].

Concerning their biocompatibility, many studies report iron oxide NPs to be highly biocompatible and to have with very low toxicity[9-14],[23]. Some papers however show contradictory results[15-19], demanding more detailed analysis to assess *in vitro* (cellular effects, ROS generation, ions

release and genetic effects) and *in vivo* (toxicokinetics, acute toxicity, genotoxicity, neurotoxicity, immunotoxicity and reproductive toxicity) mechanisms and effects. Further studies will be helpful in filling the main knowledge gaps in the iron oxide NP safety and toxicity fields.
The work reported here focuses on both aspects; understanding if uncoated SPIONs and coated ones can cross plasma membrane bypassing endocytosis would spread even more the range of possible use for these particles and would give also some clues about a mechanism of possible toxicity that has been often underestimated. The SPIONs tested in this work are maghemite (γ-Fe_2O_3, from here onward reported as Fe_2O_3 NPs) NPs, which are already used in many fields[5, 20][24, 25] and maghemite NPs functionalized with 3-aminopropyltriethoxylsilane (APTES), to achieve the surface stabilization and to make surface functionalization with biomolecules possible[26, 27].

Materials and Methods

Oocytes Collection and Preparation

See "Oocytes Collection and Preparation" section in Materials and Methods - Chapter 4.

γ-Fe_2O_3 NPs Synthesis

γ-Fe_2O_3 were synthetized following a protocol based on [26]. The synthesis was performed in an Erlenmeyer flask positioned on a heating plate with a magnetic stirrer. Because of the risk of production of nitrous gases in the heating steps, the synthesis was conducted under a working fume-hood. The synthesis yield will approximately be 50 mL of aqueous γ-Fe_2O_3 NPs dispersion.

1. Add 8.89 g $FeCl_3$ * 6 H_2O (Sigma-Aldrich n. cat: 31232) and 3.28 g $FeCl_2$ * 4 H_2O (Sigma-Aldrich n. cat: 44939) in 380 mL H_2O (in a 500 mL Erlenmeyer flask) on a magnetic stirrer for 30 min.

While stirring add slowly 1.5 mL of 37% HCl to dissolve iron salts completely.

2. Add slowly and under strong stirring 25 mL of 25% NH_4OH to iron solution: a black precipitate will appear. Stir for additional 10 min.
3. Remove flask from magnetic stirrer and let particles precipitate by placing a permanent magnet (NdFeB-magnet) under the flask and wait until all the NPs are collected to the bottom (10-20 min). NdFeB-magnet magnetic field is very strong, so caution must be paid.
4. Remove the supernatant (aqueous media) by decantation and wash twice the NPs with 100 mL of H2O MilliQ, leaving them 10 min on magnetic stirrer for each washing. During the last washing steps, transfer the suspension into a smaller Erlenmeyer flask (100 mL).
5. After the transfer, add 40 mL of 2 M HNO_3 and heat up to 90 °C for a 5 min. The suspension will turn from black to dark brown.
6. Isolate particles again with the magnet and add 60 mL of 0.34 M solution of $Fe(NO_3)_3 * 9\ H_2O$ (Sigma-Aldrich n. cat: 216828). Heat up to 90 °C and stir for 30 min.
7. Cool down to RT and remove supernatant (NdFeB-magnet).
8. Add 50 mL of H_2O (can be more) on the particles and stir properly. The particles will now "dissolve" leading to a magnetic fluid containing a well dispersion of iron oxide nanoparticles.
9. Filter NPs through 0.2 μm syringe filters for removal of larger aggregates. If dispersion cannot be filtered well, add more water to dilute the ferrofluid and use new filter.
10. Pipette into a glass bottle and store at 4 °C. If needed the iron oxide NPs solution can be dialyzed to remove any iron salts still present after the last steps.

γ-Fe_2O_3 NPs Functionalization with APTES

γ-Fe_2O_3 were functionalized with APTES (Sigma n. cat: A3648). Since newly synthetized oxide NPs were suspended in aqueous media, the corresponding of 150 mg of NPs was added to 1 mL of a solution composed by 975.4 μL of EtOH and 24.6 μL of APTES. The right amount of APTES was calculated from the total NPs surface area to have enough APTES to coat each NP. EtOH was added up to the volume of 1 mL. The reaction was maintained under mechanical stirring for 1 h (RT) and for 1 h (90 °C). Then, the synthetized γ-Fe_2O_3-APTES NPs were washed three times with H_2O MilliQ by centrifugation 5 minutes at 10000 x g and resuspended in H_2O MilliQ by ultrasonication.

Amine group on the NPs-surface determination

The amino content of the NPs was measured by the Orange II spectrophotometric assay[21, 22]: 1 mL of a solution of 1 mM Orange II pH 3 was added to 1 mg of NPs and maintained under stirring for 30 min at 40°C. The particles were precipitated and washed with an acidic water solution until all the unbound dye was removed. To desorb the bound dye, a solution at pH 12 was added to the NPs. The amount of desorbed dye was then measured at a wavelength of 480 nm with a UV/vis spectrophotometer.

NP Treatment Conditions

All NPs were prepared as 10 mg/mL (particle weight) stock suspensions in deionised water and sonicated before the addition of 10 μL to the test chamber (4 wells plate) containing 990 μL of buffered solution (pH 7.6) where oocytes were then added.

For electrophysiological experiments, the oocytes were transferred to the TEVC recording chamber within 5 min or after 20 min from the beginning of the exposure. For the fluorescence assay, recordings start

immediately after oocytes addition to the test chamber. All experiments were carried out at room temperature.

Solutions

See "Solutions" section in Materials and Methods - Chapter 4.
$FeCl_3$ (Sigma) was prepared fresh as a stock solution (50mM) in buffered solution and diluted to the working concentrations.

Spectrofluorometry

NP dissolution and release was evaluated by measuring calcein quenching (fixed concentration of 2.5 μM) in presence of increasing concentration of NPs, added to buffered solution pH 7.6 from the 10 mg/mL stocks. Jasco FP-750 fluorometer with excitation at 470 nm, emission spectra measured in the 490 to 560 nm range.

Fluorescence Assay

See "Fluorescence Assay" section in Materials and Methods - Chapter 4.

Electrophysiology

The two-electrode voltage clamp was performed with an Oocyte Clamp OC-725B (Warner Instruments, Hamden, CT, USA) that was controlled by Clampex 10.2 (Molecular Devices, Sunnyvale, CA, USA, www.moleculardevices.com). Intracellular glass microelectrodes, filled with 3 M KCl, had tip resistances in the 0.5 - 4 MΩ range. Agar bridges (3% agar in 3 M KCl) connected the bath electrodes to the experimental chamber. The holding potential (V_h) was -40 mV for all the experiments performed. The capacitance and resistance values reported were obtained applying 10 mV steps of 20 ms every 200 ms in voltage clamp conditions. The voltage pulses protocol, after 200 ms at the holding potential applied 10 mV voltage steps from -120 to +50 mV for 750 ms, and return to the holding potential for other 400 ms, the interval between stimuli was of 1 s.

Oocytes were transferred in the recording chamber (Warner-RC-1Z, warneronline.com) and impaled with microelectrodes; to recover from possible damage they were left for 2 min in a continuous solution flux. Only oocytes with resting potential equal or lower than -20 mV were used for the experiments. The number of discarded oocytes was not significantly different between treated and controls.
For Fe_2O_3 NPs, I/V relationships values were considered till +20 mV, after which there was the opening of endogenous conductances not related to the treatment (i.e. present also in the control condition) that forced us to exclude these data.

Zeta Potential

See "Zeta Potential" section in Materials and Methods - Chapter 4.

Static Light Scattering (SLS)

SLS was performed on a Mastersizer 2000 with a Hydro 2000μP Micro Precision sample dispersion unit (Malvern Instruments Limited). Baseline correction was carried out with fresh buffered solution. Next, 200 μL of 10 mg/mL stock suspension was added to the 20 mL dispersion cell to achieve a final concentration of 0.1 mg/mL (as per Oocyte assays). The dispersion unit was run at 1000 rpm and care was taken to prevent bubble formation. The stock suspension was carefully sonicated prior to introduction to the dispersion cell, after which data acquisition was immediately initiated. Size measurements then were carried out over a period of 30 min (absorption 1.0; dispersant refractive index: 1.33; particles refractive index: 2.94).

Data Analysis

See "Data Analysis" section in Materials and Methods - Chapter 4.

Results and Discussion

Fe^{3+} Uptake Evaluation

As a first step, the presence of endogenous transporters for the metal ion deriving from the NPs (Fe^{3+}) was evaluated. Increasing concentrations of $FeCl_3$, 100 μM – 300 μM – 1 mM, were perfused on the oocytes clamped at -40mV, and membrane current was recorded. Results are reported in Figure 1.

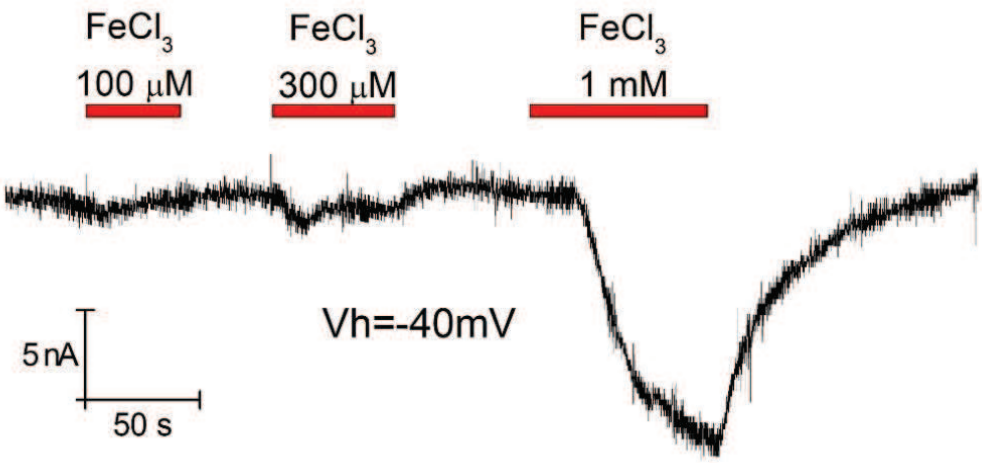

Figure 1: *electrophysiological recording at -40 mV from control oocyte in buffered solution exposed to 100 μM, 300 μM and 1 mM $FeCl_3$. Representative trace.*

As it is possible to see, a small conductance generating an inward ion flux opens at a concentration of 1 mM $FeCl_3$. Although an endogenous metal transport it is present, the concentration that triggers the metal transport it is about tenfold of the estimated concentration of Fe^{3+} ions released at the working concentration of 0.1 mg/mL of Fe_2O_3 NPs, conditions used in our study (Figure 2).

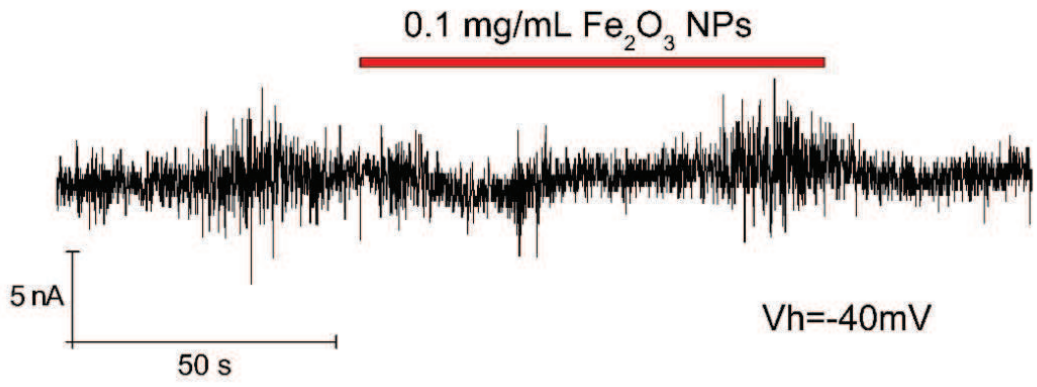

Figure 2: *electrophysiological recording at -40 mV from control oocyte in buffered solution exposed to 0.1 mg/mL Fe_2O_3 NPs. No currents were detected during exposition to NPs. Representative trace.*

The complete dissolution of the Fe_2O_3 NPs would be required to release 1.25 mM Fe^{3+}. The dissolution of any metal oxide is very hard to achieve, and it usually requires an acidic pH, rather than the neutral-slightly basic pH of the buffered solution used in this study (7.6). Total dissolution of the particles in the condition used is most unlikely. Therefore, the endogenous metal transporter presence do not affect the experimental data of this study.

Fluorescence Evaluation

The binding of the probe calcein with the ions released from the NPs was evaluated through spectrofluorometry.

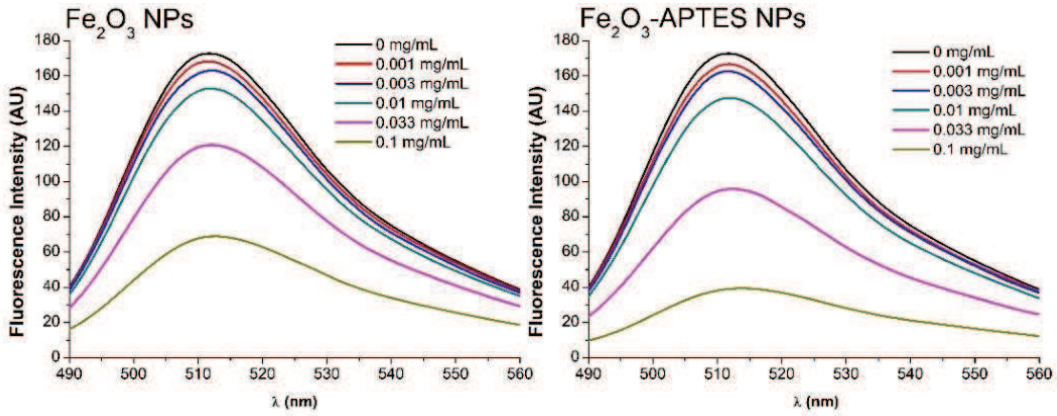

Figure 3: *emission spectra (means, n=3) obtained monitoring fixed calcein concentration with the addition of increasing concentrations of Fe_2O_3 NPs (left) and Fe_2O_3-APTES NPs (right).*

From the data shown in Figure 2, it is possible to observe that calcein was able to bind to the ions released from NPs and that they quenched its fluorescence although NPs released Fe^{3+} ions, for which the calcein affinity is reduced if compared to Fe^{2+} ions. Functionalized particles seem to release more than uncoated ones, increasing the quenching at the highest concentrations.

The calcein-injected oocytes have been used, to check if these particles were able to cross the membrane and to modify the intracellular fluorescence.

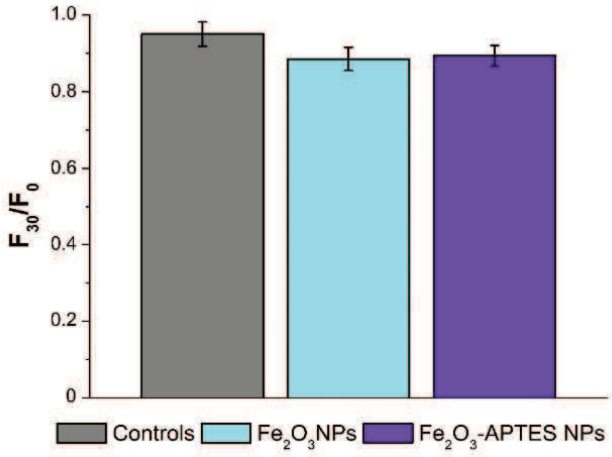

Figure 4: *Mean values of fluorescence intensity (± S.E.M.) of calcein-injected oocytes measured at 30 min from the start of the experiments and normalized at time 0 values. Controls n=14 – Fe_2O_3 NPs n=11 – Fe_2O_3-APTES NPs n=11 – 3 oocytes batches each – One-way ANOVA test with Bonferroni-Holm post-hoc correction.*

Data reported in Figure 4 show that particles were not able to quench calcein fluorescence (data are means ± S.E.M. - Controls = 95.08% ± 3.17% - Fe_2O_3 NPs = 88.57 % ± 3.03% - Fe_2O_3-APTES NPs = 89.40 % ± 2.70 %), values reported do not show statistically significant differences. To comprehend if the NPs do not cross the membrane or if the signal stability can be related to the reduced calcein affinity for the Fe^{3+} ions released from the NPs, the electrophysiological approach was applied to investigate the membrane integrity. Monitoring the membrane status permits to identify particle effects on the membrane, that could stand for a passive permeation that we are not able to detect through the fluorescence approach.

Electrophysiological Approach

Firstly, membrane capacitance, cell resting potential and membrane resistance were evaluated for oocytes exposed to each type of NPs. The parameters were measured in control condition (buffered solution pH 7.6), within 5 min from the start of the exposure and after 20 min, according to previous experiments. Values recorded for Fe_2O_3 NPs are reported in Figure 5, those obtained for Fe_2O_3-APTES NPs in Figure 6.
Transmembrane currents were measured and plotted in I/V relationships to investigate the presence of ion fluxes induced by the treatment with NPs. Results are reported in Figure 7 (Fe_2O_3 NPs) and in Figure 8 (Fe_2O_3-APTES NPs).

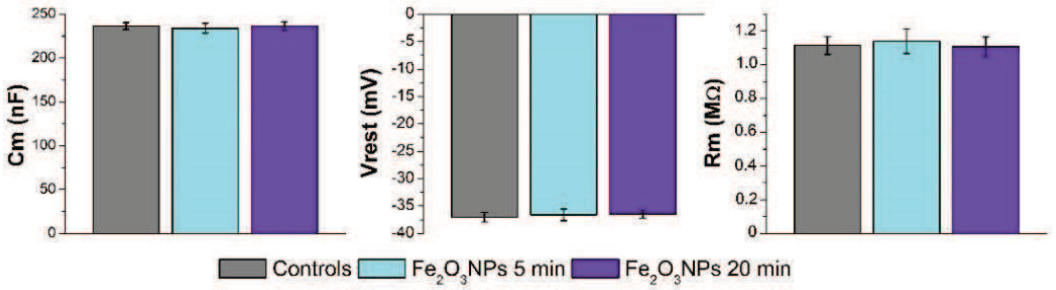

Figure 5: *Membrane capacitance (left), resting potential (center) and membrane resistance (right) (means ± S.E.M.) of oocytes in the indicated treatment conditions. Controls n=74 – Fe_2O_3 NPs 5 min n=51 – Fe_2O_3 NPs 20 min n=48 – 3 oocytes batches each – One-way ANOVA test with Bonferroni-Holm post-hoc correction.*

The Fe_2O_3 NPs were not able to modify any of the membrane parameters, neither the one related to endocytosis (capacitance) nor the ones relating to membrane integrity and passive permeation (resting potential and resistance). None of the time conditions considered resulted effective, suggesting the lack of interactions between tested NPs and the membrane, and confirming the data collected with calcein probe.

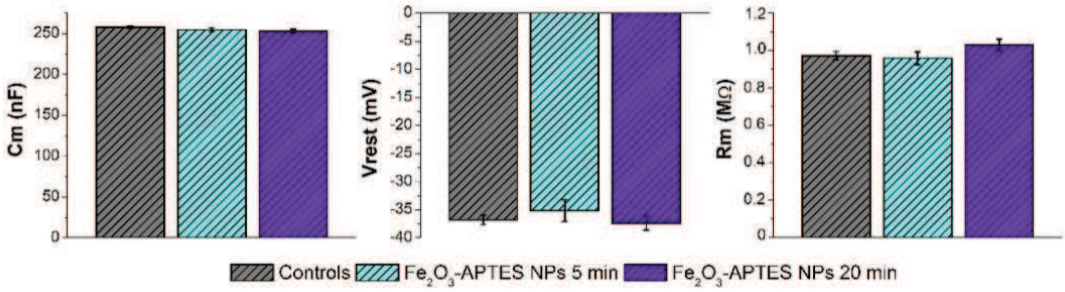

Figure 6: *Membrane capacitance (left), resting potential (center) and membrane resistance (right) (means ± S.E.M.) of oocytes in the indicated treatment conditions. Controls n=195 – Fe_2O_3-APTES NPs 5 min n=81 – Fe_2O_3-APTES NPs 20 min n=86 – 4 oocytes batches each – One-way ANOVA test with Bonferroni-Holm post-hoc correction.*

Likewise, the treatment with Fe_2O_3-APTES did not modify membrane biophysical parameters in any of the condition tested. The coating did not modify the NP interactions with the membrane.

The membrane parameters suggested the absence of membrane modification and were validated by the data reported in the I/V relationships.

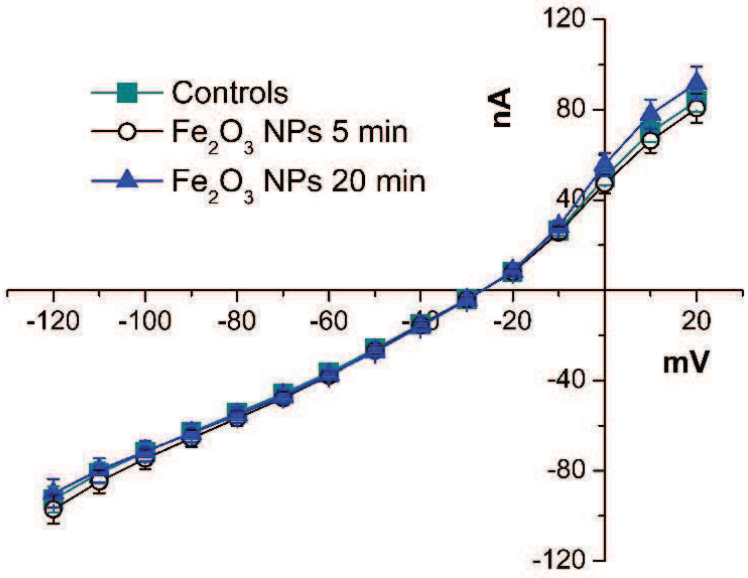

Figure 7: *I/V relationships (means ± S.E.M.) obtained from oocytes exposed to control condition (buffered solution pH 7.6), Fe_2O_3 NPs within 5 min and Fe_2O_3 NPs for 20 min. Controls n=74 – Fe_2O_3 NPs 5 min n=51 – Fe_2O_3 NPs 20 min n=48 – 3 oocytes batches each – One-way ANOVA test with Bonferroni-Holm post-hoc correction.*

I/V relationships of the Fe_2O_3 NPs treatments overlap with the control one, confirming the lack of interactions with the oocyte membrane. The data reported in the I/V curves are limited to +20 mV; at higher voltages these oocytes showed the opening of endogenous conductances, revealed in all the batches tested (evident already from 0 mV).

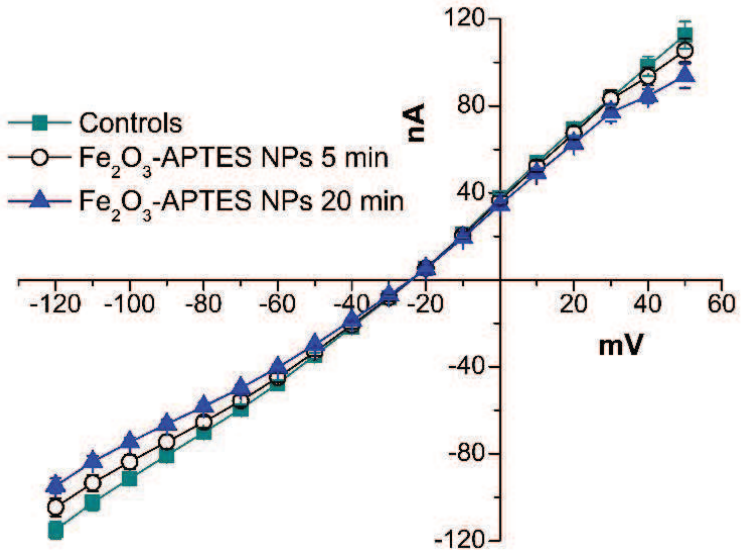

Figure 8: *I/V relationships (means ± S.E.M.) obtained from oocytes exposed to control condition (buffered solution pH 7.6), Fe_2O_3-APTES NPs within 5 min and Fe_2O_3-APTES NPs for 20 min. Controls n=195 – Fe_2O_3-APTES NPs 5 min n=81 – Fe_2O_3-APTES NPs 20 min n=86 – 4 oocytes batches each – One-way ANOVA test with Bonferroni-Holm post-hoc correction.*

Similarly, Fe_2O_3-APTES NP treatment was not able to alter in a statistically significant way the membrane currents.

Because Fe_2O_3 NPs and Fe_2O_3-APTES NPs were not able to induce intracellular calcein quenching, to modify membrane biophysical parameters and to alter transmembrane currents, a direct passive permeation of these particles can be excluded.

It is necessary to understand what are the characteristics that impeded to these NPs to cross the membrane, since Fe_2O_3 NPs are rather similar to the Fe_3O_4 NPs which have instead been proved to directly cross the membrane. In the case of the APTES functionalized particles, the result was even more surprising, since it is known in literature that cationic NPs are the most effective in porating the plasma membrane, and the coating with APTES gave to these particles 18 nM of free amine group per each particle. To this aim, the characterization of these particles in

our experimental conditions was performed, to link the particles characteristics to their biological behaviour.

NPs characterization

As a first step, zeta potential has been determined for both NP types in our experimental medium (ND96). After determining the charge, the behaviour in suspension was determined through Static Light Scattering, since our previous experience and preliminary measurements with this kind of particles suggested that this was the most appropriate instrument. Results are reported in Figure 9 (zeta potentials) and in Figure 10 (Fe_2O_3 NPs) and Figure 11 (Fe_2O_3-APTES NPs).

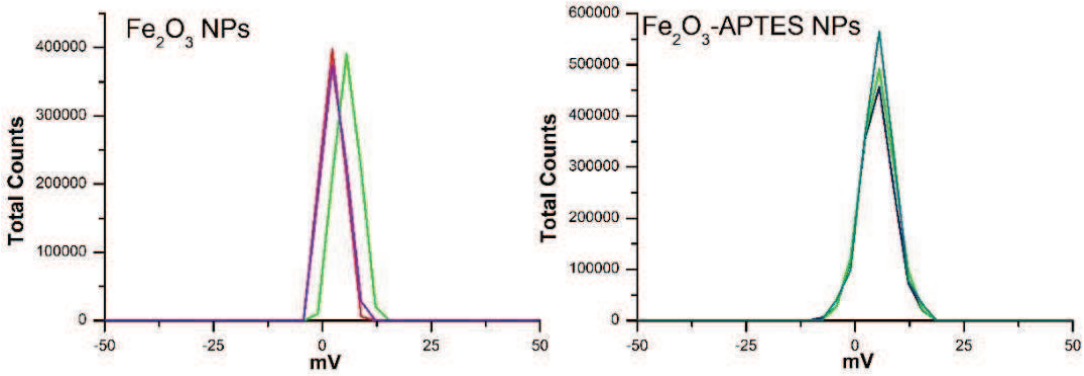

Figure 9: *zeta potential measurements (n=3 each) obtained with Laser Doppler Micro-Electrophoresis for Fe_2O_3 NPs (mean ± S.D. = 4.07 ± 2.54 mV) and Fe_2O_3-APTES NPs (mean ± S.D. = 5.02 ± 3.85 mV).*

Both particles resulted neutral in our experimental medium; if this was somehow expected of the uncoated NPs, since all the previously tested metal oxide resulted neutral, it was not for the APTES-coated NPs. The most likely hypothesis is that the coating charge (which in water is highly positive, around +35 mV) was neutralized by the anions present in the medium. The SLS data, according to these zeta potential

measurements were expected to show a marked aggregation for both types of particles.

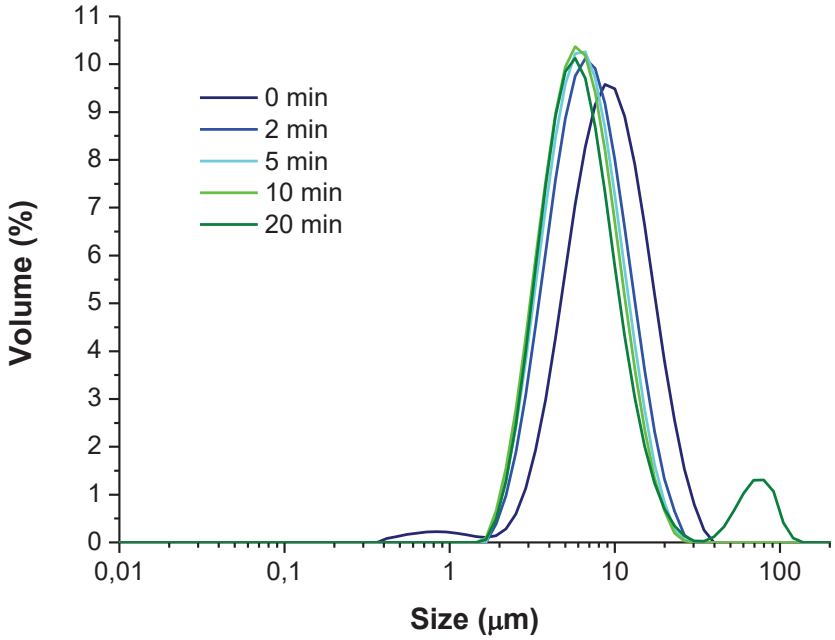

Figure 10: *Hydrodynamic size distributions of Fe_2O_3 NPs over 20 min, determined by Static Light Scattering (representative experiment).*

From the particles size distributions, it is possible to note that Fe_2O_3 NPs aggregated promptly after their addition in the experimental medium; according to our size-dependent particles crossing hypothesis, this could be the cause for their ineffectiveness on the membrane. The difference with Fe_3O_4 NPs is also quite evident.

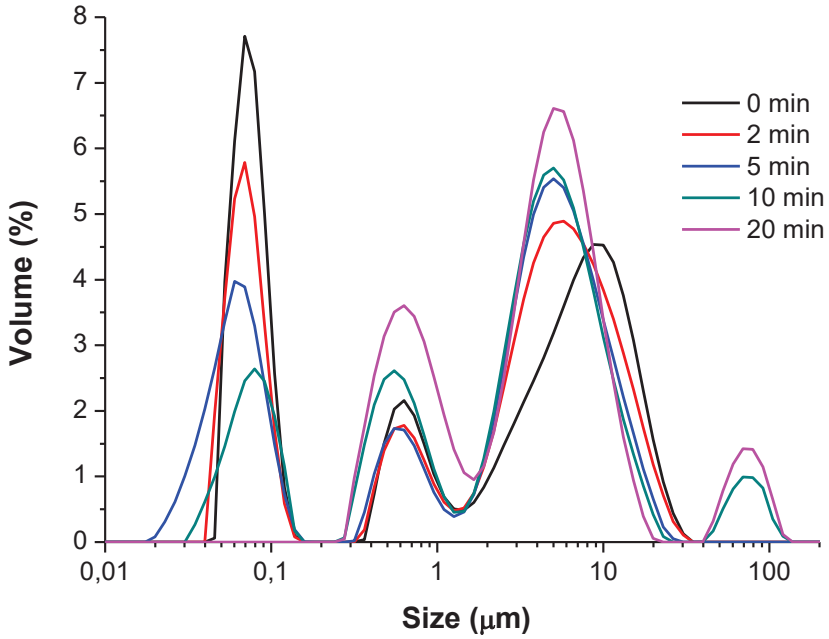

Figure 11: *Hydrodynamic size distributions of Fe_2O_3-APTES NPs over 20 min, determined by Static Light Scattering (representative experiment).*

Interestingly, even though the particles charge is neutral in our medium, the coating was successful in stabilizing (at least partially) the particles, with a robust population around 100 nm in dimension, which decreases for approximately 10 min before aggregating. The stabilization probably occurs for steric hindrance, with the particle surfaces that are no more able to interact with each other and to aggregate; similarly to what seen for BSA coating on Co_3O_4 and Fe_3O_4, a coating that stabilizes the particles can be able to abolish the effect of the NPs on the membrane.

In this case, when not coated the particles were not effective probably because they aggregate very fast becoming too big to interact with the membrane. The coating worked to partially stabilize the particles but lost positive charge in the experimental medium, resulting subsequently ineffective in promoting passive permeation of the particles; the size effects reported previously is likely to happen with particles with unmodified surface, while coating (covalent or non-

covalent) dramatically changes the interactions with the membranes of the surface-modified particles.

Conclusions

Fe_2O_3 NPs resulted unable to modify intracellular iron concentration and membrane biophysical parameters, probably because their aggregation rate in the experimental medium is too fast to let them interact with the membrane. Coating these particles with APTES partially stabilizes them, but the experimental medium utilized masked the particles positive charge that could promote membrane crossing. These particles are therefore inert in our experimental conditions.

New pathways will be used to raise the internalization of these magnetic particles; in particular, a targeted endocytosis approach is currently under development.

Validating this approach will benefit of the use of the *Xenopus laevis* oocytes transfected with specific proteins, that will provide a platform to test differently functionalized metal particles, and to determine their probability of internalization through molecular and electrophysiological approaches.

Bibliography

1. Tombacz, E., et al., Magnetic iron oxide nanoparticles: Recent trends in design and synthesis of magnetoresponsive nanosystems. Biochem Biophys Res Commun, 2015. 468(3): p. 442-53.
2. Hola, K., et al., Tailored functionalization of iron oxide nanoparticles for MRI, drug delivery, magnetic separation and immobilization of biosubstances. Biotechnol Adv, 2015. 33(6 Pt 2): p. 1162-76.
3. Martinkova, P., et al., Iron Oxide Nanoparticles: Innovative Tool in Cancer Diagnosis and Therapy. Adv Healthc Mater, 2018. 7(5).
4. Saeed, M., W. Ren, and A. Wu, Therapeutic applications of iron oxide based nanoparticles in cancer: basic concepts and recent advances. Biomater Sci, 2018. 6(4): p. 708-725.

5. Hofmann-Amtenbrink, M., H. Hofmann, and X. Montet, Superparamagnetic nanoparticles - a tool for early diagnostics. Swiss Med Wkly, 2010. 140: p. w13081.
6. Vallabani, N.V.S. and S. Singh, Recent advances and future prospects of iron oxide nanoparticles in biomedicine and diagnostics. 3 Biotech, 2018. 8(6): p. 279.
7. Estelrich, J. and M.A. Busquets, Iron Oxide Nanoparticles in Photothermal Therapy. Molecules, 2018. 23(7).
8. Crespo, P., et al., Magnetism in nanoparticles: tuning properties with coatings. J Phys Condens Matter, 2013. 25(48): p. 484006.
9. Paik, S.Y., et al., Characterization, Quantification, and Determination of the Toxicity of Iron Oxide Nanoparticles to the Bone Marrow Cells. Int J Mol Sci, 2015. 16(9): p. 22243-57.
10. Ivask, A., et al., Toxicity of 11 Metal Oxide Nanoparticles to Three Mammalian Cell Types In Vitro. Curr Top Med Chem, 2015. 15(18): p. 1914-29.
11. Karlsson, H.L., et al., Size-dependent toxicity of metal oxide particles--a comparison between nano- and micrometer size. Toxicol Lett, 2009. 188(2): p. 112-8.
12. Gupta, A.K. and M. Gupta, Cytotoxicity suppression and cellular uptake enhancement of surface modified magnetic nanoparticles. Biomaterials, 2005. 26(13): p. 1565-73.
13. Malvindi, M.A., et al., Toxicity assessment of silica coated iron oxide nanoparticles and biocompatibility improvement by surface engineering. PLoS One, 2014. 9(1): p. e85835.
14. Patil, R.M., et al., Comprehensive cytotoxicity studies of superparamagnetic iron oxide nanoparticles. Biochem Biophys Rep, 2018. 13: p. 63-72.
15. Kornberg, T.G., et al., Potential Toxicity and Underlying Mechanisms Associated with Pulmonary Exposure to Iron Oxide Nanoparticles: Conflicting Literature and Unclear Risk. Nanomaterials (Basel), 2017. 7(10).
16. Valdiglesias, V., et al., Effects of iron oxide nanoparticles: cytotoxicity, genotoxicity, developmental toxicity, and neurotoxicity. Environ Mol Mutagen, 2015. 56(2): p. 125-48.

17. Valdiglesias, V., et al., Are iron oxide nanoparticles safe? Current knowledge and future perspectives. J Trace Elem Med Biol, 2016. 38: p. 53-63.
18. Dissanayake, N.M., K.M. Current, and S.O. Obare, Mutagenic Effects of Iron Oxide Nanoparticles on Biological Cells. Int J Mol Sci, 2015. 16(10): p. 23482-516.
19. Arias, L.S., et al., Iron Oxide Nanoparticles for Biomedical Applications: A Perspective on Synthesis, Drugs, Antimicrobial Activity, and Toxicity. Antibiotics (Basel), 2018. 7(2).
20. Wu, W., Q. He, and C. Jiang, Magnetic iron oxide nanoparticles: synthesis and surface functionalization strategies. Nanoscale Res Lett, 2008. 3(11): p. 397-415.
21. Noel, S., et al., Quantification of primary amine groups available for subsequent biofunctionalization of polymer surfaces. Bioconjug Chem, 2011. 22(8): p. 1690-9.
22. Arenal, R., et al., Spatially-resolved EELS analysis of antibody distribution on biofunctionalized magnetic nanoparticles. ACS Nano, 2013. 7(5): p. 4006-13.
23. Kunzmann A, Andersson B, Vogt C, et al. Efficient internalization of silica-coated iron oxide nanoparticles of different sizes by primary human macrophages and dendritic cells. Toxicol Appl Pharmacol. 2011;253(2):81-93. doi:10.1016/j.taap.2011.03.011.
24. del Campo A, Sen T, Lellouche J-P, Bruce IJ. Multifunctional magnetite and silica–magnetite nanoparticles: Synthesis, surface activation and applications in life sciences. J Magn Magn Mater. 2005;293(1):33-40. doi:10.1016/j.jmmm.2005.01.040.
25. Feng B, Hong RY, Wang LS, et al. Synthesis of Fe3O4/APTES/PEG diacid functionalized magnetic nanoparticles for MR imaging. Colloids Surfaces A Physicochem Eng Asp. 2008;328(1):52-59. doi:10.1016/j.colsurfa.2008.06.024.
26. Balzaretti, R., Meder, F., Monopoli, M.P., Boselli, L., Armenia, I., Pollegioni, L., Bernardini, G. & Gornati, R., 2017. Synthesis, characterization and programmable toxicity of iron oxide nanoparticles conjugated with D-amino acid oxidase. Rsc Advances, 7, 1439-1442.

27. Armenia, I., Marcone, G.L., Berini, F., Orlandi, V.T., Pirrone, C., Martegani, E., Gornati, R., Bernardini, G. & Marinelli, F., 2018. Magnetic nanoconjugated teicoplanin: a novel tool for bacterial infection site targeting. Frontiers in Microbiology 9.

Chapter 6

During the three years of my Ph.D., I focused my research activity on the interactions between metal NPs and cell membrane, to investigate about the possibility that selected NPs are able to cross directly the membrane bypassing the classical endocytotic routes. This hypothesis has been tested and studied in *Xenopus laevis* oocytes. These cells have a reduced endocytotic activity, which makes them suitable to focus on alternative internalization mechanisms. Furthermore, *Xenopus* oocytes can be cultured for days in saline solution and this enables the researcher to avoid the biomolecule corona usually formed by serum protein around nanomaterials in biological fluids. This is an advantage because protein corona deeply modifies the interactions with the cells.

The second aim of my research work was to find a correlation between the effects of the various NPs tested and their physico-chemical properties, to identify key parameters leading to direct membrane crossing.

In Chapter 2, the evidences of a direct crossing of the membrane were reported for Co_3O_4 NPs. These NPs induced an intracellular Co^{2+} increase, but neither Co NPs nor Co_3O_4@BSA NPs had the same effect, highlighting existing differences between NPs and that the presence of a biomolecular corona could influence NP-membrane interactions. All the cobalt-based NPs tested were able to release ionic metal in experimental condition. Cell integrity was not compromised after 30 min of Co_3O_4 treatment and an endocytosis inhibitor had no effect on intracellular Co^{2+} concentration increase.

The application of an electrophysiological technique to study the direct membrane crossing of metal NPs is the core of Chapter 3, with the focus on the alteration of membrane biophysical characteristics. Iron-based NPs were used for this study.

Starting with the fluorescence probe experiments, it was assessed that Fe_3O_4 could induce an increase in intracellular Fe^{2+}, while neither Fe NPs nor Fe_3O_4@BSA NPs were able to do the same. Voltage clamp experiments on *Xenopus* oocytes membrane monitored the membrane status during the treatment with NPs. Membrane biophysical parameters were significantly modified by Fe_3O_4 NPs treatment only in oocytes tested within 5 min from the start of the incubation with NPs. Membrane resistance and resting potential were significantly decreased, while membrane capacitance (which is a parameter that can vary in the presence of endocytosis) was not. Treatment with Fe NPs and with Fe_3O_4@BSA NPs confirmed the absence of effects of these NPs on the membrane, as suggested by fluorescence probe experiments.

Analysing NPs physico-chemical characteristics a difference was highlighted in the particles size distributions, with a submicron population present only in the Fe_3O_4 NPs distribution, which is stable for 5 min before aggregation. BSA addition stabilized Fe_3O_4 NPs for 30 min, but the surface coating was most likely preventing the physical interaction occurring with the membrane, suggesting that the particles must maintain a submicron size and a bare surface to interact with cell membrane and cross it. After 5 min the particles aggregated and membrane resealed. The dependency of the direct crossing from the 5 min population was proven by treating oocytes with aggregated Fe_3O_4 NPs; treatment with these NPs was not effective neither on the intracellular calcein nor on the electrophysiological parameters.

In Chapter 4, the focus was monitoring biophysical membrane parameters for detecting interactions occurring in the presence of Co_3O_4, Co, Ni and NiO NPs.

Co_3O_4 NPs are effective in causing the membrane parameter modifications. Oocytes were able to reseal after 5 min, which explains why testing cells after 30 min as reported in the paper in Chapter 2 showed only non-significant difference in membrane currents. The

direct cross it is possible only in the presence of 5 min submicron population. Co NPs and Co_3O_4@BSA NPs were not able to modify the biophysical properties of the membrane, substantially confirming the fluorescence data reported in Chapter 2. Co NPs were non-effective probably because their aggregation is too rapid, as shown by their hydrodynamic size distributions; Co_3O_4@BSA NPs were stabilized (in terms of submicron population), but this surface modification could possibly prevent particles from reacting not only with each other (which is the actual stabilization we saw) but also against the cellular membrane.

Ni-based particles resulted non-effective with none of the techniques we utilized, neither in fluorescence nor in electrophysiology, either the metallic form or the oxide form. Their z-potentials are neutral in the experimental medium. Size distributions showed Ni NPs aggregate just after particles were added in the medium, while NiO NPs retained a submicron population for the whole experiment duration. a difference was highlighted comparing the hydrodynamic size distributions of Co_3O_4 and NiO NPs, where it is possible to see that Co_3O_4 submicron population was composed of smaller NPs than the NiO NPs one (indicatively smaller than 200 nm). This "below-200 nm" population could be the one responsible for particles effect.

As a final step, Fe_2O_3 NPs were tested; these particles are already applied in many fields, are considered inert and possess many interesting properties related to their magnetic susceptibility and their superparamagnetism. Bypassing endocytosis and gaining direct access to the cytoplasm would increase the applications of these particles. Furthermore, it is possible to functionalize these particles with APTES, an organosilane which provides the particles with positively charged amine residues.

Fe_2O_3 NPs and Fe_2O_3-APTES NPs failed to induce any modifications in intracellular calcein fluorescence and in membrane biophysical

parameters and membrane currents. The hydrodynamic size distributions showed that Fe_2O_3 NPs promptly aggregated when added to the experimental medium. Characterization demonstrated that particles charge resulted close to neutrality. Surprisingly, even though the covalent surface modification was successful in the experimental medium the stabilization of Fe_2O_3-APTES NPs was only partial and z-potential resulted neutral. The surface modification is thus able to stabilize the particles and to reduce their dimension, but the ability to direct cross the membranes were not changed if compared to bare NPs, pointing out a key role also for the surface coating of the NPs in dictating passive membrane crossing.

In this Ph.D. thesis several kinds of metal-based NPs were tested in *Xenopus laevis* oocytes and the results can be categorized as follows:

- The metallic NPs tested (Co, Fe, Ni) dissolve more than their oxide counterparts; however, in a medium with moderate osmolarity as the *Xenopus laevis* culture solution, they are unstable in suspension and their aggregation rate is fast. All these particles are not able to induce modifications in membrane biophysical parameters and in intracellular metal concentration, thereby excluding a direct membrane crossing mechanism for their internalization.
- The metal oxide NPs which retain a population below 200 nm (Fe_3O_4, Co_3O_4) in suspension in experimental medium induced significant modifications in membrane biophysical parameters and in intracellular metal concentration. The effects are recorded only when the population of NPs smaller than 200 nm is present, namely only within 5 min from the particles addition to the medium; after this time range, effects on membrane become milder until they disappear, stating the complete fast recovery of the membrane.

- Aggregated particles are able not to cross the membrane, confirming the role of the size in this kind of interactions.
- The metal oxide NPs that never go below 200 nm (NiO, Fe_2O_3) in suspension in the experimental medium do not cross the membrane and do not modify neither intracellular metal concentration nor membrane biophysical parameters.
- The surface coating modify particles behavior in suspension in the experimental medium. The non-covalent coating by BSA stabilized the 200 nm population for Co_3O_4 and Fe_3O_4 NPs but abolished the modifications in intracellular metal concentration and in membrane biophysical parameters. The covalent coating by APTES of Fe_2O_3 NPs partially stabilized particles around 100 nm but failed to induce membrane crossing.
- The role of particle surface is thus crucial to achieve direct membrane crossing.

Direct membrane crossing it is indeed a mechanism that has been reported in few studies, but its implications may be revolutionary. Many of the studies conducted nowadays rely on models, both *in silico* as well as *in vitro*, that are limited in replicating the biological complexity of the cells. Using voltage clamp and fluorescent probe on *Xenopus Laevis* oocytes may lay the foundation for an innovative screening platform for investigating nanocompounds which could potentially access cytoplasm directly, allowing to study the internalization and the effects on membrane. *Xenopus laevis* oocytes are easy to collect, maintain and prepare. They are flexible and adaptable to different culture conditions, allowing to study interactions in controlled environment.

Moreover, *Xenopus laevis* oocytes can also be a useful tool to study and optimize targeted internalization. Their historical use as heterologous expression system is well known, selectively express target proteins to

study specific internalization pathways of new modified nanoparticles will be one of the new goals for the therapeutic use of nanomaterial.

Scientific Production

The data reported in this Ph.D. thesis have been published in the following articles:

- "Cobalt oxide nanoparticles can enter inside the cells by crossing plasma membranes" - Elena Bossi, Daniele Zanella, Rosalba Gornati & Giovanni Bernardini - Scientific Reports | 6:22254 | DOI: 10.1038/srep22254
- "Iron oxide nanoparticles can cross plasma membranes" - Daniele Zanella, Elena Bossi, Rosalba Gornati, Carlos Bastos, Nuno Faria & Giovanni Bernardini - Scientific Reports | 7: 11413 | DOI:10.1038/s41598-017-11535-z

The national and international conferences in which the data have been presented are the following:

- Daniele Zanella, Elena Bossi, Rosalba Gornati, Nuno Faria, Jonathan J. Powell, Giovanni Bernardini - Metal oxide nanoparticles: size role in membrane interactions - NanoTox 2018, 9th International Conference on Nanotoxicology – Düsseldorf, September 2018 - Poster Presentation
- Daniele Zanella, Elena Bossi, Rosalba Gornati, Nuno Faria, Jonathan J. Powell, Giovanni Bernardini - Metal oxide nanoparticles: size role in membrane interactions - Europhysiology 2018 – London, September 2018 - Poster Presentation
- Daniele Zanella – Metal oxide nanoparticles: size role in memebrane interactions - 12TH Meeting of Young Researchers in Physiology - Anacapri, May 3-5, 2018 - Oral communication
- Daniele Zanella, Elena Bossi, Rosalba Gornati, Carlos Bastos, Nuno Faria, Giovanni Bernardini - Iron oxide nanoparticles can cross

plasma membranes - 10th SFB-Transmembrane Transporter in Health and Disease Symposium - Vienna, September 2017 - Poster Presentation

- Daniele Zanella, Elena Bossi, Rosalba Gornati and Giovanni Bernardini - Interactions of metal nanoparticles with the plasma membrane - 63° Convegno Gruppo Embriologico Italiano - Rome, June 12-15, 2017 - Poster presentation
- Daniele Zanella - Metal nanoparticles interactions with cell membranes cause alterations of cell membrane parameters - 11TH Meeting of Young Researchers in Physiology - Florence, May 25-27, 2017 - Oral communication
- Daniele Zanella, Elena Bossi, Rosalba Gornati and Giovanni Bernardini - Iron nanoparticles can enter inside the cells also by directly crossing plasma membranes - 9th SFB-Transmembrane Transporter in Health and Disease Symposium - Vienna, September 2016 - Poster presentation
- Daniele Zanella - Metal oxide nanoparticles con enter inside the cells by crossing plasma membranes - 10th Meeting of Young Researchers in Physiology - Magnano in Riviera, May 05-07, 2016 - Oral communication

Acknowledgements

My most heartfelt thanks go to my family. To my parents Maurizio and Barbara, my sisters Sara and Alessia, my aunts Lorena, Sabrina, Mariarosa, Paola and Marcolina, my uncles Roberto, Gianfranco and Walter, my grandmother Romana and the late grandparents Pietro, Natale and Luigia, for the strong and constant support they gave me during these years. Trying to become a researcher is hard, the road to the goal is long but without you I wouldn't have even started. Hope to have made all of you at least a bit proud.

To my dearest friends Davide, Michele, Simone, Marco, Ilaria, Lucia, Ilaria and Eleonora, the people that have grown up with me. Our different ways of living, thinking and feeling contributed to forge what I am now, virtues and defects alike. Our path together was not always easy, but I wouldn't ask for no one and nothing different. Brothers and sisters by choice, even half the world away.

The marvellous Cellular and Molecular Physiology Laboratory, in which I was trained and that I hope I contributed to keep going, is first of all a family. I will definitely miss it and try to recreate its atmosphere in the laboratories that will host me in my future, because I believe that nothing more than this testifies how precious to me it has become.

My deepest thank-you goes to the person who first accepted me in her laboratory and then raised me as a researcher, Professor Elena Bossi. You always let me free to do mistakes and to learn on my own skin, expressing freely my ideas and encouraging a constant exchange of ideas. You have been a wonderful mentor, I hope to have at least partially repaid the faith you had in me when I started as a M.Sc. student.

Lot of people have taken part in my years here, all share a big or smaller piece of my story in it and all deserve to be thanked.

Raffaella, your presence was always precious and discrete, you helped countless students (including myself) with your patient teachings and with your knowledge and efforts in molecular biology. I thank you most of all for the discussion and talks we had, very useful to me for proving my points of view, to have different opinions and sometimes to change my mind. Furthermore, you and Davide were stimulating lunch companions and great people to share my time with and also this deserves thanks.

To Eleonora and Alessandra, my great mentors and friends. You initiated me to electrophysiology, to MacGyverism and to lab life in general. Much of the path I have walked so far is because of you; thank you girls, one of the things I am most proud of is to call you colleagues now.

To Francesca (the younger), I found in you a complex colleague, sceptical enough to be a great scientist and optimist enough to go for it, when your mind tells you so. I hope to have been a decent colleague to you, a stubborn and selfish old goat, better defined as "elder Ph.D student". Most of all, I thank you for being a nice friend to me and I hope I have been the same to you.

To Francesca (the elder), we never had an easy relationship, but I'm happy that we managed over time to balance our characters and to live well in the lab, each enjoying his win as much as the other defeats (sportively speaking). Good luck with the teaching, it will always be nice to know a purebred "Milanese Imbruttita".

To all the students that followed me during my years here, hope to have transmitted at least some of the beauty that this work possesses, without hiding its difficulties. From the historical ones who now have entered the same path as me (Arianna "the assistant", Lavinia) to all the other that have successfully earned their B.Sc. and to the present ones, I wish you all the best, you allowed me to grow up in teaching and sometimes as a human being. To Elisa, my only M.Sc. student, fewer words more.

You were a great pupil, I loved to share my ideas with you as well as discussing about music. I know that every choice you take will be for your best, but I fell to say to you anyway: don't settle for easy stuff but aim high, because you can do it.
There is another component in this family, the physiologically peculiar "functional syncytium" with the Molecular Genetics Laboratory of Paola Campomenosi Ph.D. The cooperation made of both good human relationships and science between the two laboratories never fainted and working along was a real pleasure. Thanks for all the nice moments and for all the good people that sometimes crowded your laboratory, in particular for Sarah, former physiologist, studies companion and good friend, to whom I wish all the best.

The thanks I owe to the Cell Biology Laboratory of Professor Giovanni Bernardini and Professor Rosalba Gornati are a core part of the acknowledgments for this thesis. The collaboration established was proficuous and allowed me to enter the field of nano-science with my perspective and ideas. You provided me with the necessary instruments and funding when necessary, for which I am very grateful; moreover, I felt always well accepted and spurred when it was necessary. Collectively, I thank you for the opportunities you gave me and hope that the work done together could serve for higher goals in the future.
To Ilaria, Riccardo and Silvia, we knew each other from times before, but in these years I had the opportunity to appreciate all of you as scientist of great wit and as splendid and totally mad friends. You made the weight easy to bear, and I hope that the weight sometimes I am and was (especially for Ilaria) was bearable too. To Federica, Marina and Cristina, thank you for being nice colleagues, always ready to help and kind to me.

Finally, the international part of these acknowledgments is for the Biomineral Research Group in Cambridge; working there was an

experience that opened my mind to the international research world and changed my perspective on many aspects of this work.
To Professor Jonathan J. Powell, thank you for hosting me in your group, I felt instantly at ease and well accepted. You provided me with all that I needed, both materially and intellectually to deepen my research. It was an honour for me to be part of your group even if for a short period.
To Ravin and Nuno, the Yin and Yang of the BMR group. Nuno, a true Latin force of nature and Ravin, more British than British people itself. You were fantastic supervisors, helped me to learn a lot and were always present and helpful. You were truly of example.
To my companions Alessandra, Carlos, Will, João and Katarina. Thank you for welcoming me so nicely in the group and for all the help you gave me during my staying, if it was a fantastic experience to me it is mostly because of you. Thanks in particular to Will, for hosting me in my flash visit in September and for all the help you gave me in my first time in your lab, and to Carlos, for its help with part of this thesis and for the discussion about football; one can always rely on you for a pizza and a beer as well as for a discussion about biochemistry. Thanks to Rachel, John, Jack, Michelle, Dagma, Ahamed, great people which was nice to meet.